University of Alberta

INTERACTION OF CHEMICAL AND MECHANICAL EFFECTS IN EROSION-CORROSION OF PIPELINE STEELS IN OIL SAND WASTEWATER TRANSPORTATION

By

CHONGWEI CHEN 

A thesis submitted to the Faculty of Graduate Studies and Research in partial fulfillment of the requirements for the degree of

MASTER OF SCIENCE

IN

ENVIRONMENTAL ENGINEERING

Department of Civil and Environmental Engineering

Edmonton, Alberta

Spring, 2006

Your file Votre référence
ISBN: 0-494-13801-7
Our file Notre référence
ISBN: 0-494-13801-7

ABSTRACT

This thesis investigates the slurry erosion-corrosion behavior of two carbon steels used for piping in tailing system. The experiments were conducted with a custom-made rotating cylinder electrode system in flowing slurries comprising silica sand and tailing solution provided by Syncrude Ltd, Canada, or tap water. The experimental results show that the interface reaction dominates the corrosion of carbon steels in the flowing slurries, and the synergism contributes notably to the material loss. The synergism can be attributed to the corrosion-enhanced erosion and erosion-enhanced corrosion. In the erosion-corrosion of carbon steels in an active dissolution system, the corrosion-enhanced erosion results from the degradation in resistance of material to local plastic deformation induced by the anodic dissolution present on surface. In light of a theoretical model developed on basis of non-equilibrium thermodynamics and dislocation theory, the normalized wastage of corrosion-enhanced erosion can be formulated as a linear function of logarithm of anodic current density.

ACKNOWLEDGEMENTS

I deeply express my sincerest gratitude and appreciation to my supervisors, Dr. Tong Yu and Dr. Jingli Luo, for their supports to make my dream become truth. They have provided me with a great deal of encouragement and supervision throughout the course of this research.

I greatly thank Dr. B.T. Lu for his enthusiasm, suggestions and motivation. His support helped me to finish this research project.

I would like to acknowledge Dr. Selma E. Guigard for participating on my defense committee, and for teaching me the measurement knowledge of environmental engineering.

I would also like to extend my thanks to Mr. B. Walter for their assistance. And also, I owe a lot of debt to my colleagues and my classmates: Ms. H.X. Guo, Ms. X C. Li, Mr. S.Y. Wang, and Mr. A. Adeleke. Thanks your kindness help.

Finally, my special thanks must be given to my mother, my wife and my daughter for their love and encouragement in my school years.

TABLE OF CONTENTS

LIST OF TABLES

LIST OF FIGURES

NOMENCLATURE

B	A coefficient correlating $\Delta Hv / Hv$ and $\log(i_a / i_{th})$
C_v	Oxygen concentration in bulk of aqueous medium
C_f	Oxygen concentration on liquid/ corrosion scale interface
C_r	Oxygen concentration at bottom of pores in protective layer,
ΔC	Diffusion controlled reaction to the concentration driving force
C^j_v	Oxygen concentration in bulk of aqueous medium with j %wt. concentration sand
C_{sand}	Concentration of Sand in the slurry
D	Diffusion coefficient of oxygen
d	Average diagonal length of tube
E_{eq}	Open circuit potential
E	Potential

F	Faraday's constant
$f(\alpha)$	Function of angle injected by sand particle
Hv	Vickers hardness measured in absence of corrosion
ΔHv	Degradation of hardness caused by anodic dissolution
L_ε	Constant relative to ratio of phenomenological coefficient
L	Distance along the tube
i_a	Average anodic current density over sample surface
i_{corr}	Self-corrosion current density
i_{corr}^0	Self-corrosion current density under conditions free of erosion
Δi_{corr}	Increment of self-corrosion current density caused by erosion
i_{th}	Threshold anodic current density to cause the chemo-mechanical effect
i_0	Exchanging current density
J_{th}	Threshold flux of $Me \leftrightarrow Me^{z+} + ze^-$
J_a	Flux of anodic reaction

k^j	Mass transfer coefficient in the slurry with j %wt. sand concentration
k_v	Migration coefficient of oxygen in bulk of aqueous medium with sand
k_f	Diffusion coefficient of oxygen in corrosion scale or protective layer
k_r	Interface reaction coefficient of oxygen on the surface of metal
κ_q	Coefficients in expressions correlating w_e^0 to $\dot{\gamma}_p$
κ_p	Coefficient to correlate w_e to $\dot{\gamma}_p$
$k_r^{0\ -1}/k^{0\ -1}$	Relative contribution of the interface reaction as one of controlling steps to the corrosion process in flowing solutions without solid particles
$k_f^{0\ -1}/k^{0\ -1}$	Relative contribution of the diffusion as one of controlling steps to the corrosion process in flowing solutions without solid particles
k	Apparent mass transport coefficient in slurry
k^0	Apparent mass transport coefficient in solution free sand
k_v^0	Migration coefficient of oxygen in bulk solution free of sand
k_f^0	Diffusion coefficient of oxygen in corrosion scale or protective layer for flowing solution without sand

k_r^0	Interface reaction coefficient of oxygen on the surface of metal for flowing solution without sand
M_p	Mass of sand impacting the surface in per-liter solution
M_{Fe}	Mass weight of iron
m , p , q	Number of items in regression formula $m = q + p$
$m_1, m_2, ...m_i$	Experimental constants
n	Number of electron exchanged in the oxygen reduction
ΔP	Drop of pressure on the wall
r	Radium of cylinder sample
R	Gas constant
$R(t)$	Rate of material loss
R_v	Resistance of migration step
R_f	Resistance of diffusion step
R_r	Resistance of interface reaction step

Re	Reynolds Number
Sh	Sherwood Number
Sc	Schmidt Number
U	Apparent flow velocity at electrode surface $(=\dot{\omega}r)$
V_{sand}	Volume of sand in the slurry
V_{water}	Volume of water in the slurry
V	Total volume of sand and water
w_v	Mass flux of migration in bulk solution
w_f	Mass flux of diffusion in corrosion scale
w_r	Mass flux of interface reaction on surface of metal
w_e	Weight loss due to erosion with presence of corrosion
w_c	Weight loss due to corrosion with presence of erosion
w_e^0	Weight loss due to erosion free of corrosion
w_c^0	Weight loss due to corrosion free of erosion

w_e^c	Weight loss due to corrosion-enhanced erosion
w_c^e	Weight loss due to erosion-enhanced corrosion
w_s	Weight loss due to synergistic effect
w	Total weight loss
$w_{initial}$	Initial weight loss of specimen in the experiment
w_{end}	End weight loss of specimen in the experiment
$w_{e,initial}^0$	Initial pure erosion loss of specimen in the CP condition
$w_{e,end}^0$	Initial pure erosion loss of specimen in the CP condition
w_e^c / w_e^0	Normalized synergy of corrosion enhanced erosion
w_c^e / w_c^0	Normalized synergy of erosion enhanced corrosion
Δw	Relative errors of total weight loss
Δw_c	Relative errors of corrosion weight loss
Δw_e^0	Relative errors of pure erosion weight loss

Δw_e^c	Relative errors of weight loss of corrosion enhanced erosion
Δ	Normalized errors of total weight loss
$x_1, x_2, \ldots\ldots x_i$	Response variable
Y	Predictor variables
$Y(m)$	Response for baseline logarithmic function
z	Number of electrons exchanged in electrochemical reactions
z'	Coefficient correlative to $\Delta H_v / H_v$ and $\log(i_a / i_{th})$
Z	Coefficient correlative to w_e^c / w_e^0 and $\log(i_a / i_{th})$
$\dot{\gamma}_p$	Plastic strain rate
$\dot{\gamma}_p^s$	Plastic deformation rate in surface layer
ε_y	Residual of predictor variables
τ	Wall shear stress
$\Delta\tau_A$	Increment of shear flow stress due to strain hardening $(=\tau - \tau_0)$
υ	Kinetic viscosity

ω	Rotating angle speed of cylinder sample
$\overline{\rho}$	Average density of the slurry
ρ_{sand}	Density of sand in the slurry
ρ_{water}	Density of water in the slurry
ρ_{Fe}	Density of iron
η	Coefficient relative to corrosion process
η^j	Coefficient relative to corrosion process in the slurry with j % wt. sand concentration
η_a	Over-potential, $\eta_a = E - E_{eq}$
μ	Absolute viscosity
α, β, γ	Constants depending the corrosion mechanisms, flow conditions and geometries of test devices
α	Impact angle
$\tilde{\alpha}, \tilde{\alpha}'$	Experimental constants in slurry tests

$\tilde{\alpha}_j, \tilde{\alpha}_j{}'$	Experimental constants in slurry with j %wt. sand concentration
α_0, β_0	Constants of Re, Sh and Sc in flowing solution free of sand
$\alpha_1, \alpha_2, ...\alpha_i$	Constant of response variable
α_a	Constant of electrochemical reaction
$`\pi(m)$	A function of parameters $x_1, x_2, ...x_i$
λ_U	Constants related to flow rate with $\log(i_a / i_{th})$
λ_C	Constants related to sand concentration with $\log(i_a / i_{th})$
ξ	Power coefficient related to the sand concentration in the slurry

LIST OF ABBREVIATIONS

CE	Counter electrode
CP	Cathodic protection
D. I. water	De-ionized water
OCP	Open circuit potential
SCE	Saturated calomel electrode
RCE	Rotating cylinder electrode
RE	Reference electrode
RSM	Response surface methodology
Pd curve	Potentodynamic curve

CHAPTER 1. INTRODUCTION

Slurry erosion-corrosion is a severe problem in the mining and/or milling of minerals, in dredging operations, and in oil and gas production (Clark and Llewellyn, 2001). One example is that a large oil spill that resulted rom a hole in a Phillips Alaska's pipeline used for transporting drilling by-products at the Kuparuk oil field on Alaska's North Slope in recent years. The Anchorage Daily News (2001) reported that "The spill was apparently caused by corrosion in a 10-inch pipe, corrosion from water and erosion from abrasive material, such as, sand is a growing problem on the North Slope". The accident not only caused property damage over $39 million annually in the 1990s, but also made unpredictable damage for environment and wild animals.

Therefore, it is crucial to develop erosion-corrosion controlling techniques and new slurry erosion-corrosion resistant materials. Before winning the war against to erosion-corrosion, we need to better understand of the damage mechanisms of erosion-corrosion and various factors controlling the kinetics of erosion-corrosion.

However, the complexity of erosion-corrosion is the complex due to the synergistic effect resulting from the interaction of mechanical and chemical factors. Although several theoretical models have been established for mechanical erosion and electrochemical corrosion in fluids, the mechanism of the synergistic effect is still poorly understood. Both laboratory investigations and field surveys have shown that the contribution of synergism to the total material loss in the slurry erosion-corrosion is so

important that we cannot ignore it in the engineering practice (Buchan and Spearing, 1994). Therefore, the primary aim of this work is to investigate, experimentally, the role of chemo-mechanical interaction in the erosion-corrosion process. The erosion-corrosion of carbon steel was investigated in an environment simulated wastewater transportation systems in oil sand production. An attempt will be made to understand the mechanism of synergism and to assess the wastage caused by the synergistic effect using a chemo-mechanical model recently developed by Lu and Luo (2004).

References:

Anchorage Daily News, 2001. Pipeline leak's a doozy, 04/17/2001, Anchorage, Alaska.

Buchan, A. J. and Spearing, A. J. S. 1994. The Effect of Corrosion on the Wear Rate of Steel Pipelines Conveying Backfill Slurry. The Journal of the South African Institute of Mining and Metallurgy, Feb., 37-45.

Clark, H. M. and Llewellyn R. J. 2001. Assessment of the Erosion Resistance of Steels Used for Slurry Handling and Transport in Mineral Processing Applications. Wear, **250-251**: 32-44.

Lu, B. T. and Luo, J. L. 2004. Chemo-Mechanical Effect in Erosion-Corrosion Process of Carbon Steel, in proc. Of CORROSION 2004, March 28-April 1, 2004, New Orleans, US.

CHAPTER 2. LITERATURE REVIEW

Erosion-corrosion is the general term encompassing a spectrum of mechanisms from accelerated corrosion to a purely mechanical damage, which causes high rates of material loss in industries (Reyes and Neville, 2001). The mechanical damage in slurry-erosion is regarded mainly as a result of impingement of solid particles, while the corrosion results from certain electrochemical processes. Basically, the two mechanisms for the removal of material from surface, i.e., erosion and corrosion, operate in the erosion-corrosion process. Erosion results in removal of the surface layer gradually in form of small chopping. Corrosion is caused by the metallic atoms on electrode surface losing their electrons and then entering solution in the form of ions or some other kinds of corrosion products.

The synergism of erosion and corrosion results from the erosion enhanced corrosion and corrosion enhanced erosion because of mechano-chemical and chemo-mechanical effects and its contribution to the total material loss is of practical importance (Bjordal et al., 1995). It should be noted that the erosion-corrosion mechanism is heavily dependent on the metallurgical features of the material (Wentzel and Allen, 1997, Christodoulou et al., 1997) and the test conditions including hydrodynamic parameters (Zhou et al., 1996), sand concentration (Rincon et al., 2002), temperature and corrosivity of environment (Neville and Hodgkiess, 1997). However, the synergistic mechanism in erosion-corrosion process is still poorly understood because the complexity of problem.

A few hypotheses have been proposed to explain qualitatively corrosion-enhanced erosion phenomenon (Neville et al., 2000, Gutman, 1998 and Larsen et al., 1999). Recently, Lu and Luo (2004) modified Gutman's work and developed a theoretical model to formulate the corrosion-induced strength degradation owing to the chemo-mechanical effect. According to this model, an extra dislocation flux will appear in the surface layer if an anodic current is present on the electrode surface and the decrease of flow stress in the surface layer $\Delta\tau_A$ could be formulated as follows.

$$\Delta\tau_A = -\frac{kT}{v_d}\ln\left(\frac{i_a}{i_{th}}\right) \tag{2-1}$$

The results indicate that the material loss produced by corrosion-enhanced erosion at the open circuit potential can be formulated as a linear function of logarithm of corrosion current density.

2.1. Erosion, Corrosion and their Synergy in Slurry-Corrosion Processes

Typically, slurries comprise of aqueous solutions containing certain kinds of corrosive dissolved species and a certain amount of solid particles (sand). The pipelines subject to slurry-erosion are generally made from structural steels. Therefore, the

corrosion problems discussed here are mainly restricted in the systems that consist of steels and aqueous solutions.

Erosion is defined as a loss of material lost in form of small debris due to cutting, plastic deformation or contact fatigue caused by the caviatation in the fluid or impact of solid particles. Erosion in flowing slurry results mainly from the impingement of solid particles (Reyes and Neville, 2001).

Corrosion is the process in which metallic atoms lose a part of their electrons, leave the metal surface in the form of ions or react with certain corrosive species in the surrounding environments to form compounds (Gutman, 1981). Almost all metals and alloys are subject to corrosion, most metals are thermodynamically instable in the metallic from, they are likely to corrode and revert to a form typically found in nature, such as ores. The corrosion of pipelines in slurry erosion process is an electrochemical process. The material loss produced by the electrochemical corrosion can be calculated with Faraday's law.

The mechanical erosion and electrochemical corrosion are the two basic mechanisms of material loss in slurry-erosion processes. The material loss rate due to erosion-corrosion, w, will be, therefore,s the sum of contributions of erosion component w_e and corrosion component w_c. The relative contributions of material losses due to the erosion and corrosion in slurry-erosion processes rely heavily on the service (test) conditions and material properties. Depending on the service conditions of pipelines to

transport slurries, the damage of erosion and corrosion may be uniform or non-uniform. Normally, when the material loss is non-uniformly distributed, it will be much more dangerous because of the highly localized penetrating rate.

2.1.1. Corrosion in Flowing Slurry

From a physical-chemical point of view, corrosion reactions are heterogeneous reactions. The corrosion of metals and alloys involves at least three fundamental steps: (1). Transport of the reactant to the metal surface; (2). interface reaction; (3). Transport of the corrosion products from the surface into the solution. Each step can be further divided into several steps. For example, the interface reaction may comprise of the adsorption, electron exchange and so on. However, to simplify our analysis, we consider these three steps mentioned above as the basic ones in a corrosion process. At the steady state, the corrosion process is controlled by the slowest step. In the flowing slurry, fluid influences the corrosion processes in various ways.

The first way is that supply of reactants or removal of intermediates or products are affected by the mass transfer process. The second way is that the erosive action of the slurry happens on the metal surface, in which surface layers, passive layers, or base metal are removed, than, a more reactive surface that leads to the formation of new layers is produced. The third ways is that flow-induced formation of electrochemical macro cells is produced by breaking a passive file. (Heitz, 1991).

In the case that the anodic dissolution of iron for the anodic dissolution of iron the pH- dependent mechanism in acid solution proposed by Poalson (1983) was used

$Fe + H_2O = FeOH + H^+ + e^-$

$FeOH = FeOH^+ + e^-$ rate-determining step

$FeOH^+ + H^+ = Fe^{++} + H_2O$

The rate equation that takes into account the resistance to charge transfer and mass transport based on the above pH-dependent mechanism is follows:

$$i = i^{->} - i^{<-} = i_0 \left[\frac{[OH^-]_s}{[OH^-]_b}\right]^n \left[\exp\left(\frac{\alpha_a F\eta}{RT}\right) - \frac{[Fe^{++}]_s}{[Fe^{++}]_b}\exp\left(-\frac{\alpha_a F\eta}{RT}\right)\right] \qquad (2\text{-}2)$$

The exchange current density i_0 based on the bulk Fe^{++} and OH^- concentrations; the over-potential, η, is $E\text{-}E_{rev}$, where E_{rev} is based on the bulk Fe^{++} concentration; n is pH dependent, according to Poalson (1983), n=1 in acid solution and n=0 in near-neutral solutions.In the simply words, the local mass transfer coefficients of O_2, H^+, OH^-, and Fe^{++} in the mass transfer entrance length and fully developed region at various Reynolds numbers were determined from mass transfer equation . The self- corrosion current (I_{corr}) of O_2, H^+, OH^-, and Fe^{++} can be determined from the E/ log(i) curves (potentodynamic curves) .

The mass transfer coefficient (k) is the parameter relating the rate ($J=k\Delta C$) of a diffusion controlled reaction to the concentration driving force (ΔC), it incorporates both diffusional and turbulent transport processes,.The local corrosion rate was calculated from the local rates of oxygen mass transfer. In the case of iron the overall reaction is completed at the pipe wall and none of the Fe^{++} ions produced by the primary electrochemical reactions are transported across the mass-transfer boundary layer prior to their subsequent chemical oxidation. The corrosion rate (w_c) can be obtained from corrosion current density (i_{corr})accroding to Fardaric law:

$$w_c = \frac{i_{corr} M_{Fe}}{zF} \tag{2-3}$$

where z= 2 as $F_e^{2+} + 2e^- = F_e$; M_{Fe} is mass of iron per mole.

2.1.2. Erosion in Flowing Slurry

It is noted that slurry erosion is different from the other forms of erosion like solid particle erosion, liquid impact erosion, cavitation erosion and so on. Many factors influence the rate of erosive wear. The erosion mechanism is heavily dependent on the hydrodynamic parameters, characteristics of the erodents, microstructures and mechanical properties of target materials. The hydrodynamic parameters include the flow velocity, concentration of solid particles, impingement angle etc; The characteristics of erodent are geometry, mass and hardness of the particles; The mechanical properties of target materials influencing erosion process are hardness and strain hardening ability.

After they quoted 33 independent parameters in a recent review of 22 erosion models and predictive equations found in the literature, Meng and Ludema (1995) pointed that the flow conditions, the targeting material properties and the particle properties influence the erosion rate. The general expression for erosion rate w_e has been established empirically and taken as the form (Postlethwaite et al., 1986):

$$w_e = M_p m_1 f(\alpha) U^{m_2} \tag{2-4}$$

Where w_e is erosion weight loss; M_p is weight of partical in per-liter sloution. U is flow rate: m_1 and m_2 (typically between 2 and 3) are constants assumed to be dependent on characteristics of the erodent/target materials involved. f(α) is a functional relationship for the dependence of the erosion rate on the impact angle (Haugen et al. 1995). It can be seen that the erosion rate will be strongly dependent on the kinetic energy of the impacting sand particles, the number of impacting particles and the impact angle. All three of these factors vary for most industrial components exposed to sand loaded flows. Therefore, to maintain long service life, the internal surfaces must perform over a wide range of solid impact conditions.

There are several erosion models that try to describe the mechanism of erosion caused by hard particle impact. These are the cutting the mechanical energy density model (Rekerby, 1983), model (Finnie and McFadden, 1978),the deformation wear model (Bitter,1963), the fatigue model (Hutchings, 1981, Follansbee et al., 1981) and the localized model (Sundararajan and Shewmon, 1983, Sundararajan, 1991) etc.

Although these models gives good predictions for the erosion behavior of materials under certain conditions, none of them has been recognized as the general model which can be used to predict the effect of various parameters on erosion beahavior. The reason is that the erosion mechanism is dependent on the test conditions and metallurgical features of materials. Therefore, the erosion mechanism should be further investigated to predict the erosion rate of materials.

2.1.3. Synergistic Effect in Slurry-Erosion

The erosion-corrosion mechanism is affected by all the factors controlling corrosion and those affecting erosion. However, the complexity of erosion-corrosion problem arises mainly from the synergism in the damage process results from the interaction of mechanical and chemical factors (Reyes and Neville, 2001, and Poulson, 1999). The relationship between the total weight loss and its components is draw on the Fingure 2-1. The material loss rate in slurry-erosion is normally higher than a sum of pure corrosion (free of erosion) and pure erosion (free of corrosion) (Levy, 1995). The synergistic effect results from the corrosion-enhanced erosion and erosion-enhanced corrosion. Therefore, the wastages of erosion and corrosion in a slurry-erosion process can be expressed as

$$w_e = w_e^0 + w_e^c \tag{2-5}$$

$$w_c = w_c^0 + w_c^e \tag{2-6}$$

where w_e^0 is the material loss due to the pure erosion damage free of corrosion, w_c^0 is due to the pure corrosion damage free of erosion, w_e^c due to the corrosion-enhanced erosion and w_c^e the due to erosion-enhanced corrosion. The synergism of erosion and corrosion, w_s, can be expressed as:

$$w_s = w_e^c + w_c^e \tag{2-7}$$

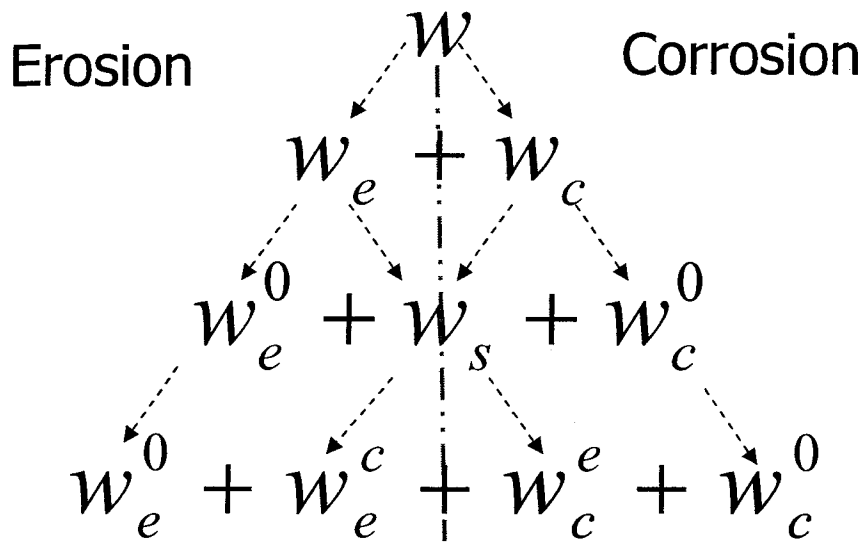

Figure 2-1. Relationshipes among the total weight loss and its componts

The synergistic effect contributes to a lot to the total materlail loss. The problem of synergistic effect in erosion-corrosion process, however, is so complicated that the mechanism for the synergism of erosion-corrosion has not been satisfactorily

apprehended, although it is considered vital for improving materials performance in industrial environment (Neville and Hu, 2001).

2.2. Factors Controlling Erosion-Corrosion

2.2.1. Flowing Velocity or Wall Shear Stress

For Newtonian fluids, such as most liquid media, the velocity field is given by the Navier-Stokes equation representing the conservation of momentum and by continuity equation based on the law of conservation of mass. The pipe flow has three kinds of flow movements in the pipe (Heitz, 1991).

The first one is Laminar that is characterized by parallel flow lines.

The second one is Turbulent, with is described as an unsteady flow that contains three dimensional, rotational fluctuations. As these fluctuations are random in space and time a turbulent flow is defined by the mean velocity of the spatial components and their fluctuation, expressed by the root mean square of single events.

The third one is attached and separated, according to their paths along solid walls.

There are some interactions of a liquid with the wall of a flow system in the water transportation. One of them is called the shear stresses. The determination of shear stress

and skin friction is a classical problem in hydrodynamics. In a laminar flow through a pipe, the pressure loss is produced by the friction between fluid and wall. This pressure loss has a linear relationship to the flow rate in the boundary layer. (Heitz, 1991)

$$\Delta P = \frac{32\mu L}{d^2} U \tag{2-8}$$

Where ΔP is drop of pressure on the wall (Pa); μ is the absolute viscosity (Pa.s); d is the pipe radius (m); L is the pipe length (m); U is the average velocity (m/s). The surface shear stress (τ) can be obtained from pressure drop (ΔP) measurements and calculated from:

$$\tau = \frac{\Delta P d}{4 L} \tag{2-9}$$

Test results available indicated that the correlation of the mass transport coefficient and flow velocity is flow-geometry-dependent. (Stack and Pungwiwat, 1998), In order to transfer the corrosion rate from one geometry to another on the basis of flow conditions, the parameter controlling the corrosion rate in the erosion-corrosion process should be well determined. The wall shear stress resulting from the flowing fluid was normally believed to be such a parameter that controlling the erosion-corrosion process (Bester and Ball, 1993). However, the wall shear stress cannot reflect the effect of particle impingement on the corrosion process (Endo and Nagae, 1996). Recently, some

experimental evidences have indicated that the mass transfer is not controlled by wall shear stress but the turbulent intensity or the kinetical energy of turbulence.

2.2.2. Mechanical Properties of Target Materials

Hutchings (1986) and Heitz (1991) have summarized the results on the erosion tests and pointed out that the mechanical erosion rates depended heavily on the relative hardness (the difference between the hardness of target material and particles). However, when corrosion is present, the relationship between the rate of total weight loss and hardness becomes intricate and the test results available are contradictive. It is normally believed that the erosion-corrosion rates of metallic materials decreases with increasing hardness (Metwally and Samy, 1994, Toro et al., 2001). However, Neville and Hodgkiess (1997) found that the resistance of high alloy stainless steels to total material loss did not follow the trend of increasing resistance as the hardness increases. For white cast iron containing tungsten in slurry, in the low hardness range, the sand slurry-erosion resistance increased linearly with hardness, but this relationship does not exist in the high hardness range. Sometimes, the sand slurry-erosion resistance of cast iron increases with its corrosion resistance. Because the sand slurry-erosion is an abrasive wear process accompanied by corrosion and cavitation, all of which aggravate each other (Rincon et al., 2002). Since the total weight-loss depends on the resistance of materials to both erosion and corrosion while the latter does not relate to the hardness of materials. Wang and Stack (2000) isolated the corrosion contribution to the total weight loss and found that only the erosion resistance of mild and stainless steels increases with increasing hardness.

Actually, the correlation between the erosion resistance and hardness of base metal depends on the erosion mechanism. Heitz (1991) pointed out that, if the mechanical damage is restricted in the surface layer, especially in corrosion product scale or passive film, it normally exists in the single-phase flow, the adherence, cohesion and hardness of surface layer determines mechanical stability. In this case, the hardness of base metal is not relevant to the erosion-corrosion process but certain chemical changes in these layers may be the cause of a breakdown with subsequent onset of erosion-corrosion. However, in the two-phase liquid/solid flow, the interaction of the solid particles and the base metal dominates and the erosion resistance is improved with increasing hardness of base metal. Theoretical analysis and experimental evident indicate that the hardness, and the strength as well, of the surface layer will decreases, as anodic dissolution current density of metal increases (Gutman, 1981). If the erosion resistance of metals depends on the hardness or strength, the corrosion-enhanced erosion owing to the chemo-mechanical effect will be expected. Such an effect has been applied in the chemo-mechanical polish (CMP) process to machine hard materials (Larsen and Liang, 1999). However, the potential effect of hardness- or strength-degradation due to the erosion-enhanced corrosion is not yet explored in research on the erosion of slurry pipes.

2.2.3. Properties of Protective Film

In many corrosion systems, a protective film is likely to form on a metal surface when it exposes to its environment and the film plays an important role in the erosion-

corrosion mechanism of materials. The passive film has an ability to inhibit erosion-corrosion damage to a certain extent through inhibiting corrosion as long as it is chemically stable in the environment (Matsumura et al., 1991). The protective function of film relates to its formation kinetics, mechanical properties and hydrodynamic conditions of fluid (Adlerm et al., 1993). The kinetics of film formation depends on the composition of materials and conditions of environment (Gooch, 1996). For a ferrous alloy, the protective ability of the film increases with increasing chromium concentration in a matrix. In alkaline slurry (0.5 M Na_2CO_3/0.5 M $NaHCO_3$/300 g/L Al_2O_3), the passive film on AISI 304 stainless steel displays much stronger protective ability than those on AISI 410 and mild steels, as a result, the material loss of the former due to corrosion is much less than those of the latter.

Because the protective film (passive film or corrosion product scale) is very thin (~10 μm or less), both the theory and experimental techniques for evaluating the mechanical properties of the protective film are not well established (Seo and Chiba, 2001).

2.2.4. Particle Properties

A particle initially produces a crater by the plastic deformation of the metal surface, depending on the impact angle. Later stages of the destruction produce surface roughness with platelet formation and local heat production. The experimental findings can be explained on the basis of the kinetic energy of particles hitting the surface. It has

been shown that the rate of erosion corrosion at the maximum of attack is proportional to the square of the velocity and directly proportional to the concentration of particles. This suggests that the kinetic energy of a single particles is a decisive parameter where the mass is directly associated with the particle concentration. This basic relationship with the square root of flow velocity can be interpreted very well by the results of the laser. Three cases of increasing energy or frequency of the particles hitting the surface can be distinguished in the Figure 2-2 (Heltz, 1991).

(1). The particle energy is too small to damage the passive layer. the metal weight loss rate is unmeasurabl. Flow effects can only be effective via mass transfer;

(2). The particle energy is sufficient to account for damage to the passive or other surface layers and for deform the outer regions of the base metal mechanically. Erosive wear and corrosion rates are of the same magnitude. Damage and healing kinetics of passive or other layers are involves;

(3). The particle energy is so great that the base metal is preferentially eroded and the attack is mainly erosive wear.

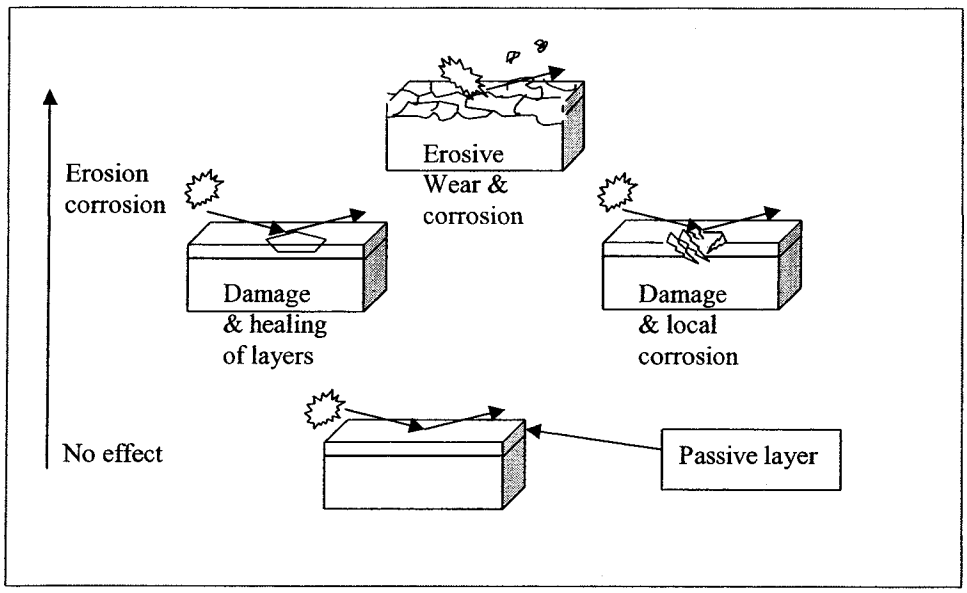

Figure 2-2. Effect of particle with mechanical energy on the passive layer

2.3. Mechanisms of Synergism in Slurry-Erosion

2.3.1. Chemo-Mechanical Effect

Theoretical models and experimental results available in slurry-erosion condition have indicated that the erosion rate decreases with hardness and or strength of steels (Schmitt et al., 2002). In light of the principle of corrosion-induced hardness/strength degradation, the corrosion-enhanced erosion phenomenon is related to the degradation of surface hardness or strength of materials due to increase of corrosion rate in flowing solution.

The role of corrosion is to roughen the pipe surface, which in turn greatly increases the erosion rate. The rough of pipe surface is very sensitive to the angle of impact of the solid particles. It was proposed that this could lead to a situation in which, although corrosion accounted for only 10% of the total wear, the elimination of the component would reduce the total wear to a low value. These conclusions were supported by the fact that the effect of chromate inhibitors and cathodic protection is to maintain a smooth, polished surface, with relatively low rates of metal loss.

2.3.2. Mechano-Chemical Effect

The erosion–enhanced corrosion is believed being caused by the retardation of formation of a protective film on surface that normally stifles the diffusion of oxygen to the corroding surface. The corrosion proceeds at a high rate in the absence of such protective films and is controlled by the rate of oxygen mass transfer through the solution to the corroding surface. For example, Protective films on carbon steel pipes are responsible for reduction of the corrosion rate to values < 1mm/ y, by providing a barrier for oxygen diffusion to the corroding surface. When abrasive solids such as sand are present, coverage of the corroding surface by the rust film is incomplete, with islands of bare metal present that can act as efficient cathodes for oxygen reduction, resulting in corrosion rates > 10 mm/y.

Existing test results have indicated that, under flow conditions close to those of tailing pipes, the corrosion process of carbon steels in the flowing neutral pH slurry is

solely controlled by the mass transport of dissolved oxygen in boundary layer of fluid (Sasaki and Burstein, 1998, Schmitt et al., 1998, and Postlethwaite et al., 1992). In this case, the correlation between the corrosion rate and hydrodynamic parameters has been well documented. If passive film or corrosion product scale exists on surface of material, it will affect the corrosion mechanism (Neville and Hu, 2001). Under slurry-erosion conditions in the practical engineering, the impingement of solid particles causes breakdown of passive film. If the passive film is totally removed by erosion, the corrosion mechanism will be similar to the carbon steel. However, if the passive film is partially breakdown, the situation is rather complicated and sometimes pitting corrosion may take place (Sasaki and Burstein, 1998). In the process the hydrodynamic parameters that control the breakdown of passive film will be important to understand the mechano-chemical effect in the erosion-corrosion of stainless steels.

2.4. Experimental Techniques for Evaluating Erosion-Corrosion Performance

Poulson (1999) had summarized the existing laboratory techniques for studying the effect of flow velocity on electrochemical corrosion processes and pointed out that the methods adopted for simulating fluid flow effects on corrosion should satisfy following basic requirements:

The hydrodynamic laminar, transitionary, and turbulent regimes and flow characteristics should be well defined.

Mass transport correleations should be readily available or should at least be easily determined.

The corroding surface should be equipotential so that the material corrodes at the the same mechanism at all points.

2.4.1. Flow Loop System

The flow loop and rotating cylinder systems (RCE) are the most suitable geometries satisfying above requirements (Chen et al., 1992). Undoubtedly, the flow–through pipe loops is the best device to directly simulate the erosion-corrosion processses of pipelines because of similarity in geometry and flow pattern. When the erosion-corrosion takes place in multiphase flow (slurry), whether the corrosion rate measured from the RCE system can be transferred to the flow through pipes is still need to be studied.

2.4.2. Rotating Cylinder Electrode (RCE) System

Comparing with the pipe loop systems, RCE system is less expensive and easily constructed. The particle impingement angles in the RCE system is close to those in

straight pipelines. For this reason, the RCE is often used in laboratory to investigate the erosion-corrosion behavior of materials selected for pipeline applications (Nesic et al., 2002). However, the hydrodynamic parameters of fluid are difficult to be measured in the RCE system.

2.4.3. Impingment Jet System

Its main advantage is that the velocity and angel of fluid imingement are both well defined so that it is widely used to study the effect of impact angle of fluid on erosion-corrosion process (Schmitt et al., 2002). The main disadvantage of the impingement jet is due to the non-uniform hydrodynamical and electrochemiccal conditions on the specimens surface suffering erosion-corrosion damage and it results in a non-uniform distribution of local thickness loss in the wear scar. Obviously, the actual erosion-corrosion rate of materials depends on the local hydrodynamic and electrochemical conditions and it cannot be accurately assessed by the total weight loss method.

2.5. Erosion-Corrosion Map

In light of the concept of wear-map proposed by Stack et al.(1993) developed the concept of erosion-corrosion map to illustrate relationships among the erosion-corrosion performance and mechanisms, service parameters including flow velocity, temperature, impingement angle. The erosion-corrosion map will be very useful for materials

engineers to solve erosion-corrosion problems. Obviously, if the effects of metallurgical features are also reflected in the erosion-corrosion map, it will be expected to be a powerful tool in the material selection for the structures encountering erosion-corrosion in service.

Stack defined the erosion-enahnced corrosion as the "addictive" effect and the corrosion-enhanced erosion as the "synergistic' effect (Stack and Pungwiwat, 2004). The "additive" effect is the enhancement of corrosion due to erosion and is essentially the situation where corrosion is enhanced by the erosion process, by the particle/ liquid stream removing film from the surfaces. Stack et al. (1999) showed such a map in the Figure 2-3. the map indicates the materials to be selected for avoidance of "synergistic" or additive" effects as defined above.

The initial attempt was to develop the map for mild steel in a bicarbonate/bicarbonate solution and to assign regimes of interaction for the different corrosion processes, as indicated in "active dissolution" and "passivation". In the Figure 2-4, a mathematical model was subsequently developed for mapping the transitions between the regimes based on combining particle erosion models with those for aqueous corrosion (Stack et al., 1998).

An important issue in the field of tribo-corrosion is the large number of variables to be considered and the difficulty in combining these variables into dimensionless groups. Stack et al. (1999) made an attempt to combine variables in such a manner

enables the different erosion-corrosion regimes on one diagram, so that the erosion-corrosion map can reflect effects of various parameters on the wastage of slurry-erosion. A technologically important development in tribo-corrosion is the concept of the wear map for aqueous sliding conditions. Very recent work by Jiang et al. (2002) is the first effort at generating such a diagram in the Figure 2-5, using a mathematical model. There are other conditions to be considered in such an approach i.e. distinctions to be made for the two very different processes of dissolution and passivation interacting with the wear process. The work, however, is the first theoretical attempt to map sliding wear in aqueous conditions and thus is an important first step in addressing this complex process. As stated by Stack, more work must be carried in this area, particularly in the aqueous erosion-corrosion field, before such maps become "user-friendly" tools for engineers dealing with such material problems.

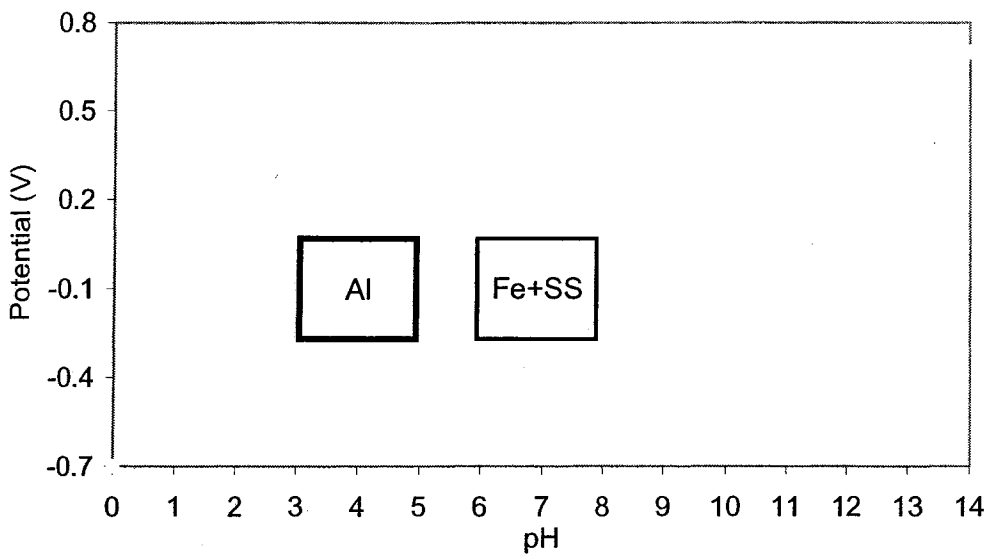

(a) "Synergistic" effects

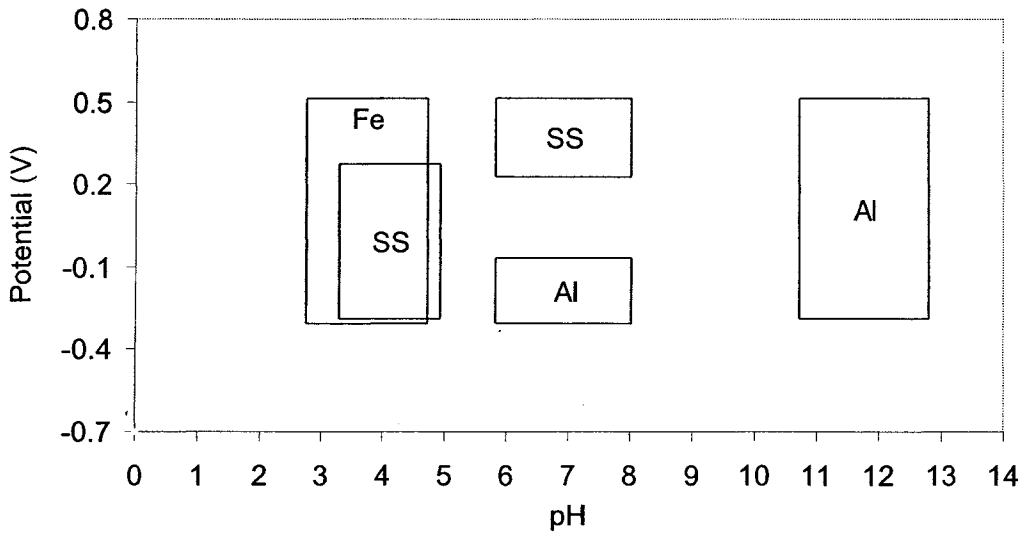

(b) "additive" effects.

Figure 2-3. Materials performance maps, for pure metals, based on erosion-corrosion resistance obtained in an impinging jet apparatus [Stack et al., 1999].

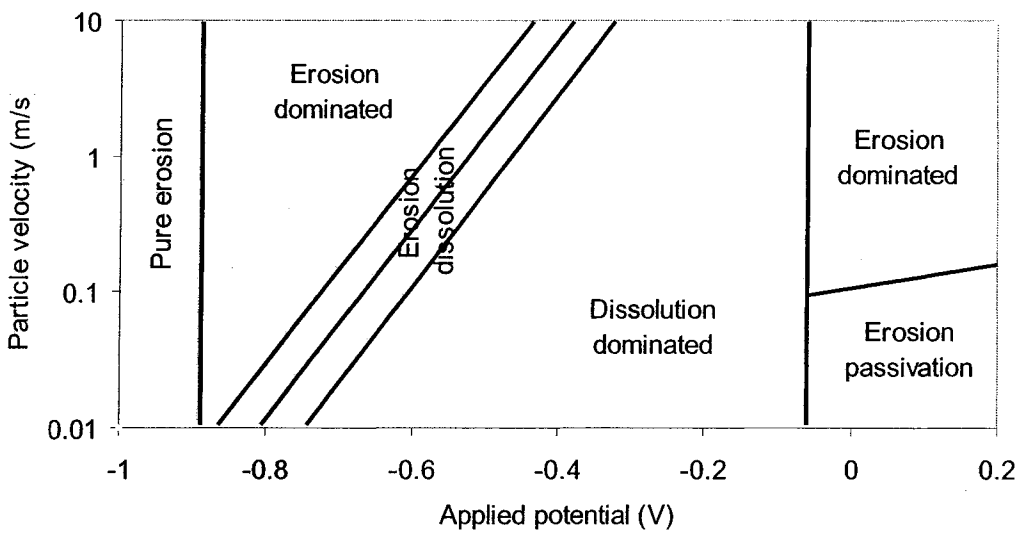

Figure2-4. Erosion–corrosion map for steel in the solution at pH5 [Stack et al., 1998].

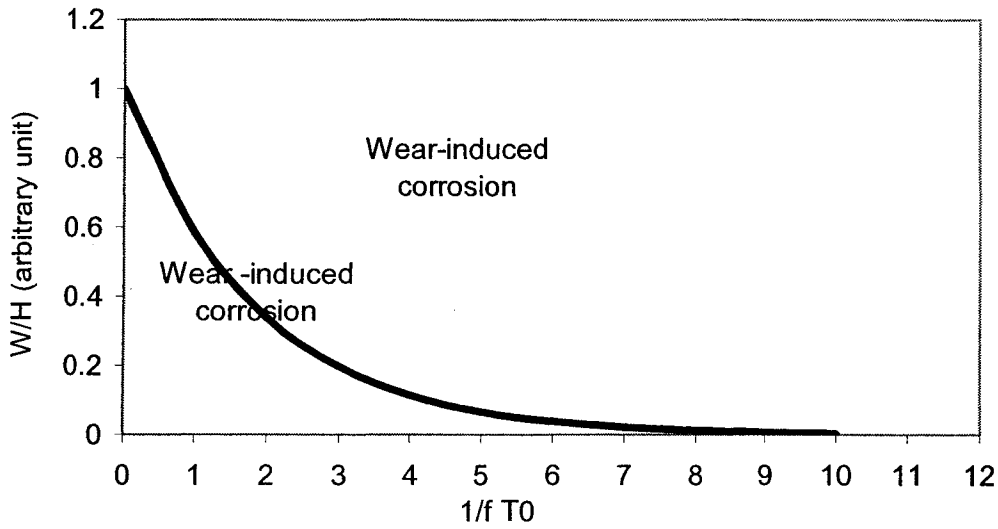

Figure 2-5. Wear–corrosion map for sliding of iron in the solution [Jiang et al. 2002].

2.6. A Theoretical Model for Interaction of Mechanical and Chemical Factors

The synergistic effect in slurry-erosion is attributed to the interaction of mechanical and chemical factors involved. During the slurry-erosion in practical engineering, the mechanical damage is mainly caused by the impingement of sand particles and the corrosion process results from certain electrochemical reactions. Based on non-equilibrium thermodynamics and dislocation theory, Lu and Luo (2004) proposed a theoretical model for the interaction of plastic deformation and electrochemical reaction. According to this model, when the anodic current appears on surface, the hardness of metallic samples will decrease due to the so-called chemo-mechanical effect. The relative degradation of hardness caused by the anodic dissolution can be formulated as follows:

$$\frac{\Delta Hv}{Hv} = -B\ln\left(\frac{J_a}{J_{th}}\right) = z\ln\left(\frac{i_a}{i_{th}}\right) \tag{2-10}$$

where J_a is the flux of dissolution and i_a is the anodic current density, J_{th} and i_{th} are the threshold flux and anodic current density to induce the chemo-mechanical effect. B is the experimental constant. In line with eq.(2-10), the hardness degradation of surface layer due to the chemo-mechanical effect is approximately a linear function of the logarithm of anodic current density present on the surface.

In line with same model, the anodic dissolution rate on the plastically deformed surface will increase simultaneously and the plastic deformation-induced anodic current density:

$$\Delta i_{corr} = k_q \dot{\gamma}_p \tag{2-11}$$

where $\dot{\gamma}_p$ is the plastic deformation rate of surface layer, κ_q is an experimental constant. With the aid of the theoretical model, the wastage of corrosion-enhanced erosion w_e^c can be expressed as follows:

$$\frac{w_e^c}{w_e^0} = z\log\left(\frac{i_a}{i_{th}}\right) \tag{2-12}$$

where w_e^0 is the wastage caused by the pure mechanical erosion and z is an experimental constant. The wastage of erosion-enhanced corrosion w_c^e is given by

$$w_c^e = k_p \gamma \dot{\varepsilon}_p \tag{2-13}$$

where k_p is an experimental constant. If the anodic current density present on surface and the plastic deformation rate in the surface layer have been determined, the wastage caused by the interaction of anodic dissolution and the surface plastic deformation can be predicted using eqs.(2-12) and (2-13).

2.7. Objective of This Study

The objective of the present investigation is to study the erosion-corrosion behavior of carbon steels in slurries of near-neutral pH. The emphasis will be put on the synergism in the slurry-erosion due to the interaction of anodic dissolution on surface and the impingement of solid particles. An attempt will be made to map the dependence of various wastage components in slurry-erosion on the hydrodynamic parameters, namely, the flow velocity and sand concentration and to establish a method to predict the wastage caused by the synergism on the basis of theoretical model developed by Lu and Luo (2004).

References:

Adlerm, T. A. and Walters, R. P. 1993. Wear and Scratch Hardness of Stainless Steel 304 Investigated with a Single Scratch Test. Wear, **162-164 (2):** 713-720.

Bester, J.A. and Ball, A. 1993. Performance of Aluminum Alloys and Particulate Reinforced Aluminum Metal Matrix Composites in Erosive-Corrosive Slurry Environments. Wear, **162-164 (1):** 57-63.

Bitter, J. G. A. 1963. A Study on the Erosion Phenomena. Wear, **6:** 5-17.

Bjordal, M., Bardal, E., Rogne, T. and Eggen T. G. 1995. Erosion and Corrosion Properties of WC Coatings and Duplex Stainless Steel in Sand-Containing Synthetic Sea Water. Wear, **186-187 (2):** 508-514.

Chen, T. Y., Moccari, A. and Macdonna, D. D. 1992. The Development of Controlled Hydrodynamic Techniques for Corrosion Testing. MTI Publication, No. T-3. Materials technology Institute of the Chemical Process Industries, Inc.

Christodoulou, P., Drooled, A and Godowsky, W. 1997. Effect of Carbon, Chromium and Silicon Content on Wear Resistance of Ferrite Fe-Cr-C Cast Alloys. Wear, **211(1):** 129-133.

Endo, S. and Nagae, M. 1996. Comparison of Experimentally Measured and Theoretically Predicted Erosion Rates of Steels in Slurries of Low Velocity, ISIJ International, **36(1):** 87-94.

Finnie, I and McFadden, D. H. 1978. On the Velocity Dependence of the Erosion of Ductile Metals by Solid Particles at Low Angles of Incidence. Wear **48:** 181-190

Follansbee, P. S., Sinclair, G. B. and Williams, J. C. 1981. Modeling of Low Velocity Particulate Erosion in Ductile Materials. Wear, **74:** 107-112.

Gooch, T. G. 1996. Corrosion Behavior of Welded Stainless Steel. Welding Journal, **75 (5):** 135-154.

Gutman, M. G. 1981. Mechanochemistry of Metals and Corrosion Protection, Metallurgiya [in Russian], Moscow, 2nd Ed.

Gutman, G. M. 1998. Mechanochemistry of Materials. Cambridge International Science Publishing, Great Abington, Cambridge, UK, 1998.

Haugen, K., Kvernvold, O., Ronold, A. and Sandberg, R. 1995. Sand Erosion of Wear-Resistant Materials: Erosion in Choke Valves. Wear 186-187 (1): 179-188.

Heitz, E. 1991. Chemo-Mechanical Effects of Flow on Corrosion. Corrosion, **47(2):** 135-145.

Hutchings, I. M. 1981. Model for the Erosion of Materials by Spherical Particles at Normal Incidence. Wear, **70:** 269-281.

Hutchings, I. M. 1986. The Erosion of Materials by Liquid Flow. MTI Publication No. 25. Materials Technology Institute of the Chemical Process Industries, Inc.,

Jiang, J., Neville, A., Stack, M. M. 2002. Modeling the Trio-corrosion Interaction in Aqueous Sliding Conditions. Tribology International, **35 (10):** 669-679

Larsen, B. J. and Liang, H. 1999. Probable Role of Abrasion in Chemo-Mechanical Polishing of Tungsten. Wear, **233-235:** 647-654

Lu, B. T. and Luo, J. L. 2004. Chemo-Mechanical Effect in Erosion-Corrosion Process of Carbon Steel. CORROSION 2004. New Orleans, March 28-April 1, 2004.

Matsumura, M., Oka, Y. H. and Yano, M. 1991. Role of Passivating Film in Preventing Slurry Erosion-Corrosion of Austenitic Stainless Steel. ISIJ. Int., **31(2):** 168-176.

Meng, H. C. and Ludema, K. C. 1995. Wear Models and Predictive Equations: Their Form and Content. Wear, **181-183 (2):** 443-457.

Metwally, W. A. and Samy, M. K. 1994. Evaluation of Abrasive-Wear and Erosion-Corrosion Resistance of High-Cr Cast-Steel. Steel Research, **65(10):** 455-458.

Nesic, S., Bienkowsky, J., Purchase, A. and Bremhorst, K. 2002. A Compact Apparatus for Testing Erosion-Corrosion under Disturbed Flow Conditions Consisting of a Rotating Cylinder with a Step. CORROSION 2002, Paper No. 504. NACE, Houston, TX.

Neville, A and Hu, X. 2001. Mechanical and Electrochemical Interactions during Liquid-Solid Impingement on High-Alloy Stainless Steels. Wear, **250-251:**1284-1294

Neville, A., Hodgkiess, T. and Dallas, J. T. 1995. A Study of the Erosion-Corrosion Behavior of Engineering Steels for Marine pumping Applications. Wear, **186-187:** 497-507.

Neville, A., Reys, M., Hodgkiess, T. and Gledhill, A. 2000. Mechanisms of Wear on a Co-base Alloy in Liquid-Solid Slurry. Wear, **238:** 138-150.

Neville, A. and Hodgkiess, T. 1997. Study of Effect of Liquid Corrosivity in Liquid-Solid Impingement on Cast Iron and Austenitic Stainless Steel. British Corrosion Journal. **32 (3):**197-205

Poalson, B. 1983. Electrochemical Measurement in Flowing Solution. Corrosion Science, **23 (4):** 391-430

Postlethwaite, J., Dobbin, M. H. and Bergevin, K. 1986. The Mechanism of Erosion-Corrosion in Slurry Pipelines. Materials Science Forum, **8:** 13-22.

Postlethwaite, J., Nesic, S. and Adamopoulos, G. 1992. Modeling Local Mass-Transfer Controlled Corrosion at Geometrical Irregularities. Materials Science Forum, **111-112:** 53-62.

Poulson, B. 1999. Complexities in Predicting Erosion Corrosion._Wear, **233-235:** 497-504.

Rekerby, D. G. 1983. Correlation of Erosion to Mechanical Properties in Metals. Wear, **84:** 393-397.

Reyes, M and Neville, A. 2001. Mechanisms of Erosion-Corrosion on a Cobalt-base Alloy and Stainless Steel UNS S17400 in Aggressive Slurries. J. Materials Engineering and Performance, **10(6):** 723-730.

Rincon, H., Chen, J. and Shadley, J. R. 2002. Erosion Corrosion Phenomena of 13Cr Alloy. CORROSION 2002, Paper No. 493. NACE, Houston, TX.

Sasaki, K. and Burstein, G. T. 1998. Generation of Surface Roughness during Slurry Erosion-Corrosion and Its Effect on the Pitting Potential. Corrosion Science, **38:** 2111-2120.

Schmitt, G., Bosch, P., Bruckhoff, U. and Siegmund, G. 1998. CORROSION 1998, Paper No. 46. NACE, Houston, TX.

Schmitt, G., Bosch, P., Plagemann, P. and Moeller, K. 2002. Local Wall Shear Stress Gradients in the Slug Flow Regime- Effect of Hydrocarbon and Corrosion Inhibitor. CORROSION 2002, Paper No. 2244. NACE, Houston, TX.

Schmitt, G., Werner, C. and Schoning, M. J. 2002. Micro Electrochemical Efficiency Evaluation of Inhibitors for CO_2 Corrosion of Carbon Steel under Higher Shear Stress Gradients, CORROSION 2000, Paper, No. 2280. NACE Houston, TX.

Stack, M. M. And Pungwiwat, N. 2004. Erosion–Corrosion Mapping of Fe in Aqueous Slurries: Some Views on a New Rationale for Defining the Erosion–Corrosion Interaction. Wear, **256 (5):** 565-576

Stack, M. M., Corlett, N. and Turgoose, S. 1999. Some Recent Advances in the Development of Theoretical Approaches for the Construction of Erosion-Corrosion Maps in Aqueous Conditions. Wear, **233-235:** 535-541

Stack, M. M. and Pungwiwat, N. 1998. Note on the Construction of Materials Performance Maps for Resistance to Erosion in Aqueous Slurries. Wear, **215:** 67-76

Stack, M. M., Corlett, N. and Zhou, S. 1999. Impact Angle Effects on the Transition Boundaries of the Aqueous Erosion-Corrosion Map. Wear, **225(1):** 190-198.

Stack, M. M., Corlett, N. and Zhou, S. 1998. Some Thoughts on the Effect of Elastic Rebounds on the Boundaries of the Aqueous Erosion-Corrosion Map. Wear, **214(2):** 175-185

Stack, M. M. and Stott, F. H. 1993. Approach to Modeling Erosion-Corrosion of Alloys Using Erosion-Corrosion Maps. Corrosion-Science, **35(5-8):** 1027-1034:

Sundararajan, G. and Shewmon, P. G. 1983. A New Model for the Erosion at Normal Incidence. Wear, **84:** 237-244.

Sundararajan, G. 1991. Comprehensive Model for the Solid Particle Erosion of Ductile Materials. Wear, **149:** 111-127.

Toro, A., Sinatora, A., Tanaka, D. K. and Tschiptschin, A. P. 2001. Corrosion-Erosion of Nitrogen Bearing Martensitic Stainless Steels in Seawater-Quartz Slurry. Wear, **251:** 1257-1264.

Wang, H. W. and Stack, M. M. 2000. The Erosion Wear of Mild and Stainless Steels under Controlled Corrosion in Alkaline Slurries Containing Alumina Particles. J. Materials Science, **38:** 5263-5273.

Wentzel, E.J. and Allen, C. 1997. Erosion-Corrosion Resistance of Tungsten Carbide Hard Metals. International Journal of Refractory Metals and Hard Materials, **15 (1-3):** 81-87.

Zhou, S., Stack, M. M. and Newman, R. C. 1996. Electrochemical Studies of Anodic Dissolution of Mild Steel in a Carbonate-Bicarbonate Buffer under Erosion – Corrosion Conditions. Corrosion Science, **38(7):** 1071-1084.

CHAPTER 3. EXPERIMENTAL PROCEDURE AND DATA ANALYSIS METHOD

3.1. Experimental materials and conditions

3.1.1. Test Materials

AISI 1045 and 1018 carbon steel rods with a diameter of 30 mm were used as the test materials. Their chemical compositions are listed in Table 3-1.

Table 3-1. Chemical compositions of test material (wt %)

Material	C	Mn	S	P	Fe
A1045CS	0.46	0.75	<0.05	<0.04	Balance
A1018CS	0.18	0.75	<0.05	<0.04	Balance

The microstructure of these test materials is typical pearlier + ferrite structure. The rotating cylinder samples with the diameter of 24.5 mm and height of 8 mm were used in the present tests.

3.1.2. Experimental Slurry

The slurries used in the present experiments, referred to as slurry 1, 2, and 3, comprised of silica sand and these different solutions.

The slurry 1 consisted of the tailings water and silica sand. The concentrations of sand ranged from 6 % wt. and 60 % wt.; the tailing solution was supplied by Syncrude, Canada, and its composition is listed in the Table 3-2. The pH of tailings solution is 8.5 . The slurry $1^{\#}$ was used for the carbon steel A1018CS in the experiments under the conditions of the galvanostatic corrosion and open circuit potential (OCP).

The slurry 2 contained the tap water and silica sand whose concentrations ranged from 10 % wt. to 50%wt. The tap solution was supplied from the distribution lines by EPCOR, Canada .The quality parameters of EPCOR's treated water are listed in the Table 3-3.. The slurry $2^{\#}$ was employed for the carbon steel A1045CS in the experiments under the OCP conditions..

Slurry 3 is a group of slurries with different pH values. Three types of the slurries are listed on the Table 3-4. The basic solution ($3^{\#}$-7.0) contained 0.1 M sodium sulfate (Na_2 SO_4) with de-ionized (D. I.) water. Its pH value was 7.0. The basic solution was adjusted to an acidic solution (pH5.5) and alkaline solution (pH8.5) with sulphuric acid (0.1M H_2SO_4) and sodium hydroxide (0.1M NaOH), respectively. The slurries 3 were used to investigate the effect of pH on the erosion corrosion behavior of carbon steel A1018CS..

The composition of the silica sand, supplied by U. S. Silica Company, are shown in Table 3-5.

Table 3-2. Chemical composition of the tailings solution

Cation	Na^+	K^+	Ca^{2+}	Mg^{2+}
mg/L	727	11.3	6.8	4.0
Anion	Cl^-	SO_4^{2-}	HCO_3^-	CO_3^{2-}
mg/L	380	211	950	<5

Table 3-3. Quality parameters of tap water (Source: EPCOR, Edmonton)

Ions	Fe^{2+}	Mg^{2+}	Na^+	K^+	Cl^-	$SO4^{2-}$
mg/L	<0.003	<0.0005	9	0.9	2.52	56.1
Parameters	Total dissolved solids (mg/L)	Alkalinity ($CaCO_3$) (mg/L)	pH	Hardness ($CaCO_3$) (mg/L)	Conductivity (µS/cm)	Caustic Soda Dose (NaOH) (mg/L)
Value	193	110	7.8	165	350	<20

Table 3-4. Detail lists of slurry 3

Type	pH	Sand Concentration (% wt.)	$Na_2 SO_4$ Concentration (M)	Other Chemical (M)
$3^{\#}$-5.5	5.5	10-50	0.1	H_2SO_4 <0.001
$3^{\#}$-7.0	7.0	10-50	0.1	
$3^{\#}$-8.5	8.5	10-50	0.1	HaOH <0.001

Table 3-5. Properties of the silica sand

Size (mesh)	Diameter (μm)	Color	Grain shape	Hardness (Mohs)	Density (g/cm^3)	Purity (SiO_2)
50-70	300 -212 ,	White	Round	7	2.65	99.70%

3.2. Experimental Apparatus

3.2.1. Rotating Cylinder System for Erosion-Corrosion Tests and Electrochemical Measurements

A rotating cylinder system (RCE), see Figure 3-1, was used for the electrochemical measurements in erosion- corrosion experiments. The cell was the same as that used in erosion-corrosion setup with the capacity 200 mL. The platinum counter electrode coil was placed near the bottom of the corrosion cell. The saturated calomel electrode (SCE) was placed outside the corrosion cell to avoid affecting the flow conditions. SCE was connected to the cell with a Luggin capillary. The rotating cylinder electrode (carbon steel A1045CS or A1018CS) was mounted in the middle section of the E3M shaft, driven by a Pine ARMSRX analytical rotator.

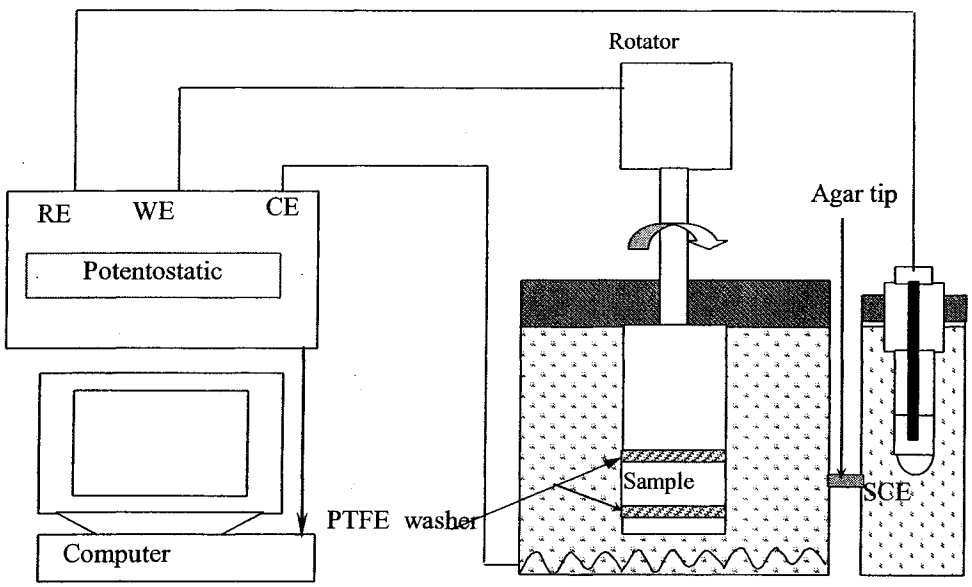

Figure 3-1. Schematic illustrations of the electrochemical measurement apparatus

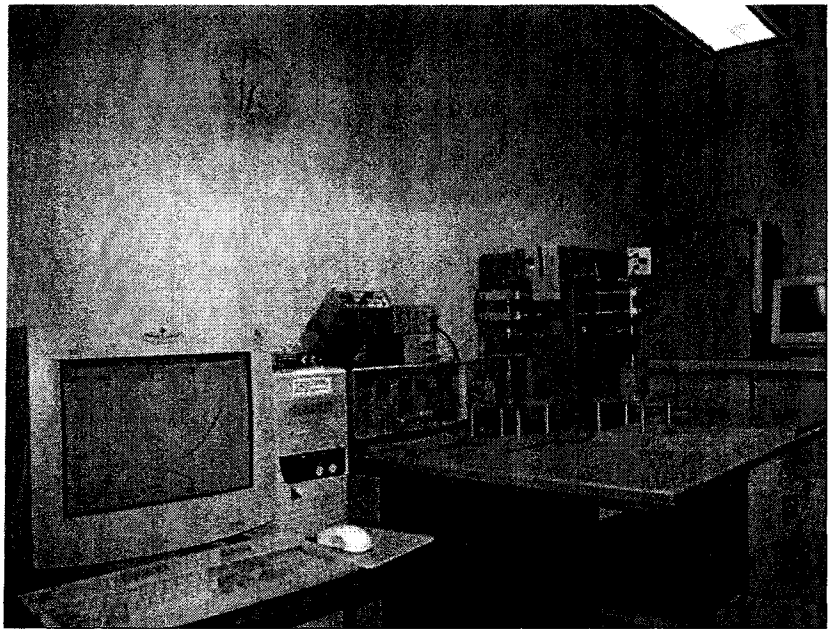

Figure 3-2. Photo-illustration of the Erosion-Corrosion Test Set-Up

The rotation rate of the electrode was precisely controlled using a custom-made four digit pushbutton controller. The rotation rate was adjusted to within 1% of the control setting over a range from 50 to 10000 RPM. When the rotator rotated, water and sand were lifted up from the bottom and flowed through the gap between the sample and the cylinder. Electrical contact was made via four springs with silver carbon contact brushes connected to the rotating shaft.

A custom-made apparatus for erosion-corrosion experiments was developed in the present investigation. As shown in Figure 3-2, this experimental apparatus consisted of two systems. First, an RCE system was used for measuring the weight loss in the slurry-erosion. It consisted of the cell with two electrodes, rotating stirrer, power supply and

multiple digital meters. A second system was an electrochemical system for testing the corrosion behaviours of the specimen. It was made of the cell with three electrodes, the Gamry instrument and Pine potentostatic instrument. The system is similar to the RCE system shown in Figure 3-1.

3.2.2. Calibration of Erosion-Corrosion Test Rig

The rotating velocities of electrochemical system in the erosion-corrosion setup were in ranges of 3000 rpm to 12000 rpm, corresponding to apparent flow velocities of 4 m/s to 16 m/s. The apparent flow rate $V = \omega r$, where ω is the rotating-angle speed and r is the radium of the specimens. Before testing, the rotating speed of the stirrer was calibrated by an optical tachometer.

In order to check the precision of the erosion-corrosion setup, the calibration of equipment was performed. In the beginning, the speeds of stirrers were corrected with an optical speed meter for three times to check the reproducibility of the experimental apparatus. The calibration was preformed using a slurry with sand concentration 50% wt. The weight loss calibration tests were conducted in rotating velocity range of 1000 to 12000 rpm. The results of weight loss in Figure 3-3, measured from four independent stirrers, were almost the same. It was indicted that the experimental reproducibility of weight loss on the specimen obtained from different system was good. The polarization curves in Figure 3-4 were measured with the RCE systems and the electrochemical system in the erosion-corrosion setup. The tests were checked in the flowing slurry

containing 50 %wt. sand and flow rate 9 m/s with potential scanning rate of 0.166mV/s. As indicated by the results of calibration the polarization curves measured from the RCE system and the custom-made electrochemical system were almost the same. It means the test results obtained from two systems were comparable.

3.2.3. Sand Degradation Consideration

It has been well known that the wastage of erosion depends heavily on the mass, and the shape of erodent (Hutchings, I. M. 1986). Owing to impingement, the sand particles will be broken and lose their sharp edge, resulting in a loss in ability of eroding. It is regarded as the sand degradation. A calibration of sand degradation on the wastage of A1018CS at the conditions of OCP is shown in Figure 3-5. The results show clearly, the rate of wastage is reduced with test duration. The rate of material loss has a power function of time. The rate R (t) can be express as the follow formula:

$$R(t) = m_3 t^{m_4} \qquad (3\text{-}1)$$

The values of constant m_3 and m_4 can be fixed by means of the regression analysis and listed on the Table 3-6. To reduce the effect of sand degradation on the erosion corrosion test results, the slurries in the erosion-corrosion tests were refreshed every two hours.

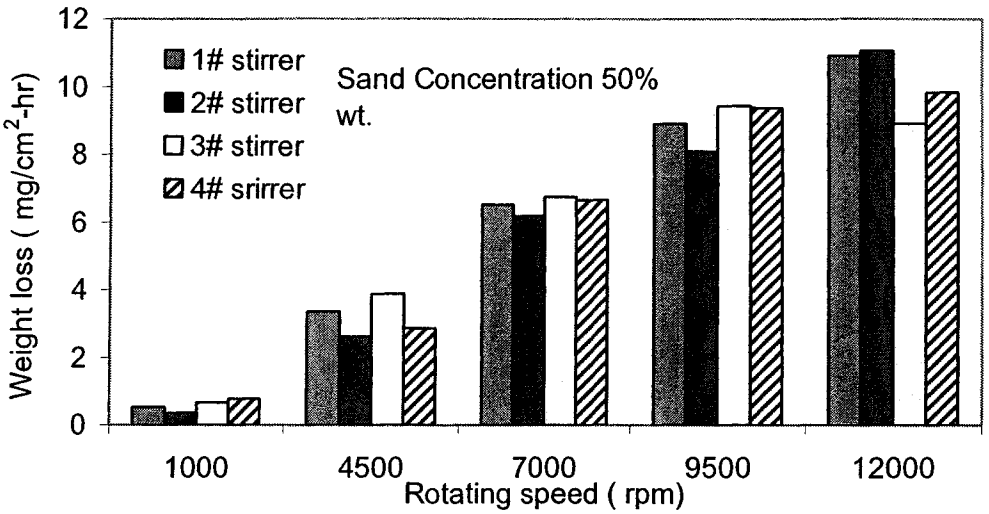

Figure 3-3. Calibration of the four individual rotating systems in the slurry

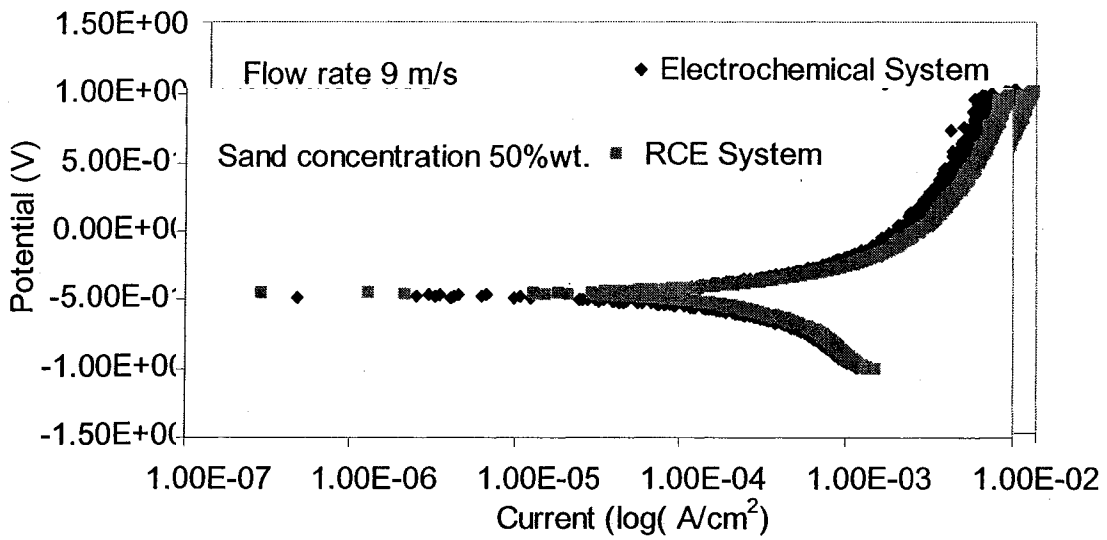

Figure 3-4. Comparison of the potentodynamic curves measured from the electrochemical system in erosion-corrosion setup and RCS system in PINE instrument.

Table 3-6. Rate of weight loss for expressing sand degradation

Flow rate	Sand Concentration	States	Coefficient	
U (m/s)	C_{sand} (%)		m_3	m_4
8	40	OCP	0.003	-0.98
8	40	CP	0.0033	-1.03
8	10	OCP	0.0004	-0.59

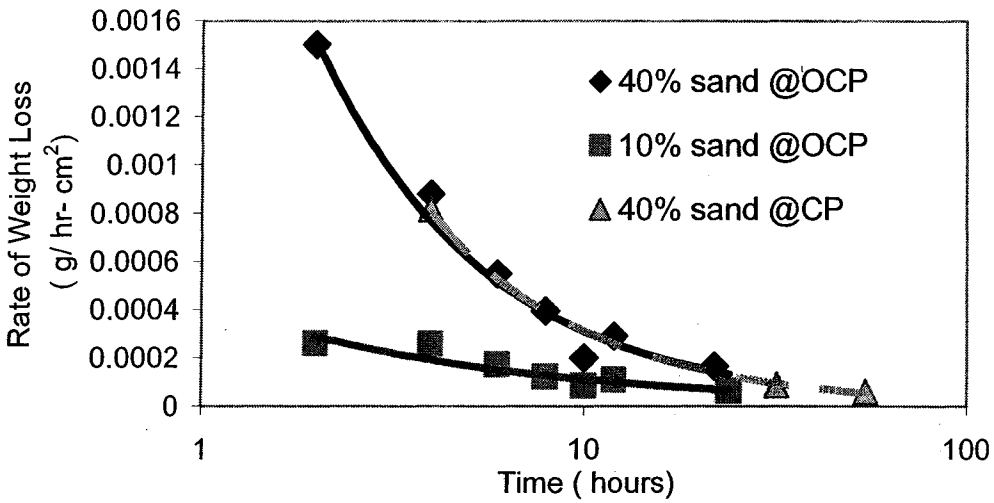

Figure 3-5. Rate of sand degradation under the OCP and CP conditions

3.3. Erosion-Corrosion Tests

In line with Figure 2-1, the relationships among the total weight loss and its components w, w_e^0, w_c and w_c^0 are directly measured from the experiments. The total weight loss w is determined by two kinds of methods. The first one is under the condition of galvanostatic current corrosion to measure the weight loss w in the fixed corrosion conditions. It is designed for determining the effect of corrosion on the erosion. Under the galvanostatic conditions the corrosion rates of samples are controlled by the applied current densities. So the corrosion rate of the samples in the slurry is kept at a constant value. The second one is in the condition of open circuit potential to measure the weight loss w in the natural conditions. Because no outside current is applied on the specimen, the corrosion on the carbon steel is a regular process.

In this investigation, the experiments are also designed under the cathodic protection to avoid the corrosion on the surface of specimen during the slurry-erosion tests. The wastage caused by the mechanical erosion w_e^0 is measured under the cathodic protection condition, namely, under cathodic potential of $-1V_{SCE}$, to prevent from corrosion occurring.

The wastages of electrochemical corrosion under the OCP in both flowing slurries and flowing electrolytes free of solid particle are considered as the weight loss of corrosion w_c and weight loss of pure corrosion w_c^0 respectively. They are calculated from the self-corrosion current densities with the Faraday's law. The self-corrosion

current densities are determined from the polarization curves measured under the corresponding test conditions.

Other components shown in Figure 2-1, the weight loss of erosion enhanced corrosion w_c^e, the weight loss of corrosion enhanced erosion w_e^c the weight loss of total erosion w_e and the weight loss of total synergy w_s, can be calculated from the above experimental results. Thus, the wastage component of erosion-enhanced corrosion is obtained from the difference in corrosion wastages ($w_c - w_c^0$). The w_c is the corrosion wastage in flowing slurry and w_c^0 is that in flowing solution without sand. The wastage component of corrosion-enhanced erosion is determined by $w - w_c - w_e^0$. The w is total material loss due to erosion-corrosion, w_e^0 is the pure erosion loss. The wastage component of erosion is determined by $w - w_c$ and the wastage component of total synergy is calculated from $w_c^e + w_e^c$.

3.3.1. Test Procedures of the Erosion-Corrosion System

The experimental processes in the erosion- corrosion systems are listed as follows:

(1). Surfaces of the specimen are grounded, cleaned with a de-ionized (D.I.) water and then with acetone, and finally, dried with the hot air.

(2). Weights of the specimen are measured with a precision analytical scale that has a accuracy of 0.1 mg. the measurements have to be operated two times and the data of initial weights are recorded.

(3). In order to avoid the corrosion and erosion on the top and bottom surface of the specimen, the top and bottom of specimen are covered by a portion of silica rubber and a piece of Teflon with the same diameter of the specimen, respectively.

(4). 200g of slurry is filled into the cell for each experiment. For example, the slurry with 20% wt. sand concentration contains 40g silica sand and 160 ml tailing water or tap water.

(5). The specimen is fixed on the shaft of the rotating stirrer and, then, was placed into the cell, enclosed the cover of the cell. It is noted that the specimen on the shaft must be set in the centre of cell.

(6). There are three kinds of operations in the erosion and corrosion system.

(6.1). In the test condition of Galvanostatic corrosion, the positive pole (+) of the power supply is connected with the working electrode (WE), that is, the specimen. The negative pole (-) of the power supply is linked with the counter electrode (CE), the platinum counter electrode coil. The applied current was measured with a multiple digital

meter. The ranges of applied anodic current densities are from 1x 10^{-4}A/cm^2 to 2.5x10^{-3}/cm^2.

(6.2). In the Cathodic protection condition, the connections between the electrodes of the cell and electric poles of power supply are opposite these in the galvanostatic corrosion conditions. That is, the (+) pole of the power supply is linked with the CE of the cell and the (-) pole of power supply is linked with the WE of the cell. The negative current density for A1018CS in the tailing water is 0.0015 A/cm^2 and for A1045CS in the tap water is 0.00015 A/cm^2. The specimen applied with this amount of currents can be totally protected from the corrosion in the flowing slurry.

(6.3). In the OCP condition the electrodes of the cell are not connected with any pole of the power supply so that the specimen don't flow any current in outside circuit during the erosion-corrosion experiments.

(7). Turn on the rotating controller and adjust the rotating speed of shaft to the value required by the test. Apply current to the specimen using a power supply and use the multiple digital meter as a current monitor. During the experiments the applied current was frequently checked.

(8). Generally, to achieve a weight loss over 0.01 g, test duration need is about 15-30 minutes for A1018CS, but 2-6 hours for A1045CS under the OCP condition. Because the hardness of A1018CS is smaller than that of A1045CS, the rate of weight

loss rate of A1018CS is much higher than that of A1045CS. According to the results of the sand degradation experiments, the rate of material loss can be kept at the linear relationship within the four hours at the beginning. In order to simulate the actual situation in a pipeline, the sand in the cell is changed in every two hour interval during the experiments to reduce the effect of sand degradation.

(9). Turn off the key on the rotating controller, the key of the power supply and the key of the digital meter at the end of experiments, respectively. Pull out the cell and take out the samples.

(10). According to the ASTM Standard G1-90 the corrosion product on the specimen surface was cleaned after running the erosion-corrosion tests. Then, the specimens are rinsed by de-ionized water and acetone successively and dried by the hot air before measuring the final mass.

(11). Determine the final weights of the specimen with the analytical balance and record the final weight. The measurements are performed in duplicate.

(12). Renew the slurry to prepare the next test.

(13). Calculate the weight loss rate using the following formula:

$$Rate\ of\ weight\ loss = \frac{Final\ weight\ - Initial\ weight}{Time\ Interval}$$

(14). Experimental data are analyzed by the Echem Analyst program provided from Garmy Company. According to Faraday's law the weight loss from the corrosion components can be calculated from the following formula.

$$Rate\ of\ weight\ loss = \frac{56}{2 \times 96500} Current\ density$$

3.3.2. lculation of Erosion and Corrosion Components

The various wastage components of are calculated using the following formula:

(1). Rate of total weight loss $w = \frac{w_{initial} - w_{end}}{\Delta T}\ (g/cm^2.hour)$ (3-2)

(2). Rate of pure erosion loss $w_e^0 = \frac{w_{e,initial}^0 - w_{e,end}^0}{\Delta T}\ (g/cm^2.hour)$ (3-3)

(3). Rate of corrosion loss $w_c = \frac{56 \times 3600}{2 \times 96500} I_{corr} (g/cm^2.hour)$ (3-4)

(4). Rate of pure corrosion loss $w_c^0 = \frac{56 \times 3600}{2 \times 96500} I_{corr}^0 (g/cm^2.hour)$ (3-5)

(5). Rate of corrosion enhanced erosion loss $w_c^e = w - w_c - w_e^0$ $(g/cm^2.hour)$ (3-6)

(6). Rate of erosion enhanced corrosion $w_e^c = w_c - w_c^0$ $(g/cm^2.hour)$ (3-7)

(7). Rate of erosion loss $w_e = w - w_c$ $(g/cm^2.hour)$ (3-8)

(8). Rate of total synergistic loss $w_s = w_e^c + w_c^e$ $(g/cm^2.hour)$ (3-9)

(9). Normalized synergy of corrosion enhanced erosion w_e^c / w_e^0

(10). Normalized synergy of erosion enhanced corrosion w_c^e / w_c^0

(11). Percentage of erosion enhanced corrosion w_e^c / w

(12). Percentage of corrosion enhanced erosion w_c^e / w

(13). Percentage of pure erosion w_e^0 / w

(14). Percentage of pure corrosion w_c^0 / w

(15). Percentage of total synergy w_s / w

The raw data of A1018CS in the tailing water slurry and their calculations are listed in the Appendix A. The experimental data of A1018CS in the slurry with different pH and their computation are listed in the Appendix B. And the Raw data of A1045CS in the tap water slurry and their calculations are tabled on the Appendix C.

3. 4. Test Matrix Design and Data Analysis Method

3.4.1. Multiple Regression

Multiple linear regressions are used for modeling material loss. In particular, they can be developed as a wide range of models of handling non-linearity in the predictor variables. The linear, polynomial, and interaction terms, as well as, more general nonlinear transformations of the predictor variables were examined for the erosion-corrosion data. The best fit is the nonlinear transformation of the regression. (Hosmer and Lemeshow, 2000)

A linear predictor regression model consists of $p-1$ predictor variables, $X_1 \ldots X_{p-1}$, in a linear relationship with the response variable Y and their constants α_1, $\alpha 2$,.. α_{p-1} . The typical expression is made by predictor variables and residual ε_y :

$$Y = \alpha_0 + \alpha_1 X_1 + \alpha_2 X_2 + \ldots + \alpha_{p-1} X_{p-1} + \varepsilon_y \qquad (3\text{-}10)$$

In the polynomial linear regression, the model contains higher-order terms of the predictor variables creating a curvilinear response function. Below is a model with only one predictor variable

$$Y = \alpha_0 + \alpha_1 X + \alpha_2 X^2 + \ldots + \alpha_{p-1} X^m + \varepsilon_y \qquad (3\text{-}11)$$

In interaction linear regression the interaction of each term can well make regression models. This case is used when the response from the level of one predictor depends on the level of another. The resulting model may be expressed as:

$$Y = \alpha_0 + \alpha_1 X_1 + \alpha_2 X_2 + \alpha_3 X_1 X_2 + \alpha_1 X_1^2 + \alpha_2 X_2^2 + \varepsilon_y \qquad (3\text{-}12)$$

In the transformed regression both the response variable as well as any of the predictor variables may be transformed into simple power or nature logarithm. It is particularly useful as a method of modeling predictor variables, which have a multiplicative relationship to the response variable. Attention should be paid to the fact that any transformation of a variable must make sense in the context of the domain. And also, transformations can add complexity to the model. As an example:

$$\log(Y) = \alpha_0 + \alpha_1 X_1 + \alpha_2 X_2 + \alpha_3 X_1 X_2 + \varepsilon_y \tag{3-13}$$

Three kinds of logistic regression models, adjacent-category, continuation-ratio, and the proportional-odds logistic models, can be derived to fit different models to the data. The method of fit is based on an alteration of the multinomial probability and its log transformation (Hosmer and Lemeshow, 2000). For the erosion-corrosion modeling problem ones are most interested in modeling an ordered response since material loss can be ordered. Logarithem or log-odds modeling can directly incorporate the ordering. The baseline log model for ordinal logistic regression is derived from above logistic regression model. The fully parameterized model for the parameter x is expressed as follow:

$$\pi(m) = X_0^{\alpha_0} X_1^{\alpha_1} \ldots X_m^{\alpha_m} \tag{3-14}$$

$$\log[Y(m)] = \alpha_0 \log X_0 + \alpha_1 \log X_1 ... + \alpha_q \log X_m + \varepsilon_y \quad (3\text{-}15)$$

$$Y(m) = \log\left[\frac{\pi_q(x)}{\pi_p(x)}\right] = \log\left[X_0^{\alpha_0} X_1^{\alpha_1} ... X_q^{\alpha_q}\right] - \log\left[X_0^{\alpha_0} X_1^{\alpha_1} ... X_p^{\alpha_p}\right] + \varepsilon_y \quad (3\text{-}16)$$

Where Y (m) is the response for baseline log function; constants p and q could be 1, 2... but $m=p+q$; π(m) is the conditional probability with m items of predictors variables X_i. In our corrosion-erosion study, modes often used to fix the data is the logistic and the proportional odds models since these better fit the requirements of our problem.

3.4.2. Test Matrix Design

Response surface methodology (RSM) is a collection of mathematical and statistical techniques widely used to determine the effects of several variables, which was already used to optimize different bioconversion processes (Toledo et al., 2001). Many applications deal with the study of the effects of two or more factors. In general, factorial designs are more efficient for this purpose than the classical method of studying one variable at a time. Besides, they are necessary to avoid misleading conclusions and allow

the effects of a factor being estimated at several levels of the other factor, yielding results that are valid over a wide range of experimental conditions (Montgomery, 2000).

In this study, a 3^5 full-factorial design combined with RSM has been used to determine the flow rate, sand concentration and corrosion current levels on the synergy of erosion enhanced corrosion and also to identify the optimum erosion-corrosion conditions. According to chemo-mechanical theoretical model and the logistic and proportional-odds regression model (Schabbach, et al., 2001) the factors, A, B and C, could be designed with a form of logarithmical transfer. Such as, Table 3-7, in which the three factor, flow velocity, sand concentration and corrosion current, are divided as five levels 0, -1, +1, -α and +α. In the basic experiments the values of level |α| is equal to 1.66. For the additional experiments the level |α| ranges from 0 to 2 according to the requirement of experiments.

Table 3-7. Selection of parameters and parameters' levels

Level	A Flow rate (m/s)	B Sand (wt. %)	C Current (mA/ cm^2)
-1.66	4.6	6.5	0.22
-1	5.9	10	0.4
0	8.5	20	1
1	12.3	40	2.5
1.66	15.7	62.5	4.6

Response Surface Methodology (RSM) is used to obtain the number of experiments, depending on the number of parameters and levels agreed upon. RSM is a set of techniques, which are used for finding the best value or values of response, depending on the parameters and levels involved in the design (Kalil, et al., 2000) Although, this design of experiment technique is generally utilized for optimization purposes, it is also utilized as a great tool to understand, the overall response system, for the processes or products investigated. The main experiments designed for the present study, is tabulated in Table 3-8. The experiments were run in random order to avoid a statistical bias in the analyses.

Following each run, the specimen was put into the cell and the experiments under the given conditions. Specimens were then weighed by utilizing the same balance to obtain the weight difference before and after the test. Based on the results, the regression and ANOVA analyses were conducted to understand the effect of each parameter on the weight loss. Furthermore, surface plots were made to illustrate the outcome of the response analysis.

Regression and ANOVA analyses were made to see whether data about the synergy of erosion enhanced corrosion were 'statistically significant' and 'which

parameter' can be used to define this effect best. Analyses were conducted using Essential Regression program in Excel for Microsoft Wear.

Table 3-8. Test Matrix

Setting	Factors			Speed	Sand	Current
No.	A	B	C	Scale	g	mA
1	-1	-1	-1	4	20	2.5
2	1	-1	-1	8	20	2.5
3	-1	1	-1	4	80	2.5
4	1	1	-1	8	80	2.5
5	-1	-1	1	4	20	15.5
6	1	-1	1	8	20	15.5
7	-1	1	1	4	80	15.5
8	1	1	1	8	80	15.5
9	0	0	0	5.6	40	6.3
10	-1.66	0	0	3	40	6.3
11	0	-1.66	0	5.6	13	6.3
12	0	0	-1.66	5.6	40	1.4
13	1.66	0	0	10	40	6.3
14	0	1.66	0	5.6	120	6.3
15	0	0	1.66	5.6	40	28.9

References:

Hosmer, D. W. and Lemeshow, S. 2000. Applied Logistic Regression, 2nd. Joho Wiley & Sons. Inc., New York.

Hutchings, I. M. 1986. The Erosion of Materials by Liquid Flow. MTI Publication No. 25. Materials Technology Institute of the Chemical Process Industries, Inc.,

Kalil, S. J., Maugeri, F. and Rodrigues, M. I. 2000. Response Surface Analysis and Simulation as a Tool for Bioprocess Design and Optimization. Process Biochem, **35:** 539–550.

Montgomery, A. D. 2000. Design and Analysis of Experiments, 4th. Joho Wiley & Sons. Inc., Arizona State.

Schabbach, L. M., Fredel, M. C. and Hotza, D. 2001. Three-Component Lead Borosilicate Frit. Am. Ceram. Soc. Bull. **80 (7):** 57–63

Toledo, E. C. V., Santana, P. L., Maciel, M. R. W. and Filho, R.M. 2001. Dynamic Modeling of a Three-Phase Catalytic Slurry Reactor. Chem. Eng. Sci. **56:** 6055–6061.

CHAPTER 4. CORROSION - ENHANCED EROSION BEHAVIOR IN GALVANOSTATIC CONDITONS

4.1. Corrosion-Enhanced Erosion in Glvanostatic Conditions

Since the uniform electrochemical corrosion rate during the galvanostatic tests was under the control of applied anodic current, the total weight loss was the sum of contributions of pure erosion, corrosion and corrosion-enhanced erosion, so that the synergistic component of in the slurry-erosion process, in line with Equations.(2-5) through (2-8), results only from the wastage of corrosion-enhanced erosion.

$$w_e^c = w_s = w - w_e^0 - w_c \tag{4-1}$$

where w and w_e^0 are the wastages under the action of constant anodic current density and the cathodic protection, respectively, and the w_c can be calculated from the applied anodic current density using the Faraday secondary law.

$$w_c = M_{F_e} \frac{i_a}{zF} \tag{2-3}$$

For low carbon steels, M_{F_e}=56g/mol. In this way, the wastage of corrosion-enhanced erosion could be experimentally determined.

In line with the theoretical model developed by Lu and Luo (2004), the corrosion-enhanced erosion results mainly from the degradation of resistance to mechanical erosion because of the effect of anodic dissolution-promoted plasticity, and the wastage of corrosion-enhanced erosion can be formulated a linear function of logarithm of anodic current density present i_a on the test surface

$$\frac{w_e^c}{w_e^0} = Z \log\left(\frac{i_a}{i_{th}}\right) \tag{2-12}$$

where i_{th} is the threshold current density; Z is an experimental constant. According to Equation (2-12), the normalized corrosion-enhanced erosion rate w_e^c / w_e^0 will increase with increasing anodic dissolution rate and the relationship between them can be approximately formulated as a linear function of the logarithm of anodic current density. It is confirmed by the erosion test data in Figure 4-1 measured under action of applied anodic current, indicating the erosion will be enhanced by the chemo-mechanical effect when corrosion occurs simultaneously.

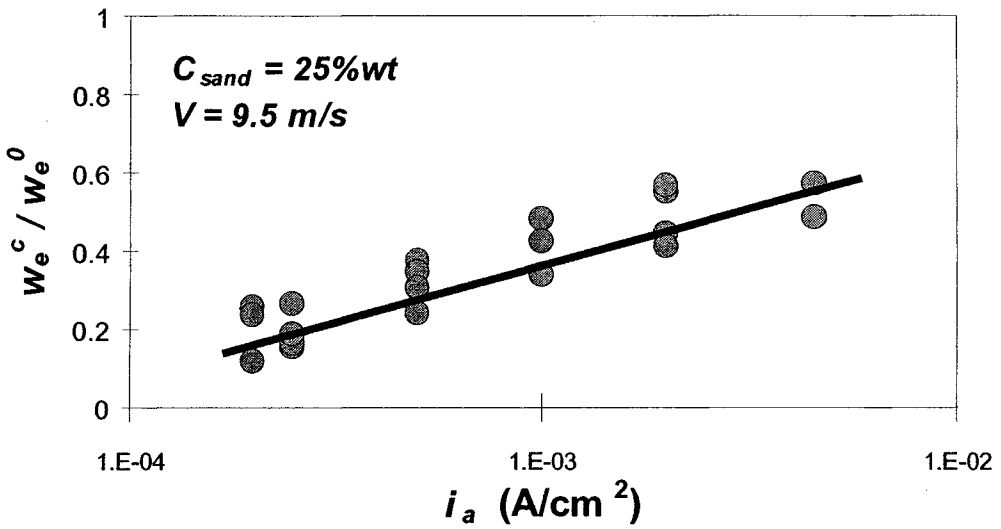

Figure 4-1. Dependence of flow rate on corrosion enhanced corrosion

4.2. Dependence of Corrosion-Enhanced Erosion on the Hydrodynamic Parameters

The synergies of corrosion-enhanced erosion not only rely on the corrosion current but also are dependent on the follow velocity and sand concentration. (Madsen, 1985, Yue et al., 1987, and Poulson, 1999). The test data in Figures.4-2 and 4-3 indicate that, when the flow rate or sand concentration increase, the normalized wastage of corrosion-enhanced erosion under a given applied anodic current density decrease but the slope of the curves of w_e^c / w_e^0 vs. i_a hold almost unchanged. As indicated by the results in Figures.4-4 and 4-5, under the action of anodic current density the relationships of w_e^c / w_e^0 vs. U and w_e^c / w_e^0 vs. C_{sand} can be approximately formulated, respectively, with empirical expressions as follows:

$$\frac{w_e^c}{w_e^0}\Big|_{i_a=const.} = \lambda_U \ln U \tag{4-2}$$

$$\frac{w_e^c}{w_e^0}\Big|_{i_a=const.} = \lambda_C \ln C_{sand} \tag{4-3}$$

With the aid of Equations (2-29), (4-2) and (4-3), it is possible for us to establish the expression to formulate the dependence of normalized wastage of corrosion-enhanced erosion under both galvanostatic conditions and open circuit potentials on the hydrodynamic parameters using multiple regression method.

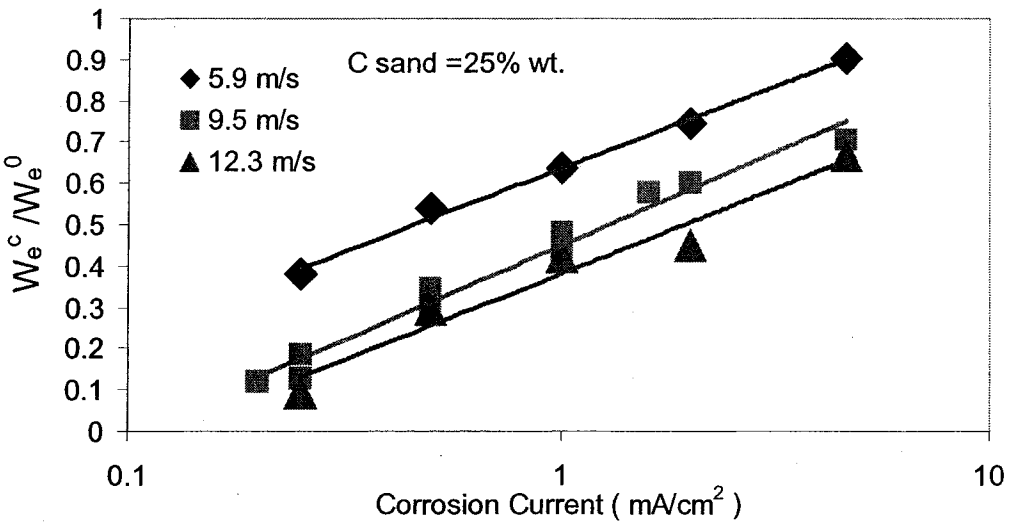

Figure 4-2. Effect of flow velocity on the relationship of the normalized wastage of corrosion-enhanced erosion w_e^c / w_e^0 vs. anodic current density

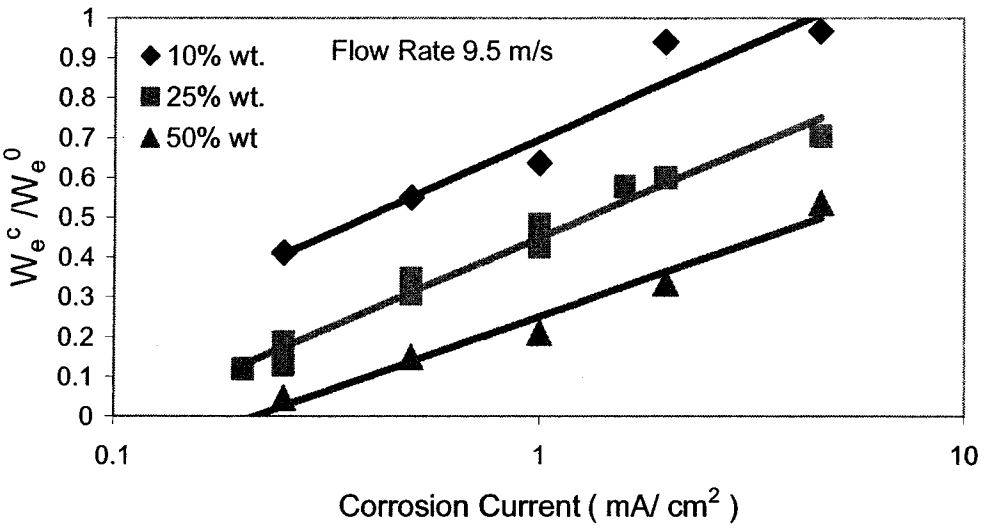

Figure 4-3. Effect of sand concentration on the relationship of the normalized wastage of corrosion-enhanced erosion w_e^c / w_e^0 vs. anodic current density

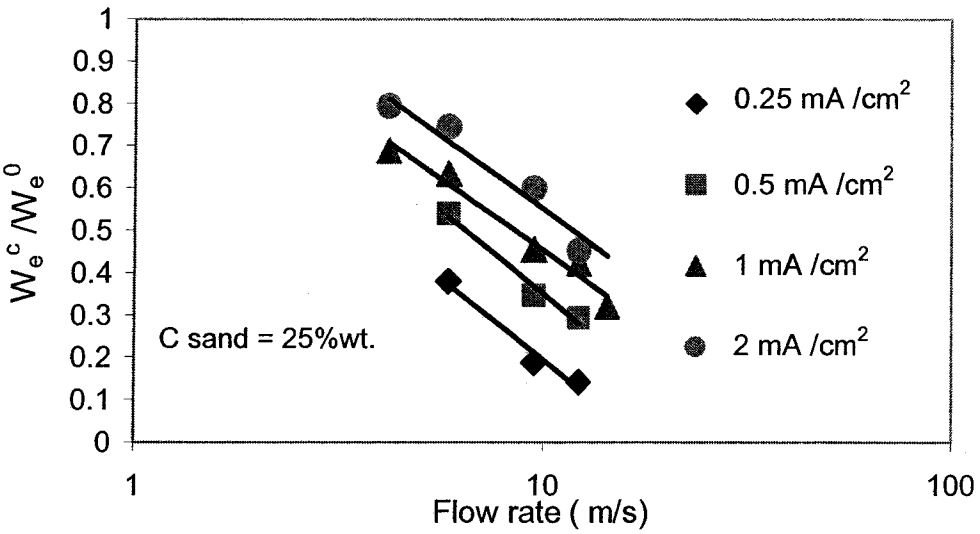

Figure 4-4. Dependence of normalized wastage of w_e^c / w_e^0 on the flow rate

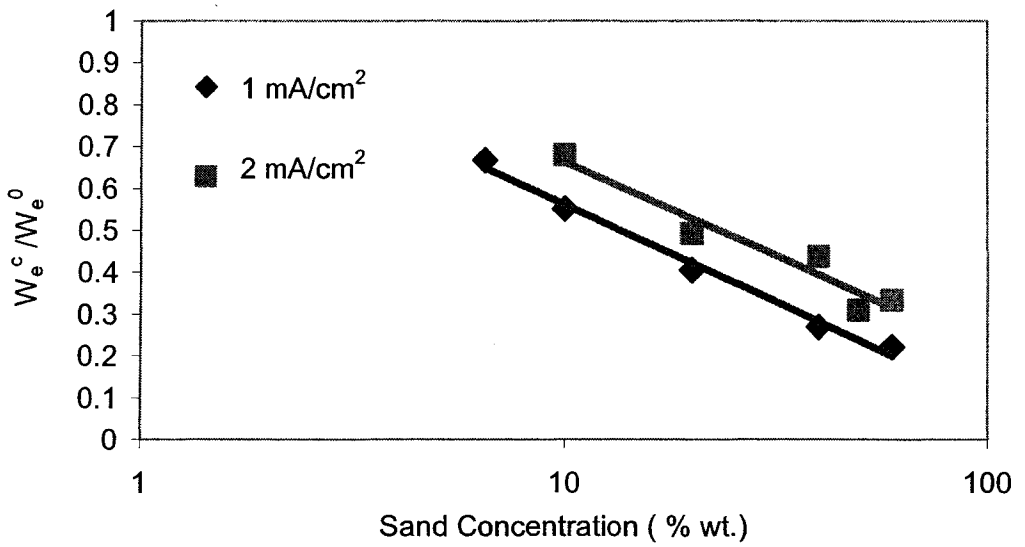

Figure 4-5. Dependence of normalized wastage of w_e^c / w_e^0 on sand concentration

4.3. General Expression for Wastage of Corrosion-Enhanced Erosion

As mentioned precisely, the experiments run under the design conditions are listed in Table 3-8. Companying with the additional experiments, the relationship among the normalized wastage of erosion-enhanced corrosion, w_e^c / w_e^0 the anodic current density and the hydrodynamic parameters, the apparent flow velocity and sand concentration, is determined with multiple regression method and ANOVA analysis (Appendix D). The results of analyses are given in Tables 4-1 through 4-3. As seen in Table 4-1, the coefficients of determination, R^2, and R^2_{adjusted}, were, respectively, 0.68 and 0.65, very close to each other. The value of multiple R indicates that quality of fit to be 82%. It

means about 82% of test data fall in the range of standard error (± 16.9%) deviating from the response surface. These analyses were made at a confidence level of 95%.

Table 4-1. Parameters obtained from regression

Regression Statistics	
Multiple R	0.82
R Square	0.68
Adjusted R Square	0.65
Standard Error	0.17
Observations	88

Table 4-2. Parameters used in ANOVA analysis

	df	*SS*	*MS*	*F*	*Significance F*
Regression	7	4.86	0.69	24.33	2.04E-17
Residual	80	2.28	0.03		
Total	87	7.14			

Table 4-3. Coefficients and statistical parameters obtained from ANOVA analysis

	Coefficients	Standard Error	t Stat	P-value	Judgment
K	0.48	0.02	24.31	1.08E-38	Sign.
A	-0.15	0.02	-6.19	2.40E-08	Sign.
B	-0.10	0.02	-4.00	1.42E-04	Sign.
C	0.15	0.02	8.62	5.01E-13	Sign.
AB	-0.05	0.04	-1.49	0.14	
AC	-0.04	0.02	-2.10	0.04	
BC	-0.02	0.02	-0.86	0.39	
ABC	0.02	0.03	0.61	0.55	

The significance of this model is also seen in ANOVA results shown in Table 4-3. Usually, the judgment is made by means of the significance F_{signif} of variables. It should be bigger than the value of F listed in Table 4-3 if the regression model is significant. The lower value of F_{signif} indicates the higher significance of the model. The result shows that the regression formula is very high significant.

The normal probability plot in Figure 4-6 shows that the distribution of standard residuals can be well fitted with a straight line, except a few of residual data with high values. It means that residuals follow approximately the normal distribution. The

dependence of the residuals on the predicted values of w_e^c / w_e^0 is shown in Figure4-7. The residuals are even distributed on the band around the zero (in the two dash line). It means that the residuals are random distributed residuals and they are independent of the w_e^c / w_e^0 values. Above results indicate that the relationship among test data of w_e^c / w_e^0, the anodic current density and the hydrodynamic parameters can be well formulated with the expression of response surface.

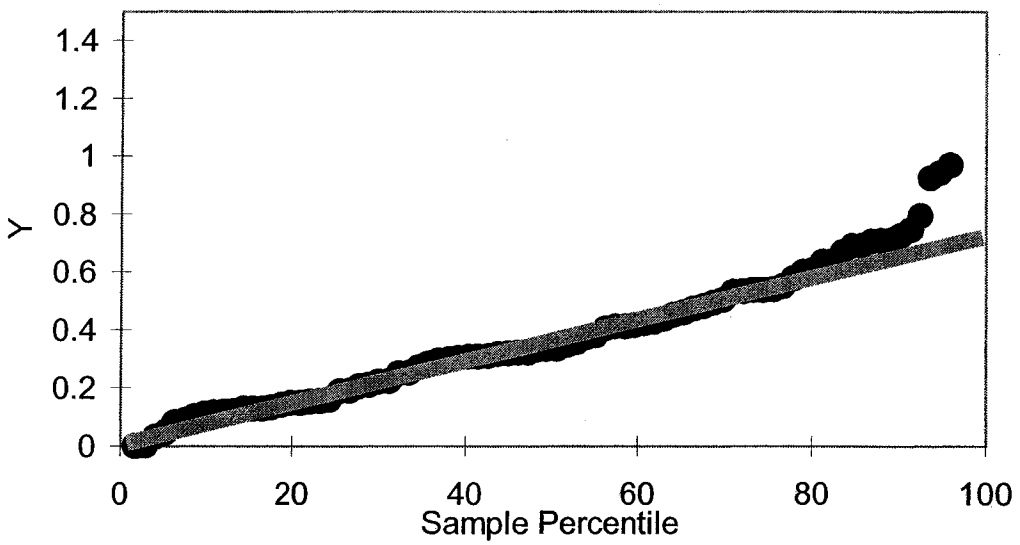

Figure 4-6. Plot of Normal probability of residuals, over 95% residuals distributed along the green line

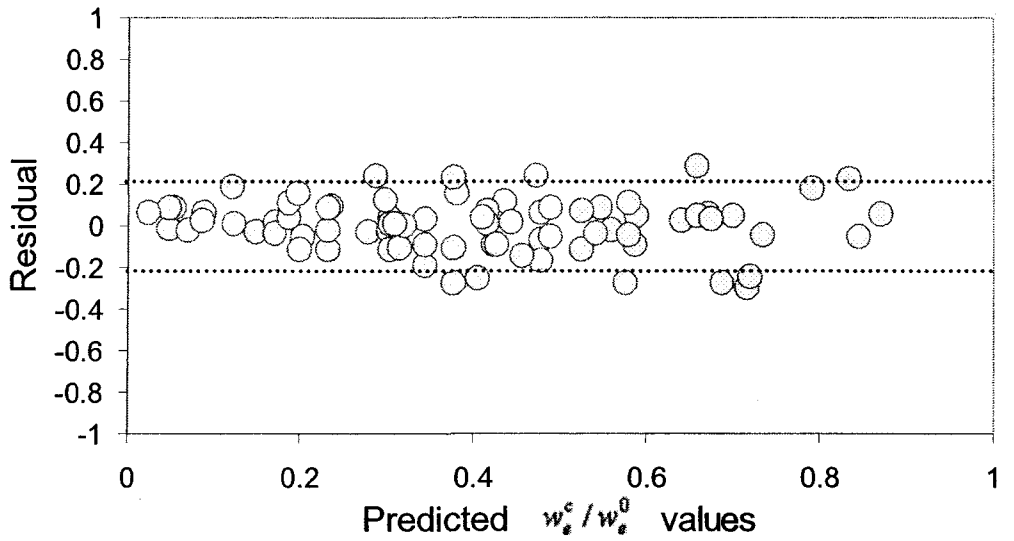

Fig 4-7. Plot of residuals vs. the predicted synergy of w_e^c / w_e^0 residuals fall in the band whose centre line is zero.

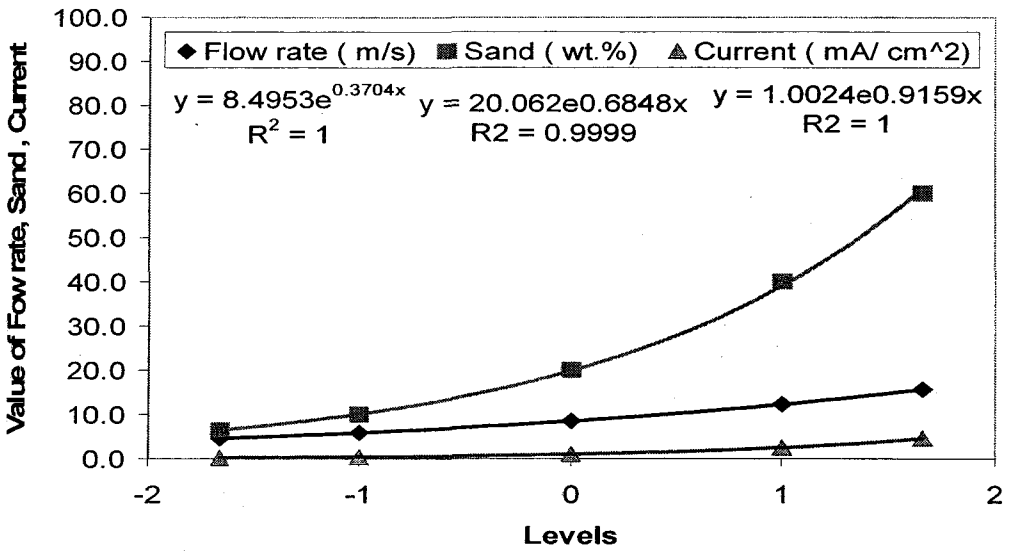

Figure 4-8. Curves used to transfer the formula of flow rate, sand concentration and corrosion current in the regression.

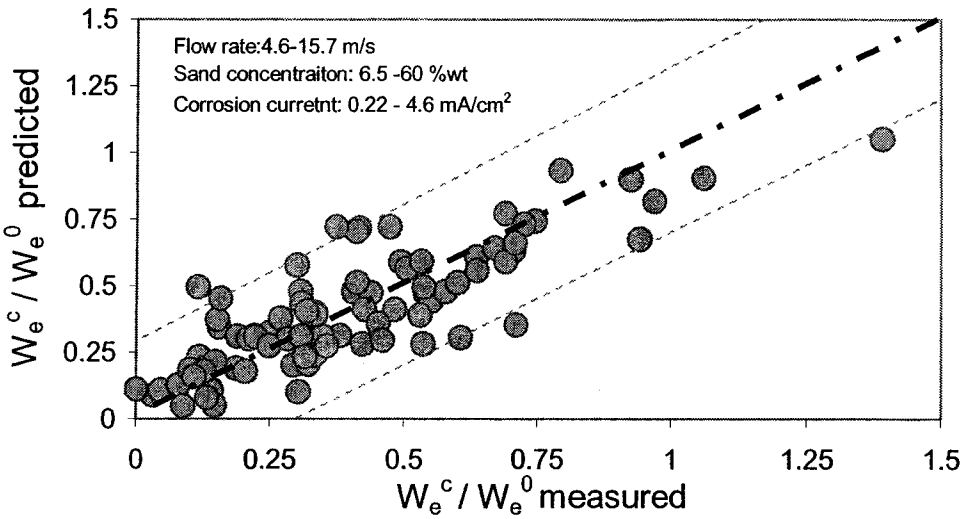

Fig 4-9. Plots of the W_e^c / W_e^0 values predicted from regression formula and values measured from experiment. Their values distributed around the tangle line

In line with the data in Table 4-3, the significant components are found to be the flow velocity, sand concentration and corrosion current as their P-values are far less then α_{critic}, so they are selected in the regression formula. The interaction items of three factors are bigger than α_{critic}, therefore, in the formula these items can be negligible. The expression to formulate the relation among independent parameters and normalized wastage of corrosion-enhanced erosion w_e^c / w_e^0 is:

$$Y = 0.477 - 0.146A - 0.10B + 0.148C \qquad (4\text{-}4)$$

According to the Table 3-7 of 3^5 full factorial designs the follow transfer equation of flow velocity, sand concentration and corrosion current are obtained from Figure 4-8.

Flow Rate (m/s) U $$A = \frac{1}{0.37} \ln \frac{U}{8.5} \tag{4-5}$$

Sand Concentration C_{sand} $$B = \frac{1}{0.685} \ln \frac{C_{sand}}{20} \tag{4-6}$$

Corrosion Current i_a $$C = \frac{1}{0.916} \ln i_a \tag{4-7}$$

Therefore, the expression for the response surface

$$\frac{w_e^c}{w_e^0} = 0.37 \log \left(\frac{i_a}{1.84 \times 10^{-5} U^{2.44} C_{sand}^{0.91}} \right) \tag{4-8}$$

The Equation (4-8) shows the normalized wastage of corrosion-enhanced erosion is a log function of corrosion current, flow velocity and sand concentration. In the Fig 4-9, the values of w_e^c / w_e^0 determined from the experimental data and those predicted from the response surface obtained by the regression analysis are compared. Their values are well a good agreement.

4.4. Effects of Synergism in the Slurry of pH

In this section, the effect of chemical composition of solutions for preparing slurries is examined. The base solution used was 0.1 M Na_2SO_4 and its pH value was adjusted with sulfuric acid or sodium hydroxide. The pH of slurries is 5.5, 7 and 8.5, respectively. The sand concentrations range from 10%wt. to 50%wt.

The effects of anodic current on the normalized wastage of corrosion-enhanced erosion in the acidic slurry are depicted Figure 4-10. The results indicate that the corrosion-enhanced erosion is promoted by the anodic dissolution present on the surface and the slope of the curves of w_e^c / w_e^0 vs. ln (i) is approximately independent of the flowing velocity.

When the pH of slurries increases, the corrosion-enhanced erosion becomes, generally, more pronounced but the dependence of the normalized wastage w_e^c / w_e^0 on the anodic current density is reduced, as demonstrated in Figs. 4-11. Under the condition of the sand concentration 25% and flow rate 9.5 m/s, the straight lines' slopes of the normalized synergy resulted from corrosion enhanced erosion are increased as the pH values are increased in the slurry. This may relate the tribological characteristics of specimen surface in the solution with different pH. However, this statement need to be further checked.

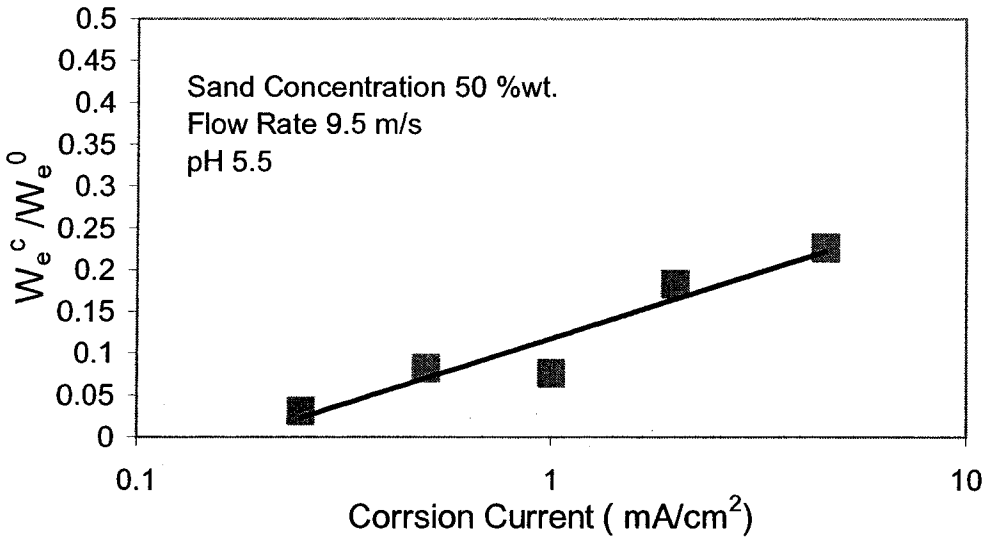

Figure 4-10. Normalized synergy of w_e^c / w_e^0 vs. corrosion current at acid slurry

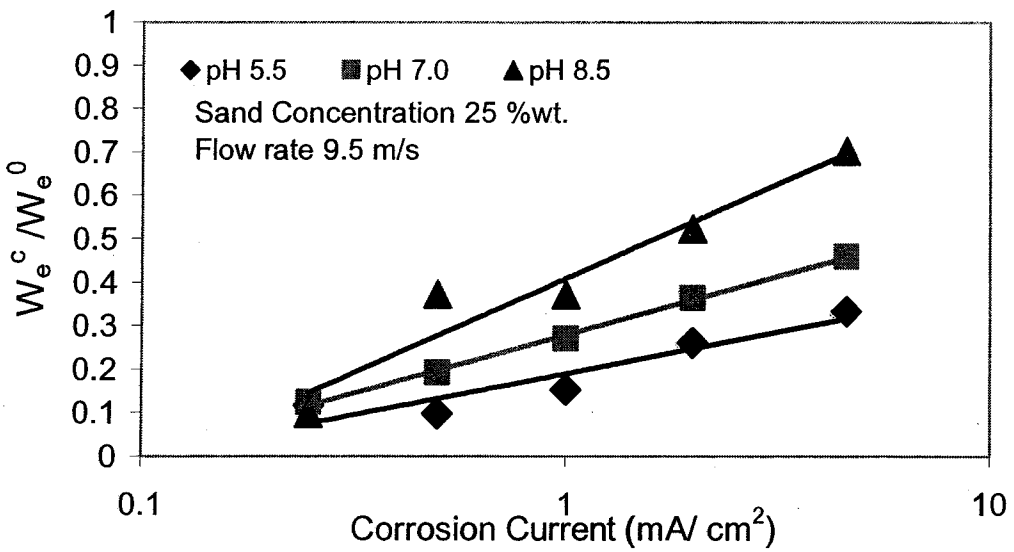

Figure 4-11. Normalized synergy of w_e^c / w_e^0 vs. corrosion current at acid, natural and base slurry.

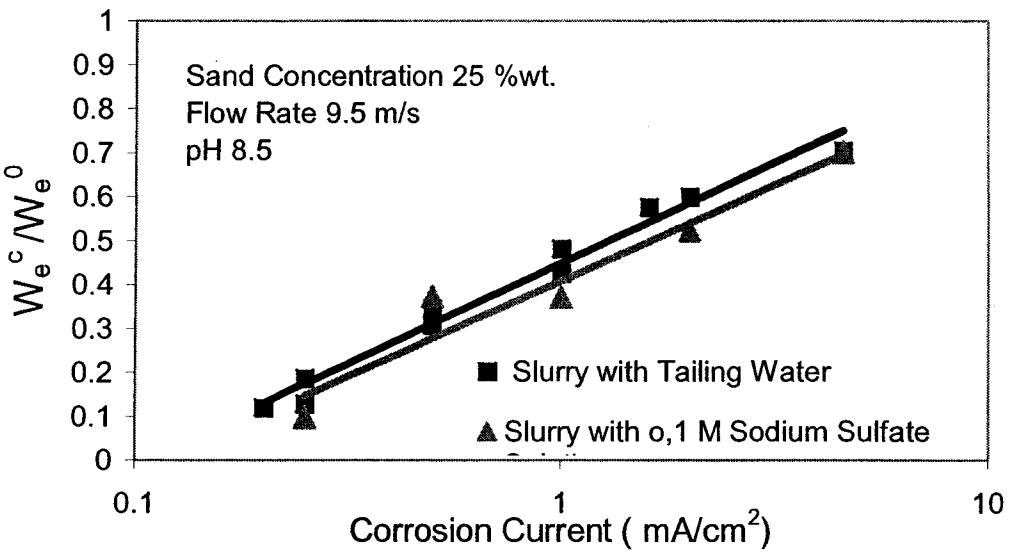

Figure 4-12. Normal synergy of w_e^c / w_e^0 vs. corrosion current test in the tailing water slurry (pH8.5) and man-made base slurry (pH 8.5).

To understand the impact of slurry chemistry, the erosion-corrosion tests were conducted in the slurries prepared with the basic Na_2SO_4 solution and the tailing solution offered by Syncrude. Both slurries have same pH value and sand concentration. The test results in the Figure 4-12 show that, when the pH of the solution is kept unchanged, the modification in the chemical composition in slurry dose not alters the corrosion-enhanced erosion behavior. The wastage of corrosion-enhanced erosion is mainly controlled by the anodic dissolution rate on the specimen surface.

In sumary, it is known that the synergy caused in chemo-mechanical effect is related to the flow rate, sand concentration, corrosion current and pH of the slurry. The normalized synergies in the different pH slurry versus the regression formula are drawn

in the Figure 4-13. The pH values affect on the slopes of the synergistic curves. Based on equation 4-8 the formula to express their relationship can be written with pH as follow:

$$\frac{w_e^c}{w_e^0} = m_5 pH^{m_6} \log\left(\frac{i}{m_7 U^{m_8} C_{sand}{}^{m_9}}\right) \tag{4-9}$$

were, Constants are $m_5 = 0.0046$, $m_6 = 2.1$, $m_7 = 1.84 \times 10^{-5}$, $m_8 = 2.44$, $m_9 = 0.91$ in our case. The values predicted from Equation (4-9) and the values measured from experiments are compared in the Figure 4-14. The anodic current during test was constant under the galvanostatic conditions. It is means that under the conditions of controlled rate of corrosion, synergy of corrosion enhanced erosion have a power relationship with the pH values in the slurry. The reason should be further explored.

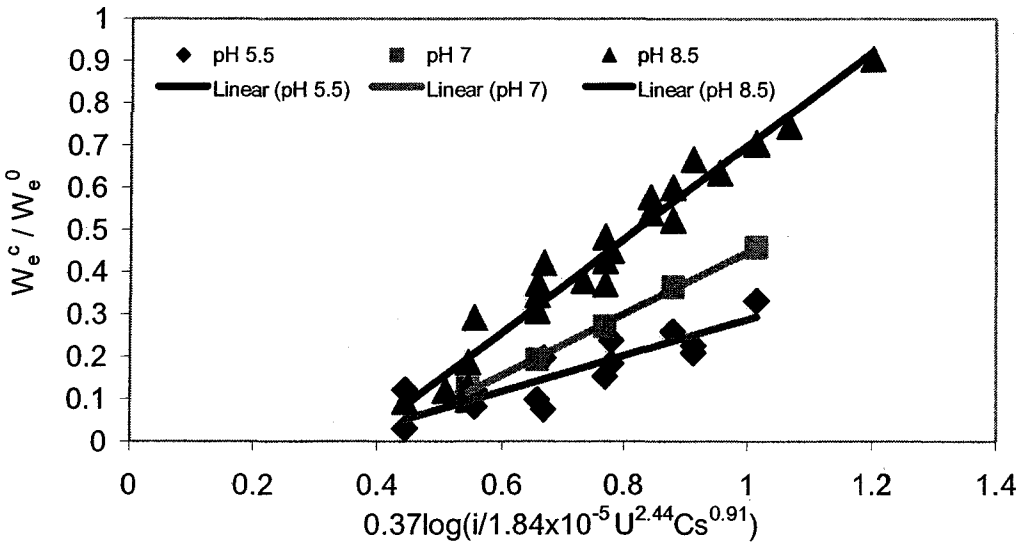

Figure 4-13. Synergy of w_e^c / w_e^0 vs. regression formula at different pH

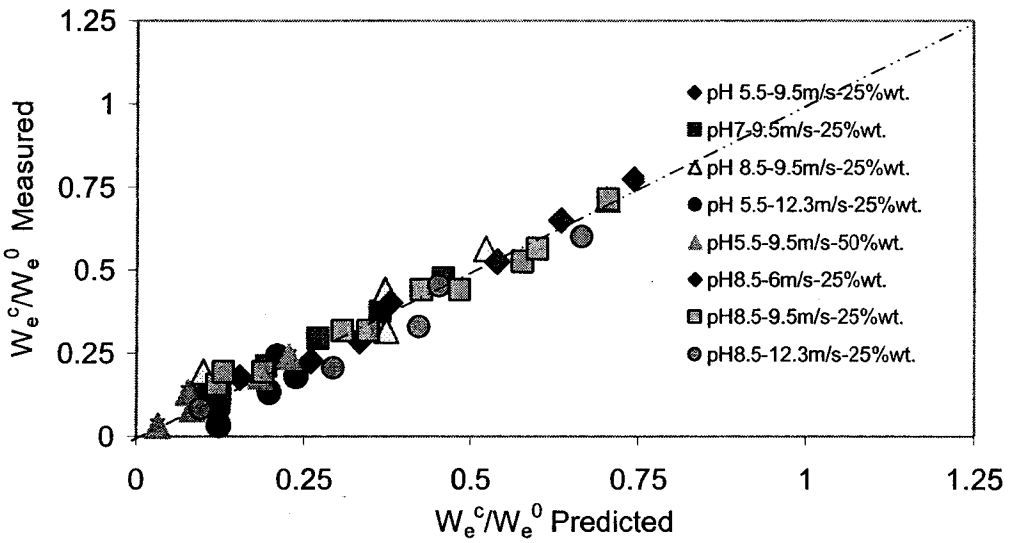

Figure 4-14. Comparison of measured values and experimental values for synergy of corrosion-enhanced erosion

References:

Lu, B. T. and Luo, J. L. 2004. Chemo-Mechanical Effect in Erosion-Corrosion Process of Carbon Steel. CORROSION 2004, New Orleans, March 28-April 1, 2004.

Madsen, B. W. 1985. Study of Parameters Using a New Constant Wear-Rate Slurry Test. Wear of Materials, ASME, New York, 345-354.

Poulson, B. 1999. Complexities in Predicting Erosion Corrosion. Wear, **233-235:** 497-504.

Yue, Z., Zhou, P. and Shi, J. 1987. Some Factors Influencing Corrosion-Erosion Performance of Materials. Wear of Materials, ASME, New York, 763-771.

CHAPTER 5. INTERACTION OF MECHANICAL AND ELECTROCHEMICAL FACTOR IN SLURRY EROSION AT OPEN CIRCUIT POTENTIAL

5.1. Contributions of Different Components of Wastage to the Total Material Loss in Slurry Erosion-corrosion under OCP

It has been recognized that the erosion resistance of materials depends mainly on their mechanical properties and the corrosion resistance is governed by their chemical characteristics (Lutz and Postlethwaite, 1990).The erosion-corrosion mechanism not only depends heavily on the metallurgical features of a material but also depends on the test conditions including hydrodynamic parameters, sand concentration and corrosivity of the environment (Neville and Hu, 2001). As mentioned previously, the total wastage of erosion-corrosion can be attributed to the pure erosion w_e^0, pure corrosion w_c^0, erosion-enhanced corrosion w_e^c and corrosion-enhanced erosion w_c^e. The relative contributions of each component to the total material loss of A1045CS and A1018CS steels are illustrated from Figure 5-1 to Figure 5-4, respectively.

The weight loss of pure corrosion contributes small percentages to the total weight loss. The corrosion weight loss contributes to about 0-3% of the total material loss under the current test conditions. Specially, for the A1018CS in Figure 5-3 and 5-4 it is

less than one percentage of the total weight loss. The corrosion can increase the surface rougher of the sample surface,. The rough surface will increase the impact angle of the solid particles. Therefore it will enhance the erosion damage.although corrosion accounted for only a small part of the total wear, it can accelerate the erosion process considerably.

Table 5-1. Percentages of each component w_s , w_e^0 , w_c^0 , w_e^c and w_c^e to total loss w of A1018CS at different flow rate.

No.	Flow Rate m/s	[Sand] %wt.	W_s/W %	W_e^o/W %	W_c^0/W %	W_c^e/W %	W_e^c/W %
1	4.5	30	59	41	0.23	1.30	57
2	6.5	30	19	81	0.18	1.61	17
3	8.5	30	17	83	0.16	2.39	15
4	11.5	30	11	88	0.21	2.01	9
5	13	30	10	90	0.22	1.98	8
6	16	30	2	98	0.22	1.92	0

The weight loss of pure erosion dominates the total weight loss. It is noted that slurry erosion is very large at high flow rate or high sand concentration, for example, in the Figure 5-1 and 5-2 when the sand concentrations are over 40% and flow rate are over 11m/s for A1018CS the percentage of pure erosion weight loss is over 90%. Even at low flow rate or low sand concentration, it is still over 40% for both of carbon steel. The ratio of the weight loss of pure erosion to the total weight loss is very big values, almost tens time for A1045CS and hundreds times for A1018CS then the ration of the weight loss of pure corrosion. It is indicted that the erosion dominates the whole process in the test

conditions. So, any effect, promoted on the erosion process, will be important ones in the erosion-corrosion process.

Table 5-2. Percentages of each component w_s , w_e^0 , w_c^0 , w_e^c and w_c^e to total loss w of A1018CS at different sand concentration

No.	Flow Rate m/s	[Sand] %wt.	W_s/W %	W_e^0/W %	W_c^0/W %	W_c^e/W %	W_e^c/W %
1	11.5	6	63	37	0.23	1.11	62
2	11.5	12	19	81	0.25	1.80	17
3	11.5	20	9	91	0.18	1.47	8
4	11.5	34	5	94	0.15	1.51	4
5	11.5	40	1	99	0.13	1.11	0
6	11.5	60	1	99	0.10	1.00	0

The percentages of total synergy , depending on the service conditions of slurry pipelines, change from 0% to 60% in the present experiment. The experimental results have indicated that the contribution of synergism to the total material loss due to erosion-corrosion is so important that it could not be neglected in engineering practice. In the most cases of experiments the synergy of the carbon steel A1045CS contributes about 20% to 60% of the total weight loss in the range of flow velocity from 4 m/s to 8 m/s (Table 5-3) and sand concentration from 10%wt. to 40%wt (Table 5-4). The results are quite close to those reported by Madsen (1985) who pointed out that pointed about 23-33% of the total weight loss of low alloy steels could be attributed to the synergistic effect. In the special case of our experiment, the highest percentage of total synergy for A1045CS can reach to 80% of total weight loss at the condition of flow rate 2.6 m/s and

sand concentration 10 % wt. It suggests that, when the slurry pipes of carbon steel are eroded in near-neutral pH slurry, which happens often in engineering practice, the synergistic effect should be very strong under the low flow rate and sand concentration.

Table 5-3. Percentages of each component w_s, w_e^0, w_c^0, w_e^c and w_c^e to total loss w of A1045CS at different flow rate.

No.	Flow Rate m/s	[Sand] %wt.	W_s/W %	W_e^0/W %	W_c^0/W %	W_c^e/W %	W_e^c/W %
1	4	20	56	42	3	5	50
2	5	20	33	65	2	5	28
3	6	20	28	70	2	5	23
4	8	20	22	76	2	3	19

The wastage component of erosion enhanced corrosion contributes only a small section to the total synergy. It only contributes to one or two percent of the total weight loss under the test conditions in this investigation, because it is result of the differences in the weight loss of corrosion in slurry and weight loss of pure corrosion in flowing water. This kind of synergy is relative to the electrochemical reaction during the erosion-corrosion process.

Table 5-4. Percentages of each component w_s, w_e^0, w_c^0, w_e^c and w_c^e to total loss w of A1045CS at different sand concentration

No.	Flow Rate m/s	[Sand] %wt.	W_s/W %	W_e^0/W %	W_c^0/W %	W_c^e/W %	W_e^c/W %
1	4	10	77	22	2	3	74
2	4	20	56	42	3	5	50
3	4	30	46	53	1	3	43
4	4	40	32	68	0	1	31

The weight loss of corrosion enhanced erosion is a bigger part of total synergy. Its percentage for A1018CS dramatically drops as if the sand concentration or flow rate increases. At the end, its values become zero if sand concentration is over 40% and flow rate is over 16 m/s (Figure5-3 and Figure 5-4). It means that the Mechano-chemical effect will become less and less at high concentration sand and high flow rate. The same results for A1045CS show on the Figure 5-1 and Figure 5-2. It could be reasonable to say synergy of corrosion enhance erosion is dependent on hydrodynamic parameters, that is its weight loss is relative to the interaction of particle kinetic energy and frequency of collection between the particle and surface of metal.

Above results further confirm that the synergistic effects play the significant role at the range of low flow rate and sand concentration, but it is less affection on the high flow slurry with high sand concentration.

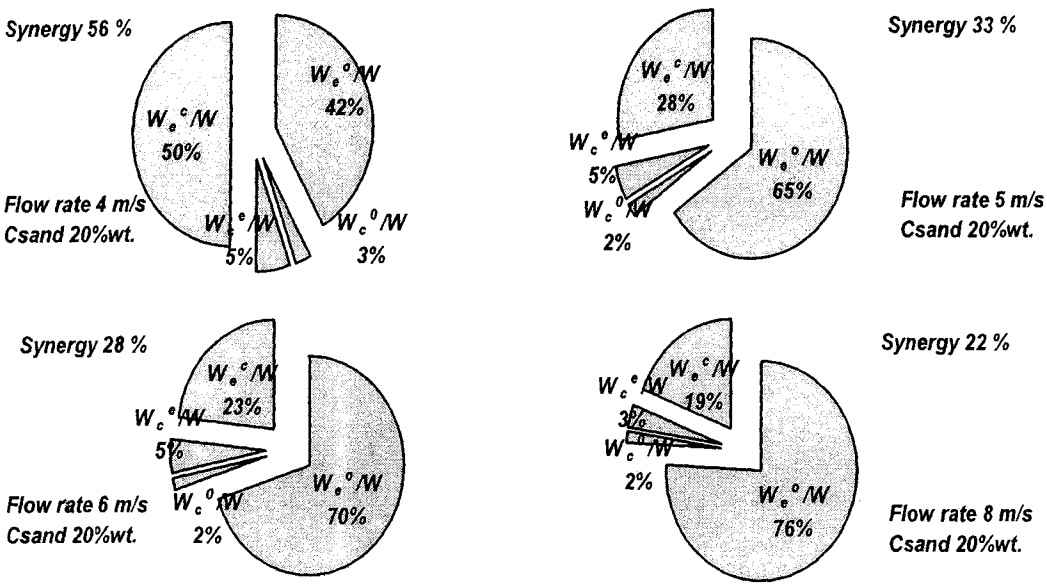

Figure 5-1. Relative contributions of each component w_e^0, w_c^0 w_e^c w_c^e and w_s to the total material loss of A1045CS at the variation of flow rate.

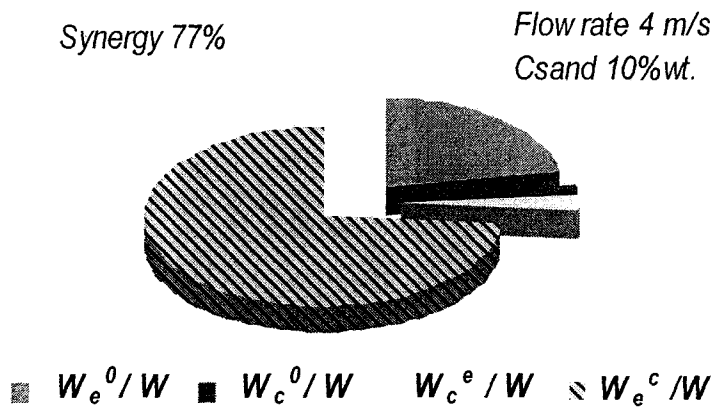

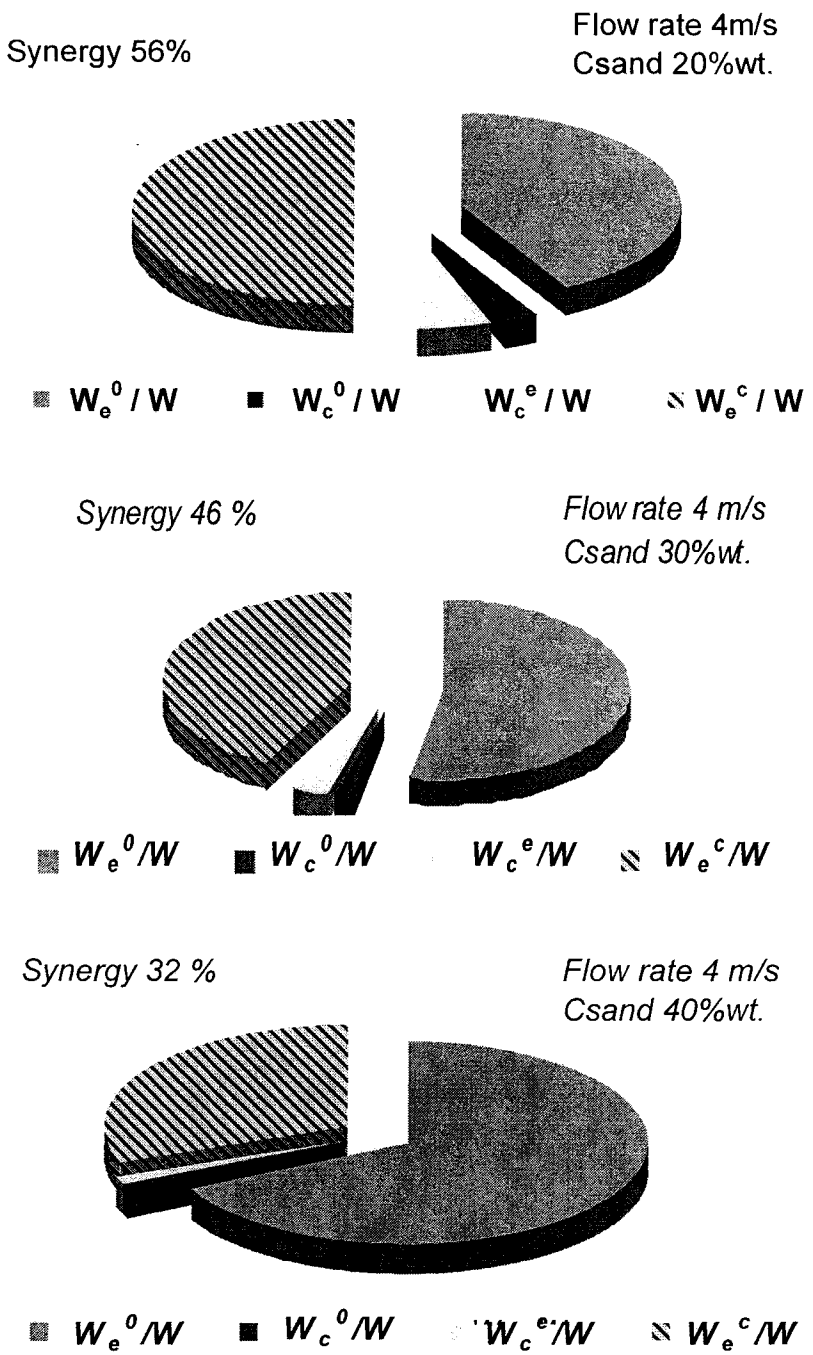

Figure 5-2. Relative Contributions of the w_e^0, w_c^0 w_e^c w_c^e and w_s to the total loss of A1045CS at the variation of sand concentration.

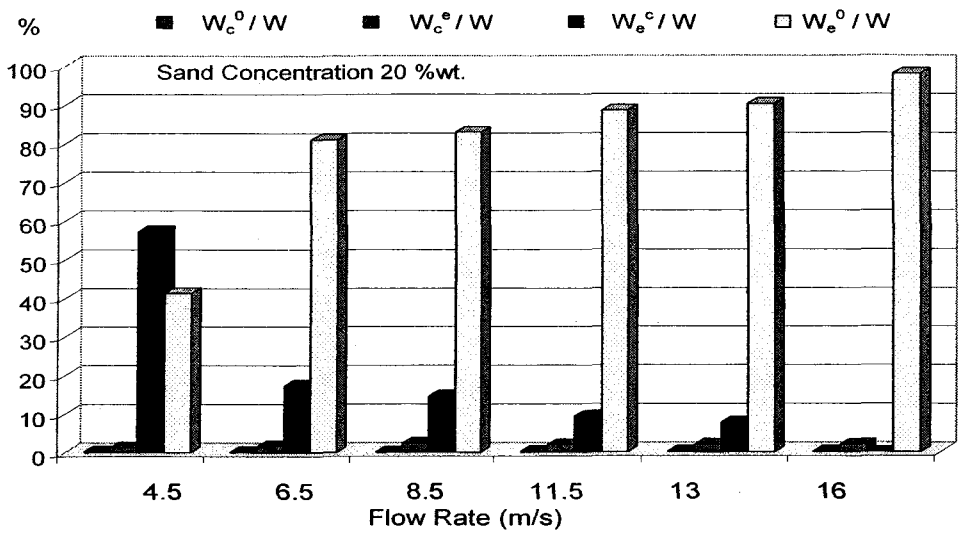

Figure 5-3. Relative contributions of each component w_e^0, w_c^0 w_e^c w_c^e and w_s to the total material loss of A1018CS at the variation of flow rate.

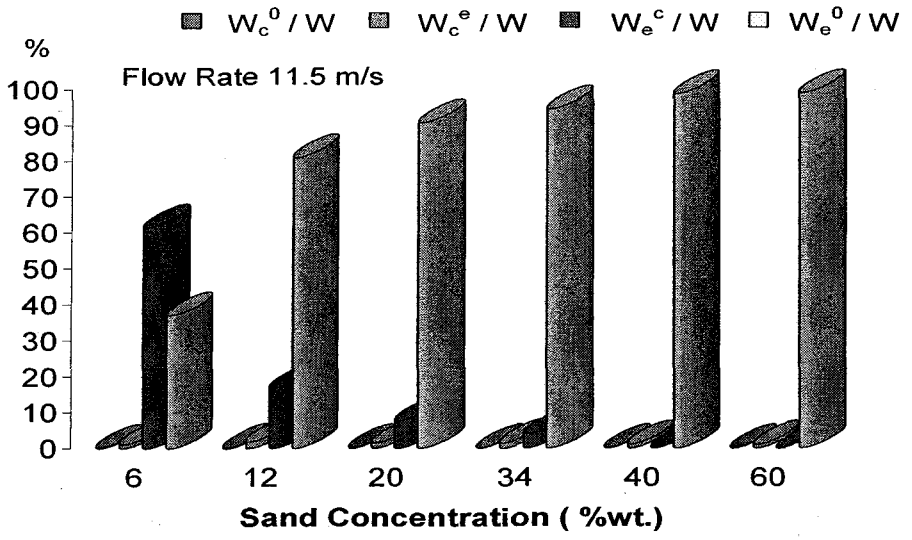

Figure 5-4. Relative contributions of each component w_e^0, w_c^0 , w_e^c , w_c^e and w_s to the total material loss of A1018CS at the variation of sand concentration.

5.2. Effects of Hydrodynamic Factors on Mechanical Erosion and Electrochemical Corrosion

5.2.1. Basic Theoretical Concepts.

It is generally accepted that the corrosion rate in a fluid can be formalted with the empirical expression (5-1) in the non-dimensional form (Kolman et al., 1998, and Coeuret and Legrand, 1981).

$$Sh = \alpha \, \mathrm{Re}^{\beta} \, Sc^{\gamma} \qquad (5\text{-}1)$$

The non-dimensional parameters in Equation (5-1) are written here,

Sherwood Number: $Sh = \frac{k\,d}{D}$

Reynolds Number: $Re = \frac{Ud}{\nu}$

And Schmidt Number: $Sc = \frac{\nu}{D}$

where α, β and γ are constants depending on the corrosion mechanisms, flow conditions and geometries of test devices; k is the apparent mass transport coefficient; d is the pipe diameter; D is the diffusion coefficient; U is the flow velocity; $\nu(=\mu/\rho)$ is the kinematic viscosity of fluid (μ and ρ are viscosity and density of fluid). According to theoretical considerations the exponents' β and γ in the fully developed pipe flow and high Schmidit Numbers should be close to 9/10 and 1/3, respectively. For example (Poulson, 1983).

$$Sh = 0.023\,\mathrm{Re}^{0.8}\,Sc^{0.33} \tag{5-2}$$

According to Faraday's law, it is genially accepted that the corrosion rate w_c has a linear function of self-corrosion current i_{corr}. The relationship between them is formulated as flow:

$$w_c = \frac{i_{corr} M_{Fe}}{zF} \tag{2-3}$$

Where M_{Fe} is mass of iron per mole; F= 96500c/mol; z =2 as $Fe^{2+} + 2e^- \Leftrightarrow Fe$. Iron Fe^{2+} formed from anodic electrode may combine with iron OH^- formed from cathodic electrode to precipitate Fe $(OH)_2$ on the corroding surface. Fe $(OH)_2$ may undergo further change to form a porous adherent metal oxide on the corroding surface.

In case of corrosion process, such as, drawn in the Figure 5-5, inside a pipe surface cavered with a layer of corrosion scale, , and boundary layer of lquaid. Kinetic studies of the industrial corrosion in which dissolved oxygen acts as a depolarizer have revealed that the cathodic reduction of oxygen involves three steps. (Postlethwaite et al., 1986)

The frist step is the magriation in the boundary layer. Dissolved oxygen passes through the boundary layer from the bulk flowing solution to the scale/ liquid interface. The rate of this step is given by:

$$w_v = k_v(C_v - C_f) \tag{5-3}$$

The second step is the diffusion in the corrosion scale. The oxygen diffuses through the pores of the corrosion deposited layer from the scale/liquid interface to matel/scale interface. This step can be represented by:

$$w_f = k_f(C_f - C_r) \tag{5-4}$$

The third step is the interface reaction on the surface of metal. The oxygen reacts with the iron on the pipeline surface at the bottom of the pores. the equilibrium rate of the reaction is given by

$$w_r = k_r C_r \tag{5-5}$$

Where, w_v is a mass flux resulted from migration of dissolved oxygen. w_f is a mass flux come from diffusion of oxygen in the double layer or product's deposited layer. w_r is a mass flux caused from reaction of oxygen. C_v is the oxygen concentration in the bulk of the aqueous medium; C_f is the oxygen concentration on the surface of protective layer; C_r is the oxygen concentration at the bottom of the pores in the protective layer; k_v is mass transfer coefficient as a function of the flow rate U; k_f is a coefficient as a function of the pore structure of the surface layer and k_r is a coefficient as a function of the potential. Because the three steps are in series:

$$W_v = W_f = W_r \tag{5-6}$$

The three steps of the mass transfer process can be thought as a equilibrium circuit in which the interface reaction resistance R_r, the diffusion resistance R_f and migration resistance R_v connect each other in series. The corrosion current flows out from the metal surface to the bulk solution. Because the mass transfer resistance R is equal to one over mass transfer coefficient k. If the passive film or corrosion product scale exists on the surface, the apparent mass transport coefficient K is formulated as follows:

$$\frac{1}{k} = \frac{1}{k_v} + \frac{1}{k_f} + \frac{1}{k_r} \tag{5-7}$$

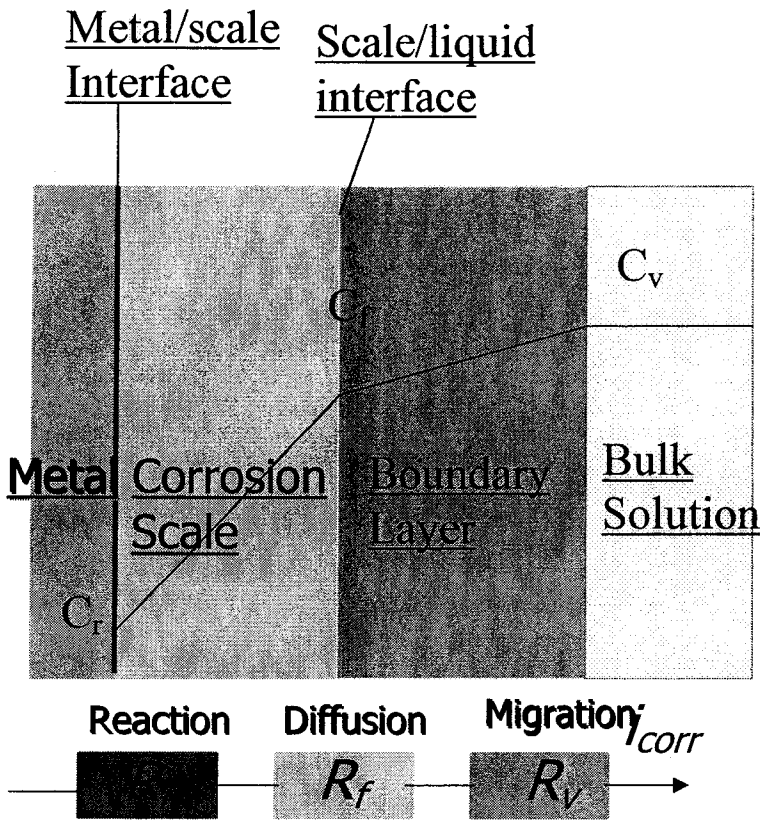

Figure 5-5. Illumination of mass transfer process

Because the three steps link each other in series, the rate of overall reaction is controlled by the slowest step. It is indicated that the slowest one of three steps in the process is the key step.

According to equation (5-6) the overall reaction rate should be equal to the diffusion rate in the boundary layer. it has been well documented that, when the corrosion process is controlled by the boundary layer diffusion, the reaction rate is equal to the

diffusion rate. It can be expressed with equation (5-1). Follow this vein, it is reasonable to assume that , when the corrosion process is not solely contorted by the boundary layer diffusion . the diffusion rate (= reaction rate) can still formulated with equation (5-1). In the case:

$$i_{corr} = nFk_v(C_v - C_f) = nF\eta C_v k_v \tag{5-8}$$

Where, n is equal to 4 as $O_2 + 4H^+ + 4e^- \Leftrightarrow 2H_2O$ and C_v is the bulk concentration of dissolved oxygen. C_f is the oxygen concentration at scale/ liquid interface. k_v is migrate coefficient in the boundary layer and η are the coefficients that have a functional relationship with the mass transfer process.

The rate of corrosion w_c in the slurry has a relationship with Reynolds Number. It can be formulated by combining the equation (5-1), (2-3), and (5-8)

$$w_c = \eta C_v \frac{n}{z} M_{Fe} \frac{D}{d} \alpha Sc^{\gamma} \mathrm{Re}^{\beta} \tag{5-9}$$

From above equation, a dimensionless mass transfer correlation using the groups Sh, Sc, Re is developed to connect with corrosion rate, from which the liquid phase mass transfer k can be predicted under turbulent flow conditions. Therefore, the practical meaning lies in the fact that corrosion rate w_c has a relationship with Reynolds Number

Re, which is dependent on hydro-parameters of the process in fully developed mass transfer.

$$w_c = \alpha' \mathrm{Re}^{\beta} \tag{5-10}$$

Where $\alpha' = \eta\ C_v \frac{n}{z} M_{Fe}\ \frac{D}{d} \alpha\ Sc^{\gamma}$

5.2.2. Mass Transfer Coefficient with Reynolds Number in Slurry

In the two-phase liquid/solid flow, effect of sand concentration should be considered. According to Shadley et al. (1996) and Blatt et al. (1989) the corrosion current density increases with increasing sand concentration. This is further confirmed in the Figure 5-6 and 5-7. When the flow rate increases the potentodynamic curves move from left to right. It means that the self-corrosion current increased as the flowing rate increases under the condition of sand concentration 20 %wt. If the sand concentration is increased in the slurry with flow rate 12 m/s the corrosion current is slightly increased with increasing the sand concentration.

The dependence of the self-corrosion current on the Reynolds Number is depicted on Figure 5-8 for A1018CS in tailing water slurry and Figure 5-9 for A1045CS in tap water slurry. These are clearly shown that the impingement of solid particles promotes

the corrosion process. The slopes of curves $\log i_{corr}$ vs. *Re* measured in the flowing slurry are almost constant in Figure 5-9, but they are lower than the slope determined in the flowing solution free of sand.

Basic on equation (5-10) the corrosion rate and corrosion current in the individual sand concentration can be formulated as follow:

$$w^j{}_c = \alpha_j' \mathrm{Re}^{\beta_j} \tag{5-11}$$

$$i^j{}_{corr} = \alpha_j \mathrm{Re}^{\beta_j} = nF\eta^j C_v^j k^j \tag{5-12}$$

Where $\alpha_j' = \eta^j C_v^j \frac{n}{z} M_{Fe} \frac{D}{d} \alpha_j Sc^{\gamma}$ and $\alpha_j = \frac{zF}{M_{Fe}} \alpha_j'$.

The above equations show the relationship between the corrosion weight loss or corrosion current and Reynolds Number . It is an improtant that the corrosion weight loss or corrosion current can be directly calcuated from the hydro-paramenter if the corrosion peocess is in the active dissolution system. By means of the Reynolds Number to express the formula, the corrosion weight loss or corrosion current connect with the unless-dimensional parameter insterd of the dimensional paramenters , such as flow rate and sand concentration.

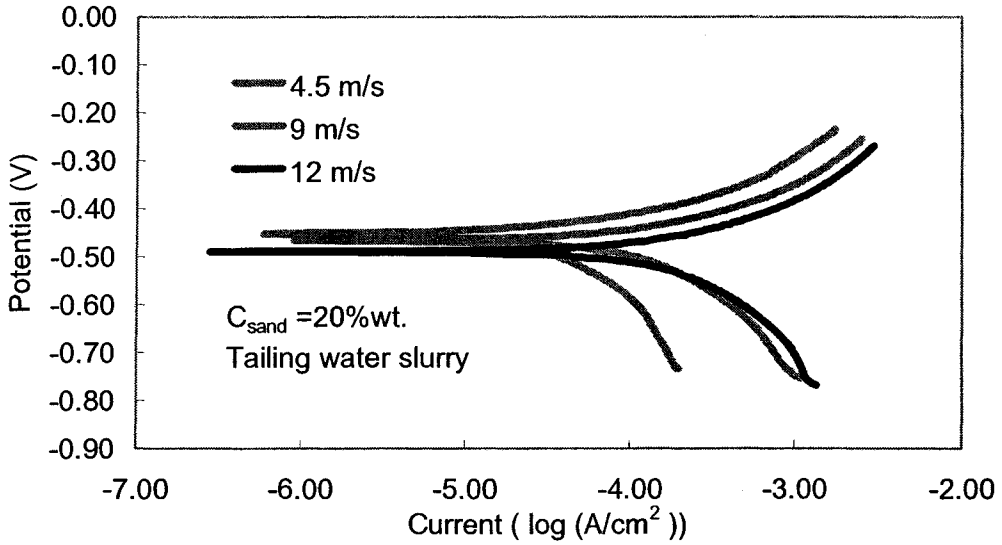

Figure 5-6. Potentodynamic curves at 20%wt. sand concentration

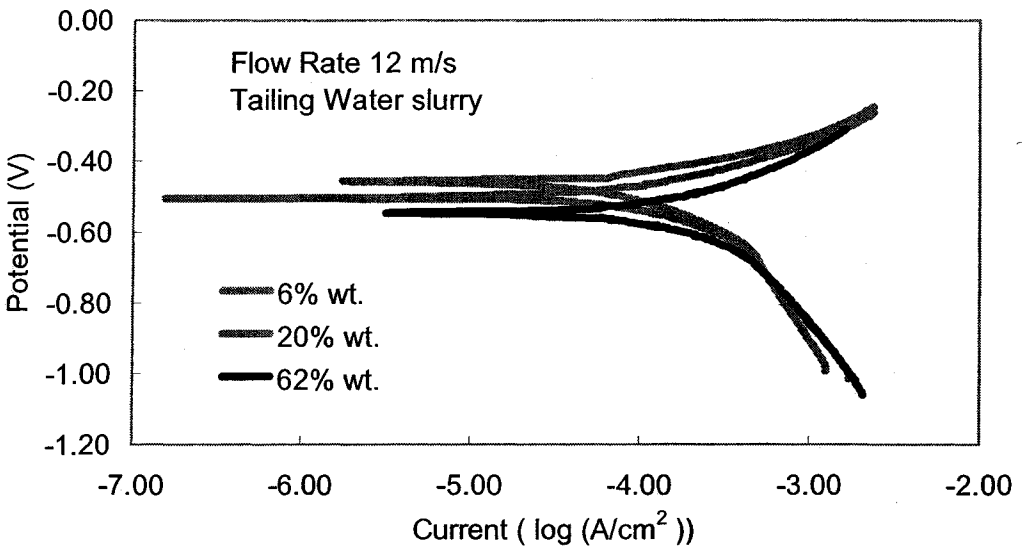

Figure 5-7. Potentodynamic curves at fixed flow rate condition

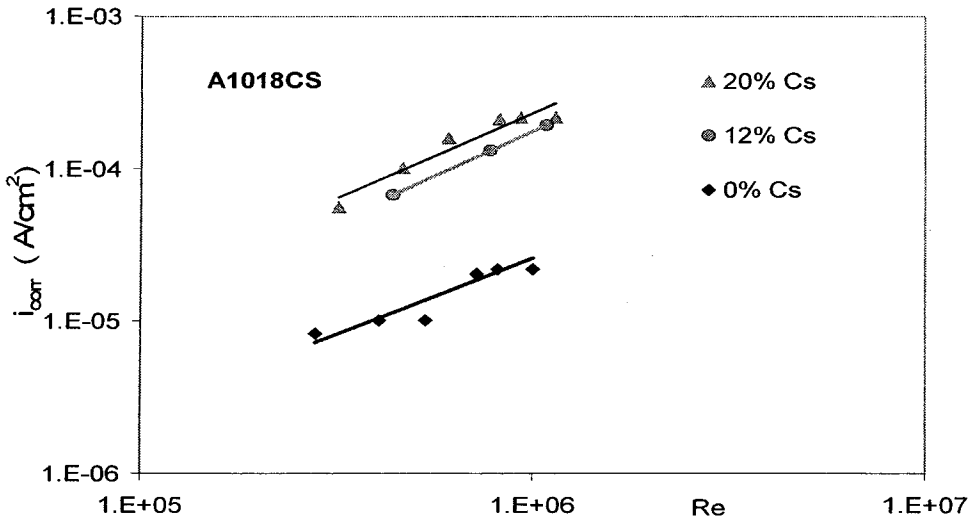

Figure 5-8. Self-corrosion current vs. Reynolds Number for A1018CS in tailing slurry

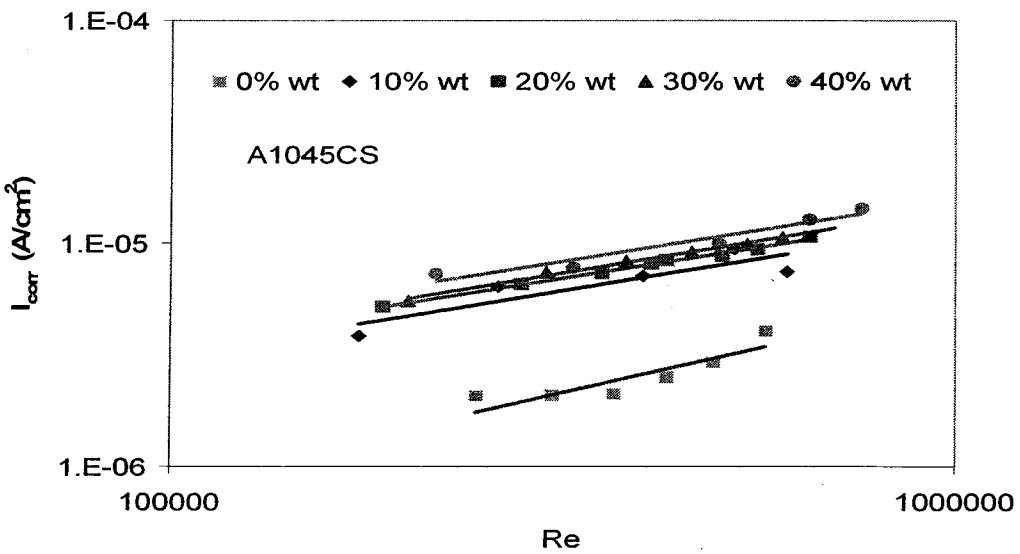

Figure 5-9. Self-corrosion current vs. Reynolds Number for A1045CS in tap water slurry

The parameters under the individual sand concentration for A1018CS in Figure 5-4 and A1045CS in Figure 5-5 are listed in Table 5-5.

Table 5-5. Parameters α_j and β_j in Equation (5-12)

Material	*Cs* (%wt)	α_j (A/cm2)	β_j
A1018CS	12	2×10^{-11}	1.17
	20	5×10^{-11}	1.12
A1045CS	10	4×10^{-9}	0.58
	20	6×10^{-9}	0.56
	30	5×10^{-9}	0.58
	40	7×10^{-9}	0.56

As the density of the solution with sand is different from that of flowing solution free of sand, the average density of the slurry $\bar{\rho}$ can be introduced in the empirical expression (2-1) in the non-dimensional form. By means of water density ρ_{water} and sand density ρ_{sand}, the average density of the slurry $\bar{\rho}$ can be calculated from the follow assumption:

$$C_{sand}+C_{water}=1\ ;\ V_{sand}+V_{water}=V\ ;\ \rho_{water}=1.0(g/cm^3);\quad \rho_{sand}=2.65(g/cm^3);$$

Therefore,

$$\bar{\rho} = \frac{W}{V} = \frac{W_{sand} + W_{water}}{V_{sand} + V_{water}} = \frac{C_{sand} + C_{water}}{C_{sand}\rho_{water} + C_{water}\rho_{sand}} \rho_{sand}\rho_{water} \tag{5-13}$$

$$\bar{\rho} = \frac{\rho_{sand}}{C_{sand}(1-\rho_{sand}) + \rho_{sand}} \tag{5-14}$$

$$\frac{1}{\bar{\rho}} = 1 + C_{sand}\left(\frac{1}{\rho_{sand}} - 1\right) = 1 - 0.62C_{sand} \tag{5-15}$$

Based on above information it is indicated that the effect of sand impingement on the corrosion rate can be approximately formulated as follow:

$$w_c = \alpha \, \mathrm{Re}^{\beta}(1 + C_s)^{\xi} \tag{5-16}$$

Or $$i_{corr} = \alpha \mathrm{Re}^{\beta}(1 + C_s)^{\xi} = nF\eta C_v k \tag{5-17}$$

Where $\alpha = \frac{zF}{M_{Fe}} \alpha'$.

Experimental constants α , β , ζ for different materials are given in Table 5-6 by means of solver program in Microsoft Excel.

Table 5-6. Parameters $\tilde{\alpha}$, β and ζ in equation (5-17)

Material	$\tilde{\alpha}$ (A/cm2)	β	ζ
A1018CS	1.39×10^{-9}	0.86	0.40
A1045CS	6.93×10^{-9}	0.57	0.54

The morphology of the samples after running experiments showed that not any rust exists on the surface of the specimen in Figure 5-10. The porous oxide film was destroyed and the corrosion scale was removed because of the impingement of solid particles, so that the mass transport in surface film or corrosion scale can be ignored, $1/k_f \approx 0$. Under the conditions of the high turbulence slurry, the corrosion current can be expressed with the contributions of the interface reaction k_r and the mass transport in boundary layer k_v by combing the equation (5-6) and (5-8).

$$\left(\frac{i_{corr}}{nF\eta C_v}\right)^{-1} = \frac{1}{k} = \frac{1}{k_r} + \frac{1}{k_v} \qquad (5\text{-}18)$$

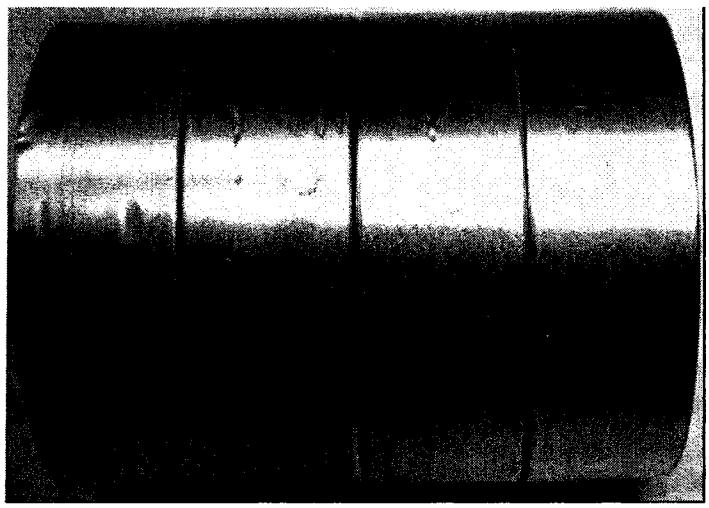

Figure 5-10. Morphology of specimen's surface after running experiments

In our experiments, the self-corrosion current densities for the A1045CS steel in slurries made from tap water were in range of 2×10^{-6} to 1×10^{-5} A/cm^2, which is much lower than the limited current densities (8×10^{-4} to 2×10^{-3} A/cm^2) (Sankaran, 2004). This is indicated that the process of corrosion is not totally controlled by the diffusion step because the corrosion current should be closed to the limiting current in the diffusion control (Gosman et al., 1981). It suggests that the corrosion is mainly controlled by the reaction step. So, the interface reaction dominates the corrosion process in the slurry. The reason is that under the conditions of high shear stress and impingements of suspended solids, the thickness of the boundary layer are strongly tabulated. It can be thought as the relative thickness of the boundary layer become less and less. Oxygen molecular easily migrates from the bulk liquid to the metal/liquid interface. The interface reaction coefficient k_r is far smaller than the migration coefficient k_v. So, the point is that the rate of interface reactions decides the rate of corrosion, that is, the mass transfer

coefficient k is almost equal to interface reaction coefficient k_r in the slurry. Basic on the equation 5-17, the mass transfer coefficient in the slurry can be expressed as follow:

$$\frac{1}{k} = \frac{1}{k_r} = \left(\frac{\partial \mathrm{Re}^{\beta}(1+C_s)^{\xi}}{nF\eta C_v} \right) \tag{5-19}$$

The comparison of the data measured from experiments and calculated form Equation (5-17) is depicted on the Figure 5-11 for A1045CS and Figure 5-12 for A1018CS. It is indicated that the new equation (5-17) can be used to calculate the experimental results.

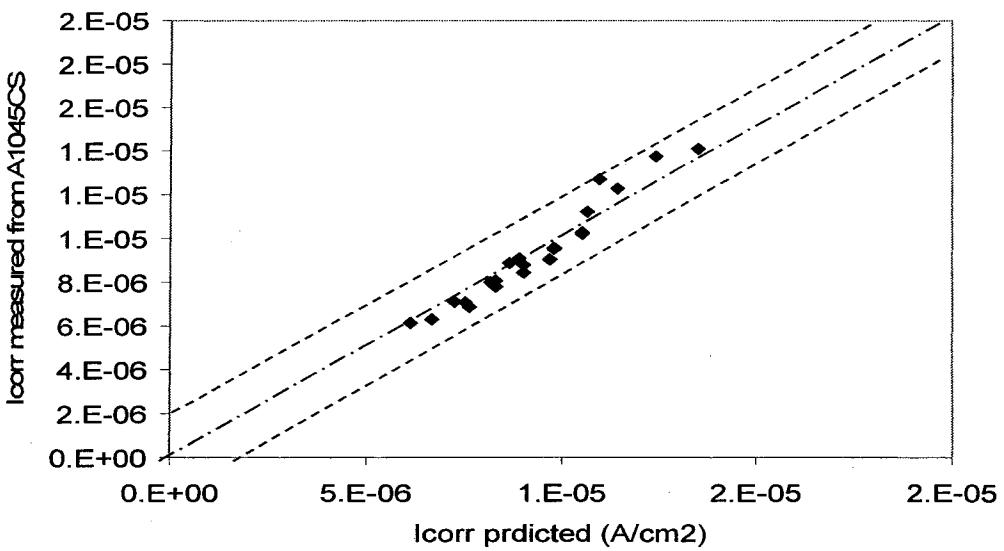

Figure 5-11. Compression of self-corrosion current predicted from Equation (5-17) and measured from experiments for A1045CS

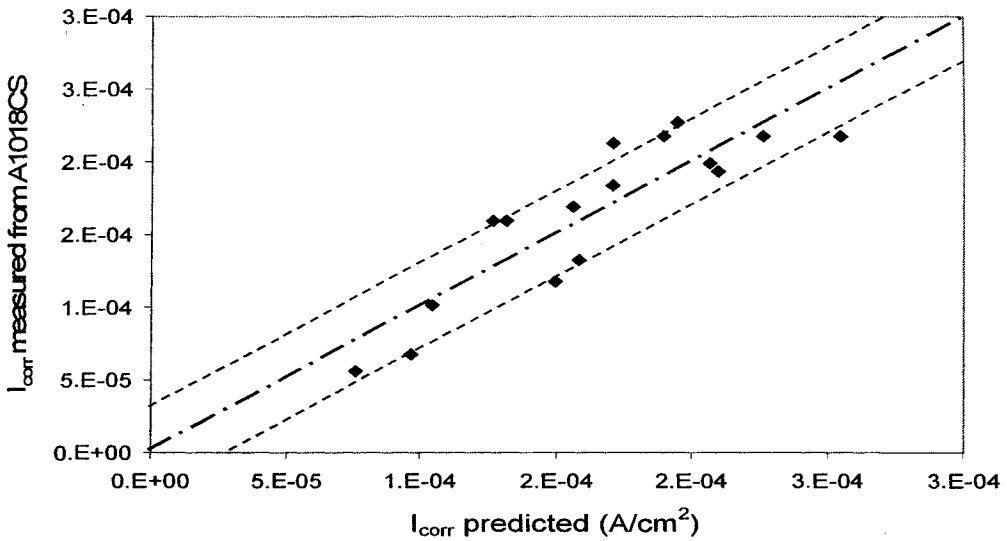

Figure 5-12. Compression of self-corrosion current predicted from Equation (5-17) measured from experiments for A1018CS

5.2.3. Mass Transfer Coefficients in Flowing Solution

Under the conditions of flowing solution free sand, the rate of corrosion w^0_c has a relationship with Reynolds Number. According to equation (5-10) it can be expressed as:

$$w^0_c = \alpha_0 \rho' \, \mathrm{Re}^{\beta_0} \tag{5-20}$$

The corrosion rate can be converted to corrosion current from equation (2-3) and (5-8)

$$i^0_{corr} = \alpha_0 \rho \mathrm{Re}^{\beta_0} = nF\eta_0 C_v k^0 \tag{5-21}$$

where $\alpha_0 = \frac{zF}{M_{Fe}} \alpha_0'$

The experimental data in the flowing solution are analyzed by a linear regression method in Macro Soft wear. The parameters of the equation (5-21) for A1018CS and A1045CS are listed in Table 5-7.

Table 5-7. Parameters α_0 and β_0 in the equation (5-21)

Material	α_0 (A/cm2)	β_0
A1018CS	2×10^{-11}	1.01
A1045CS	9×10^{-11}	0.87

Comparing with Table 5-5 and 5-7, the results show that the presence of sand particles promotes the corrosion reaction, and the corrosion current densities in the fluids containing sand are about 3-5 times of those in the flowing corrosive solution free of sand. The different exponents in the fluid with and without sand indicate different mechanisms controlling the corrosion process in the flowing slurries and flowing solutions. This statement is supported by the surface morphology of corroded samples after the tests. When the samples were tested in flowing solutions free of sand, the corroded surface covered with the thick corrosion scale of brown color. If the tests were conducted in flowing slurries, the test surfaces were free of corrosion scale. The exponents of test materials under the present slurry-erosion conditions are approximately independent of

the hydrodynamic parameters. It suggests that, under the present test conditions, the corrosion in the fluid with and without sand is controlled by different mechanism.

Based on the equation (5-6), the mass transfer coefficient k^0 in the flowing solution free of sand is rewritten as the equation (5-22) with the migration coefficient k_v^0, diffusion coefficient k_f^0 and interface reaction coefficient k_r^0, where the superscript "0" stress for the parameters in fluid free of solid particle.

:

$$\frac{1}{k^0}=\frac{1}{k_v^0}+\frac{1}{k_f^0}+\frac{1}{k_r^0} \qquad (5\text{-}22)$$

In the continuous flowing condition the migration of oxygen in bulk of solution is very fast. So the concentration of oxygen C_v is almost equal to concentration of oxygen on the surface of corrosion production layer C_f. As mention previously, the resistance of interface reaction R_f is far bigger than the migration resistance R_v in the slurry it is indicted that the migration resistance in the flowing solution can be ignored comparing with the interface reaction resistance R_r and diffusion resistance R_f. Therefore, the resistances $\frac{1}{k^0_r}+\frac{1}{k^0_f}$ of the mixed mode should be far bigger than the migration resistance $\frac{1}{k^0_v}$ in the flowing solution free of sand. The equation (5-22) can be simplified as;

$$\frac{1}{k^0} = \frac{1}{k^0_f} + \frac{1}{k^0_r} \tag{5-23}$$

Equation (5-23) is applicable for the corrosion of carbon steels in flowing tap water and tailing solution, owing to the existence of corrosion scale on the test surface. Combining equation (5-21) and (5-23) the relationship between the mass transport coefficients k^0_r, k^0_f and self-corrosion current densities i^0_{corr} in flowing solutions free of sand is developed at follow:

$$\left(\frac{i^0_{corr}}{nF\eta_0 C_v}\right)^{-1} = \frac{1}{k^0} = \frac{1}{k^0_f} + \frac{1}{k^0_r} \tag{5-24}$$

By inserting equation (5-21) to equation (5-24), the relationship of mass transfer coefficient and Reynolds Number in the solution free sand can be written as follow:

$$\frac{1}{k^0} = \frac{1}{k^0_f} + \frac{1}{k^0_r} = \left(\frac{\alpha_0 \mathrm{Re}^{\beta_0}}{nF\eta_0 C_v}\right) \tag{5-25}$$

5.2.4. Process Control in the Flowing Solution without Sand

Because the corrosion current is a function of mass transfer coefficient, the black line in the Figure 5-13 represents the function of reaction coefficient in slurry, and the pink line represents the function of the mass transfer coefficient in the flowing solution

free of sand. So the difference between the two lines can be thought of the contribution of the diffusion coefficient. How much does the diffusion step contribute to the corrosion process? It can be explained as follow.

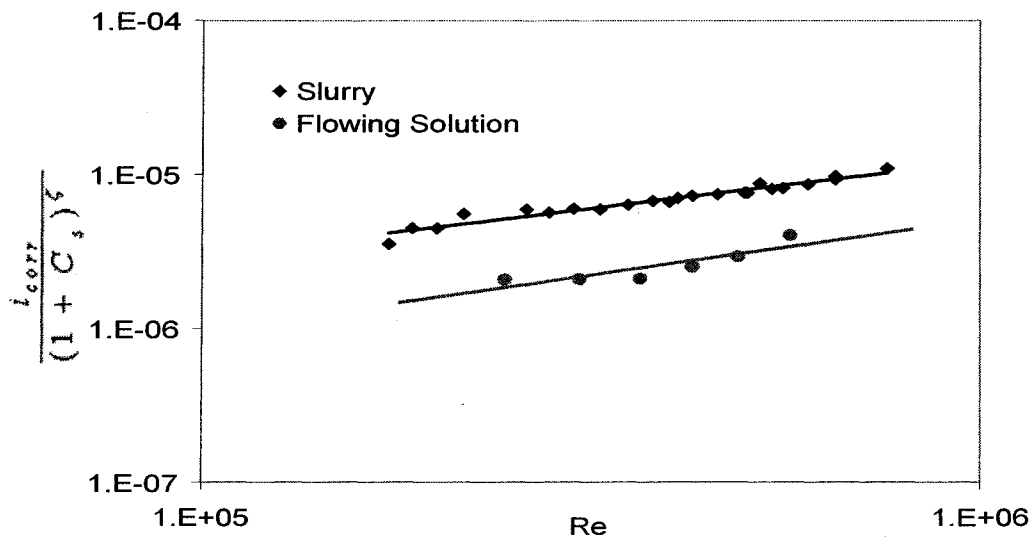

Figure 5-13. The contribution of mass transfer coefficients in the slurry and in the flowing solution free of sand

According to Equation (5-17) and (5-21), the ratio of corrosion current densities in flowing slurry and flowing solution free of sand can be expressed as:

$$\frac{i_{corr}^{0}}{i_{corr}} = \frac{k^{-1}}{k^{0\ -1}} = \frac{k_r^{-1}}{k_r^{0\ -1} + k_f^{0\ -1}} \tag{5-26}$$

Supposing the sand concentration is equal to zero, that is, the *Cs* in Equation (5-17) equal to zero, and also the coefficient $\eta\big|_{C_s=0} = \eta_0$ we have:

$$\frac{i_{corr}^{0}}{i_{corr}\big|_{C_s=0}} = \frac{k_r^{-1}\big|_{C_s=0}}{k^{0\,-1}} = \frac{\%}{\%}\mathrm{Re}^{\beta_0-\beta} \tag{5-27}$$

Assume $k_r\big|_{C_s=0} = k_r^0$ when the Reynolds number is hold unchanged, then

$$\frac{k_r^{0\,-1}}{k^{0\,-1}} = \frac{1}{1+k_f^{0\,-1}/k_r^{0\,-1}} = \frac{\%}{\%}\mathrm{Re}^{\beta_0-\beta} \tag{5-28}$$

The normalized value of $k_r^{0\,-1}/k^{0\,-1}$ represents the relative contribution of the interface reaction as one of controlling steps to the corrosion process in flowing solutions without solid particles.

Because of $\frac{k_r^{0\,-1}}{k^{0\,-1}} + \frac{k_f^{0\,-1}}{k^{0\,-1}} = 1$ in the corrosion process, the normalized value of $k_f^{0\,-1}/k^{0\,-1}$ represents the relative contribution of the diffusion step as one of controlling steps to the corrosion process in the flowing solutions.

The Reynolds numbers involved in the present test conditions are in range of 2×10^5 to1×10^6. The values of $k_r^{0\,-1}/k^{0\,-1}$ and $k_f^{0\,-1}/k^{0\,-1}$ for A1018CS and A1045CS are summarized in Table 5-8. The results of normalized coefficient showed whether the interface reaction step or diffusion step control the corrosion process in the flowing solution free of sand are dependent on the hydro parameter, that is, Reynolds Number, and corrosivity of media. When the Reynolds Number is raised, which corresponds high turbulence, the thickness of corrosion scale will be less and less and the interface reaction will play a more important role in controlling corrosion process. Because the tailing

solution is more corrosive than the tap water, the self-corrosion current densities of carbon steel in the tailing water are about one order of magnification higher than those in the tap water.

Because the interface reaction in the Figure 5-14 contributes to corrosion process over 56%., the corrosion process of carbon steel A1045CS in the flowing tap solution free of sand is dominated by mixed control, that is, interface reaction and diffusion steps. But, as the diffusion step in Figure 5-15 contributes to corrosion process about 90%, the corrosion of the carbon steel A1018CS in the flowing tailing solution free of sand is mainly dominated by the diffusion step.

The experimental results in Figure 5-8 show that the values of corrosion current i_{corr} for A1018CS measured in the tailing solution freed sand range from 1×10^{-5} A/cm^2 to 2×10^{-5} A/cm^2, but the values of limiting current in Figure 5-16 are around 4×10^{-5} A/cm^2 . Therefore the corrosion current is slightly small than values of the limiting current. So the corrosion process of A1018CS is mainly controlled by the diffusion step. According to above results the percentage contributed from diffusion step or from the reaction step is relative on the materials and corrosion media.

Table 5- 8. Normalized values of $k_r^{0\ -1}/k^{0\ -1}$ and $k_f^{0\ -1}/k^{0\ -1}$

Material	$k_r^{0\ -1}/k^{0\ -1}$		$k_f^{0\ -1}/k^{0\ -1}$	
	Re=2×10^5	Re=1×10^6	Re=2×10^5	Re=1×10^6
A1018CS	0.08	0.10	0.92	0.90
A1045CS	0.56	0.96	0.44	0.04

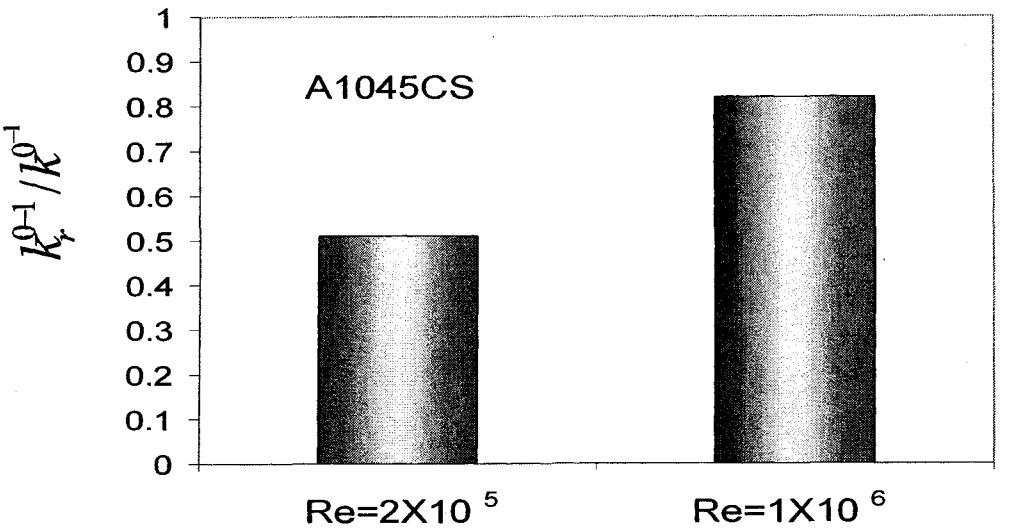

Figure 5-14. The percentage of the interface reaction step contribute to corrosion process in flowing tap solution

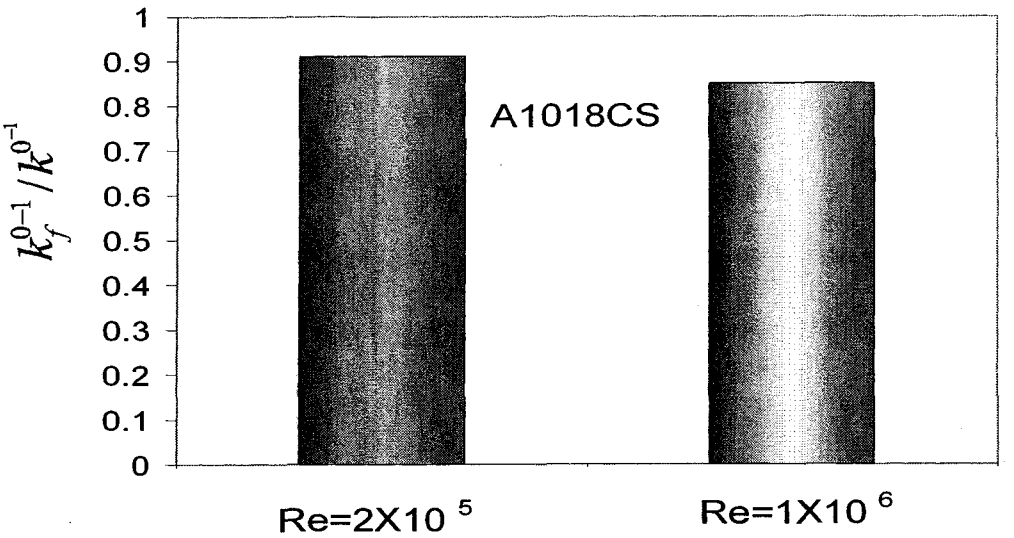

Figure 5-15. The percentage of the diffusion reaction step contribute to corrosion process in flowing tailing solution

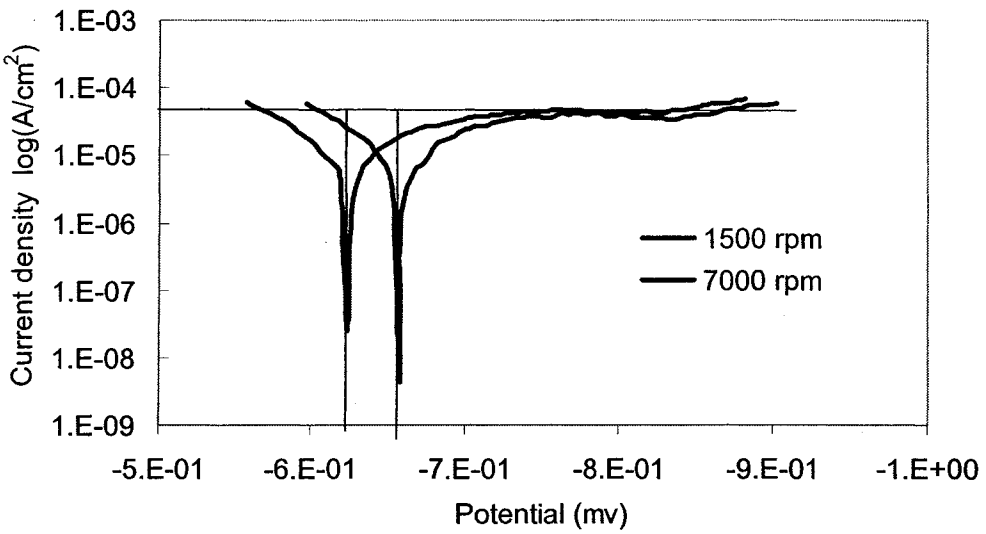

Figure 5-16. Relationships between mass transfer coefficients and Reynolds Number in flowing solution.

5.3. Chemo-Mechanical Effect in Slurry Erosion at OCP

5.3.1. Evaluation of Corrosion-Enhanced Erosion at OCP

In the Section 4, we established a predictive model for the wastage of corrosion-enhanced erosion based on test data of slurry erosion-corrosion under the galvanostatic conditions and a theoretical model of non-equilibrium thermodynamics, as given by Equation (4-8)

$$\frac{w_e^c}{w_e^0} = 0.37 \log\left(\frac{i}{1.84\times10^{-5} U^{2.44} C_{sand}{}^{0.91}}\right) \tag{4-8}$$

The applicability of Equation (4-8) at the condition OCP was checked and the results are shown in Figure 5-17. It is indicated that the Equation (4-8) can be used to predict the wastage of corrosion-enhanced erosion at OCP for both test materials. The relative large scatter band, especially in region of small w_e^c, may result from the test method for measuring w_e^c. Up to now, we are only able to measure w_e^c in an indirect way. It is determined from the test data of total weight loss w, pure erosion w_e^0 and corrosion W_c:

$$w_e^c = w - w_e^0 - w_c \tag{5-29}$$

The absolute error of w_e^c can be induced by the error of each quantity involve

$$\left|\Delta w_e^e\right| = \left|\Delta w\right| + \left|\Delta w_e^0\right| + \left|\Delta w_c\right| \tag{5-30}$$

Divide both side of Equation (5-29) and arrange it, we have

$$\frac{w_e^c}{w}\left|\frac{\Delta w_e^c}{w_e^c}\right| = \left|\frac{\Delta w}{w}\right| + \frac{w_e^0}{w}\left|\frac{\Delta w_e^0}{w_e^0}\right| + \frac{w_c}{w}\left|\frac{\Delta w_c}{w_c}\right| \tag{5-31}$$

Or

$$\Delta_e^c = \frac{w}{w_e^c}\left(\Delta + \frac{w_e^0}{w}\Delta_e^0 + \frac{w_c}{w}\Delta_c\right) = \frac{w}{w_e^c}\left(\Delta + \frac{w_e^0}{w}\Delta_e^0\right) + \frac{w_c}{w_e^c}\Delta_c \tag{5-32}$$

Where Δ_e^c, Δ Δ_e^0 and Δ_c the relative errors of corresponding quantities. Because the values of w and w_e^0 were measured with weight loss method, $\Delta = \Delta_e^0$ obviously, the value of w/w_e^c become small, the error of w_e^c will increase greatly.

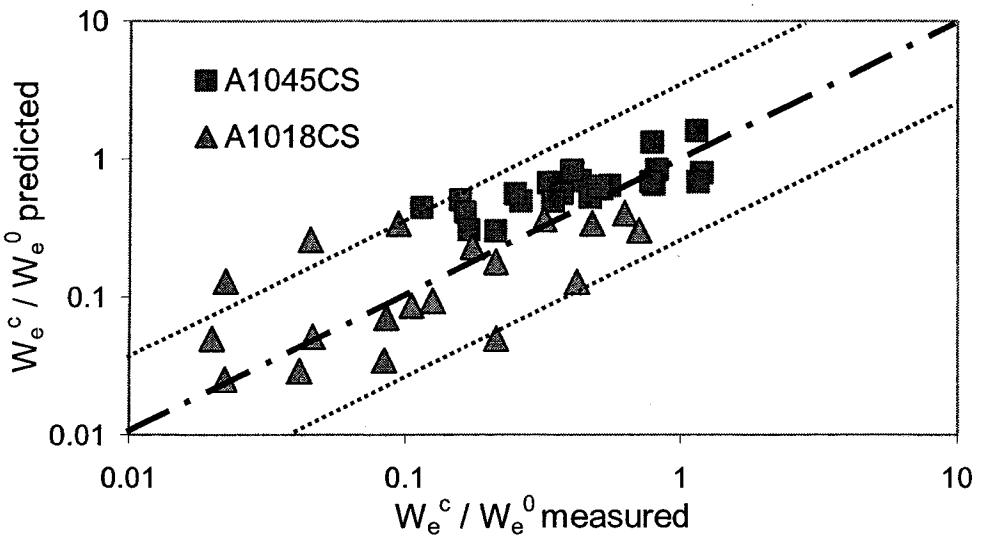

Figure 5-17. Synergy of corrosion enhanced erosion measured and predicted at OPC

5.3.2. Threshold Current i_{th} and Self-Corrosion Current i_{corr}

The threshold current density is a critical current density that is relative to many kinds of parameters in the slurry erosion, such as, flow rate and sand concentration (Zheng et al., 2000). If the corrosion current is below the threshold current no chemo-mechanical effect can be detected. Comparing Equation s (2-12) and (4-8), we have:

$$i_{th} = 1.84 \times 10^{-5} U^{2.44} C_s^{0.91} \quad (5\text{-}33)$$

The response surface obtained in line with Equation (5-33) is shown in Figure5-18, where we can see the value of i_{th} increases with flow velocity and sand concentration. In our test, the value of the synergy caused from chemo-mechanical effect ranges form 0 to 1. As if it is equal to zero, there is no any synergy of corrosion enhanced erosion because the total weight loss is equal to weight loss of pure erosion. Therefore, corrosion current equal to threshold current, that is, the values of corrosion current is on the response surface. So do that, below the response surface, no corrosion-enhanced erosion can be found. The corrosion-enhanced erosion can only be detected at the test conditions represented by the points above the response surface. So the threshold current is a critical current for producing the synergy.

The dependence of i_{th} and i_{corr} on the hydrodynamic parameters is shown in Figure5-19 and 5-20, in which the threshold current is calculated from Equation 5-33 and the normalization synergy is counted from Equation 4-8 as well as the data of w_e^c / w_e^0 and i_{corr} measured from experiments. The results indicate that the difference between the i_{th} and i_{corr} is reduced as the flowing velocity and sand concentration are increased. It suggests that the wastage of corrosion-enhanced erosion will decrease with the flowing velocity and sand concentration and, when the flowing velocity and sand concentration are sufficiently high, the difference between the i_{th} and i_{corr}, the corrosion-enhanced erosion caused by the chemo-mechanical effect will disappear.

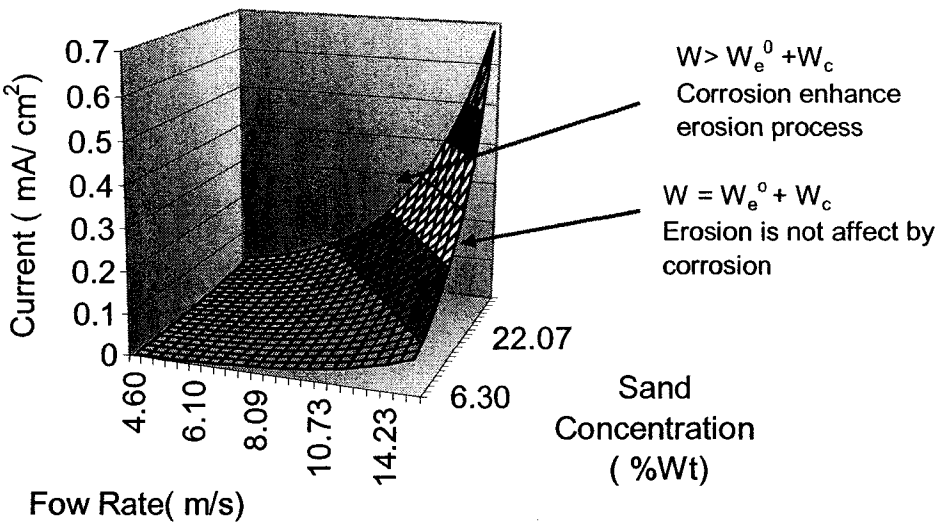

Figure 5-18. Response surface of thresholds current i_{th}

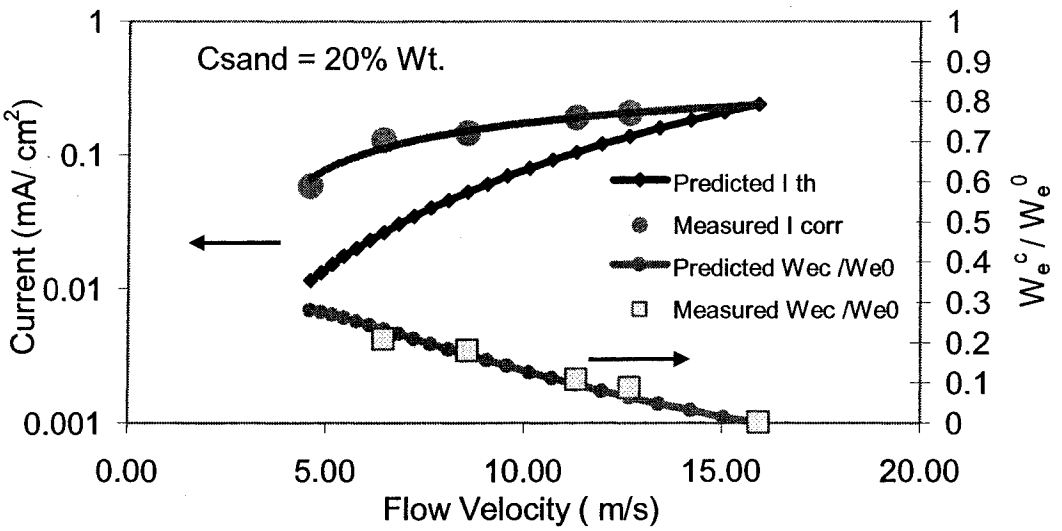

Figure 5-19. Difference of predicted i_{th} and measured i_{corr} vs. flow velocity at sand concentration 20% wt.

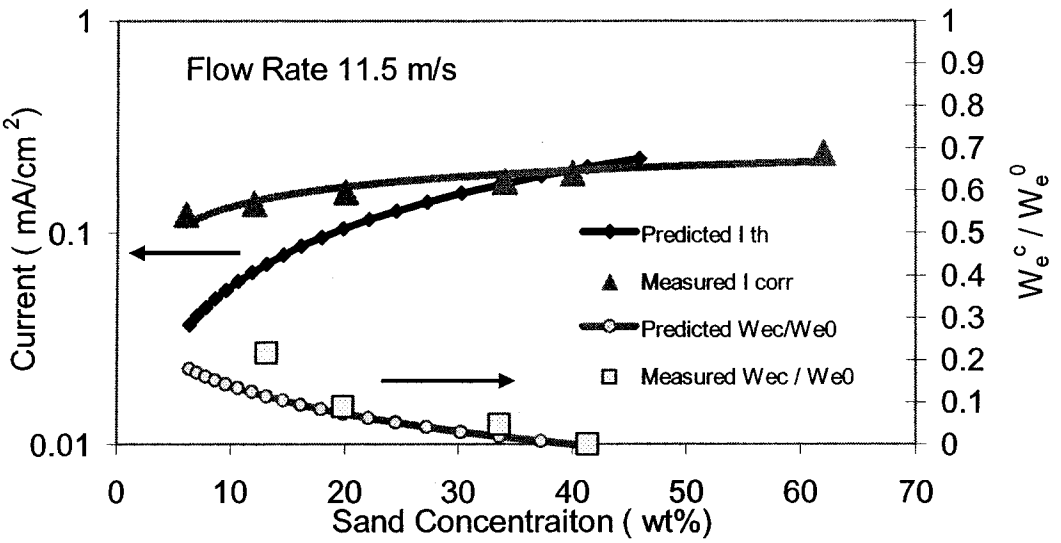

Figure 5-20. Difference of predicted i_{th} and measured i_{corr} vs. sand concentration at flow rate 11.5m/s

For both carbons steel the synergy resulted from chemo-mechanical effect is detected under the open circuit potential. The synergy of erosion-enhanced corrosion is decreased as increasing flow rate and sand concentration at the condition of OCP. The relative contribution of Mechano-chemical effect is expected to be more important when the sand concentration is low and the flow rate is lower. The results from A1018CS can be expressed as a logarithm function of relationship between the normalized synergy and hydro-parameters. The two characters can be seen in the Figures 5-21 and 5-22. One of them is the slop of curves kept the same values under the fixed sand concentration or fixed flow velocity. Another one is the curves of normalized synergy shift up or down when the fixed parameter is changed. Those agree with the results calculated from the Equation 4-8, that is, the regression formula of synergy about corrosion enhance erosion can be used to predicted the normalized synergy under the condition of OCP.

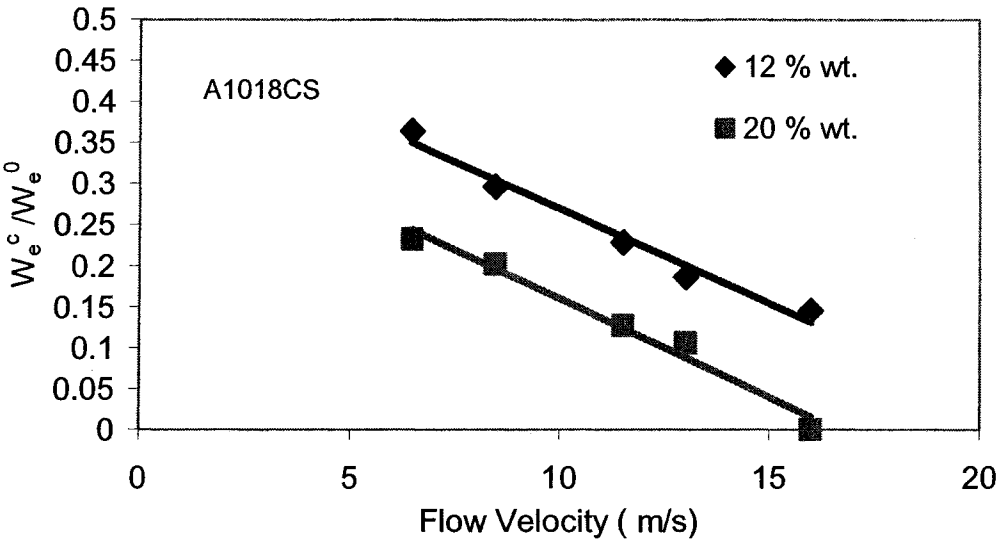

Figure 5-21. Normalized synergy w_e^c / w_e^0 of A1018CS vs. flow velocity under the fixed sand concentration at OPC condition

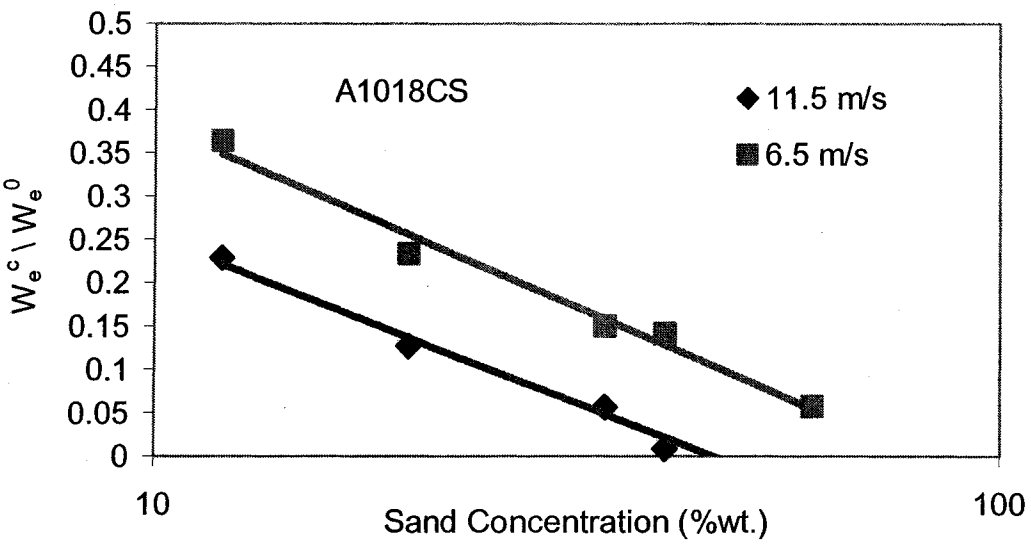

Figure 5-22. Normalized synergies w_e^c / w_e^0 of A1018CS vs. sand concentration under the fixed flow velocity at OCP condition

5.4. Mechano-Chemical Effect in Slurry erosion-corrosion at OCP

5.4.1 Erosion-Enhanced Corrosion at OCP

The weight loss of erosion enhanced corrosion in Figures 5-23 and 5-24 is a power function of flow rate and sand concentration. These results have indicated that the tendency of weight loss caused by mechano-chemical effect have the same tendency of weight loss caused by corrosion, in which the correlation between corrosion rate and hydrodynamic parameters has been well discusseded. Under slurry erosion-corrosion conditions in the practical engineering, Erosive action on the metal surface by removal of surface layers, passive layers, or base metal. Thus, it produces a more reactive surface and leads to the formation of new layers. For example, The stainless steel is put into the media containing chloride and reveals high corrosion rates due to the continuously fresh surface (Yong et al., 2000). In our case, the impingement of solid particles causes to turbulent the diffusion layer, rough the surface of metal and produce more active surface. Consquantally, the mechano-chemical effect makes the diffusion of oxygen fast and increase the rate of corrosion.

5.4.2 Evaluation of Erosion-Enhanced Corrosion at OCP

The results in Section 5.2 have shown clearly that the increases in flowing velocity and concentration of solid particles in slurry will promote the corrosion process at the OCP. It suggests the existence of mechno-chemical effect resulting in erosion-

enhanced corrosion. According the defination, the wastage of erosion-enahnced corrosion is given by

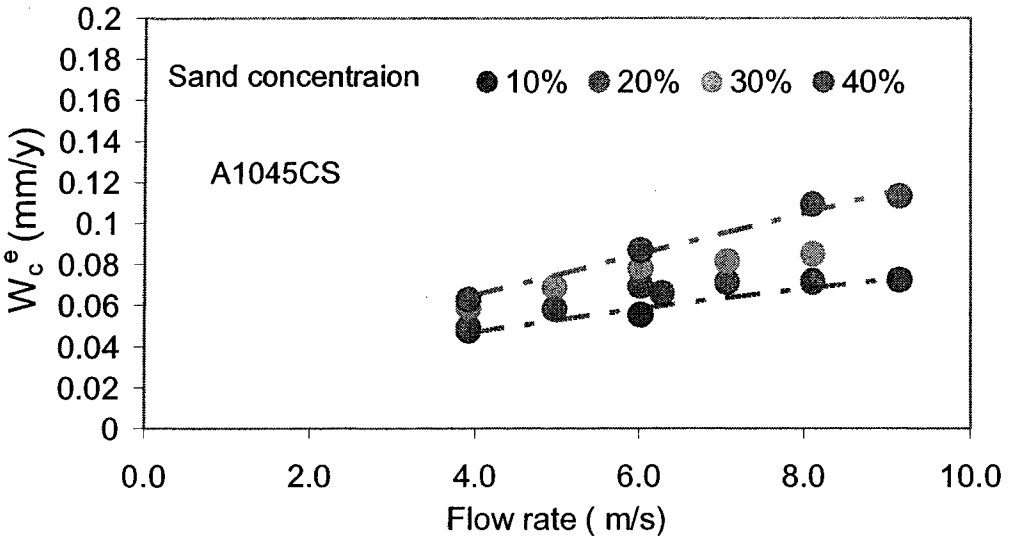

Figure 5-23. Synergism of w_c^e vs. flow rate for A1045CS in tap water slurry

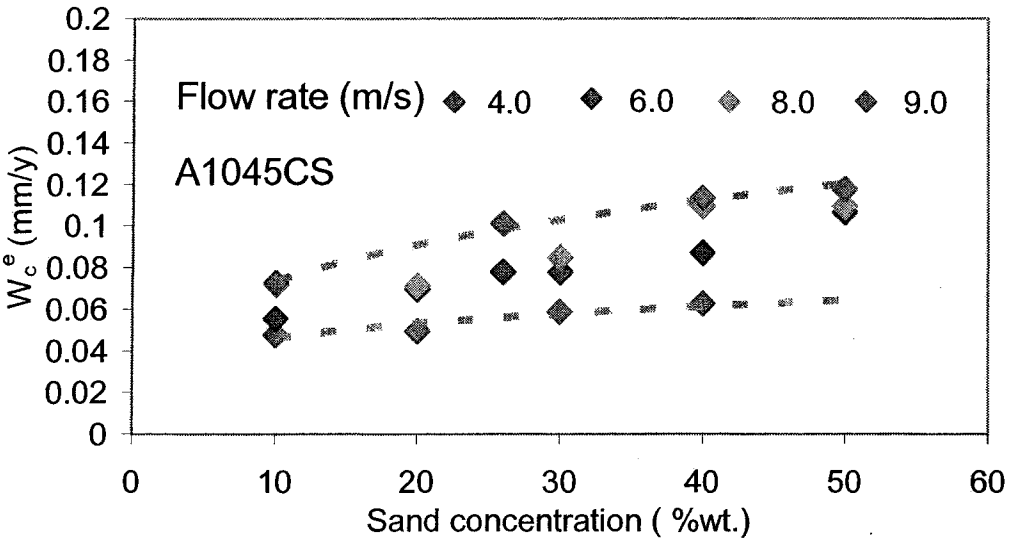

Figure 5-24. Synergism of erosion enhanced corrosion vs. sand concentration for A1045CS in tap water slurry

$$w_c^e = w_c - w_c^0 \tag{5-34}$$

It can also expressed by the increment of self-corrosion current density due to erosion

$$\Delta i_{corr} = i_{corr} - i_{corr}^0 \tag{5-35}$$

In line with theoretical model developed by Lu and Luo (2004), the erosion-enhanced corrosion in slurry erosion-corrosion results mainly from the dynamically plastic deformation at the surface caused by the impingement of sand particles, if the corrosion is governed by the interface electrochemical reaction, and the wastage of erosion-enhanced corrosion can be formulated as follows

$$w_c^e = ML\dot{\varepsilon}_p \tag{5-36}$$

Where $\dot{\varepsilon}_p$ is the plastic deformation rate at surface caused by the mechanical erosion process, M is atomic weight of test material and L is a constant related to ratio of the phenomenological coefficients in Onsager's reciprocity relations, L is a constant related to ratio of the phenomenological coefficients in Onsager's reciprocity relations. Obviously, the dynamically plastic deformation will be promoted by increasing turbulence strength and impingement frequency of solid particle and the intensity of mechanical erosion. The former relies mainly on the Reynolds number and the latter is a function of the concentration and the velocity of sand particles (Lindsley and Marder,

1998, and Sapate et al., 2000). Insert Equation (5-11) and (5-17) into Equation (5-34) or (5-35), for the normalized synergy of erosion enhanced corrosion is expressed as follow;

$$\frac{\Delta i_{corr}}{i_c^0} = \frac{\alpha_0}{\alpha_\beta} \mathrm{Re}^{\beta-\beta_0}(1+C_s)^{\zeta} - 1 \tag{5-37}$$

$$\frac{w_c^e}{w_c^0} = \frac{\alpha_0}{\alpha_\beta} \frac{M}{zF} \mathrm{Re}^{\beta-\beta_0}(1+C_s)^{\zeta} - 1 \tag{5-38}$$

The data in Figure5-25 shows that Equation (5-31) can give a good prediction on the wastage of erosion-enhanced corrosion measured from the test materials.

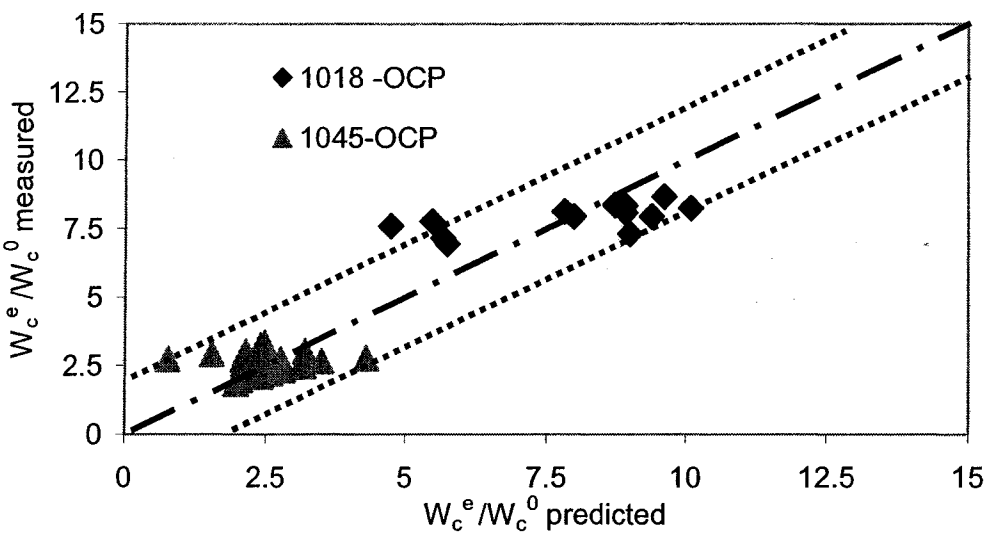

Figure 5-25. Data measured from experiments and predicted from Equation (5-38)

5. 5. Empirical Formula of Total Weight Loss

In our experiments the total weight loss can be formulated as a power function of flow rate, sand concentration and corrosion current corrosion.

$$w = m_{14} U^{m_{15}} C_s^{m_{16}} i^{m_{17}} \tag{5-39}$$

Where, constants m_{14}, m_{15}, m_{16}, m_{17} are experimental constants and are listed in the Table 5-9.

The comparison of predicted values and experimental values is plotted in Figure5-26. It is showed that the measured data can be fixed by the experimental formula under the three different conditions.

Table 5-9. Values of constants in equation (5-39) in different conditions

States	m_{14}	m_{15}	m_{16}	m_{17}
A1045CS in OCP	25.88	1.74	0.82	1.04
A1018CS in OCP	1.45	0.96	0.58	0.17
A1018CS in Galvanostatic	6.05	0.72	0.64	0.15

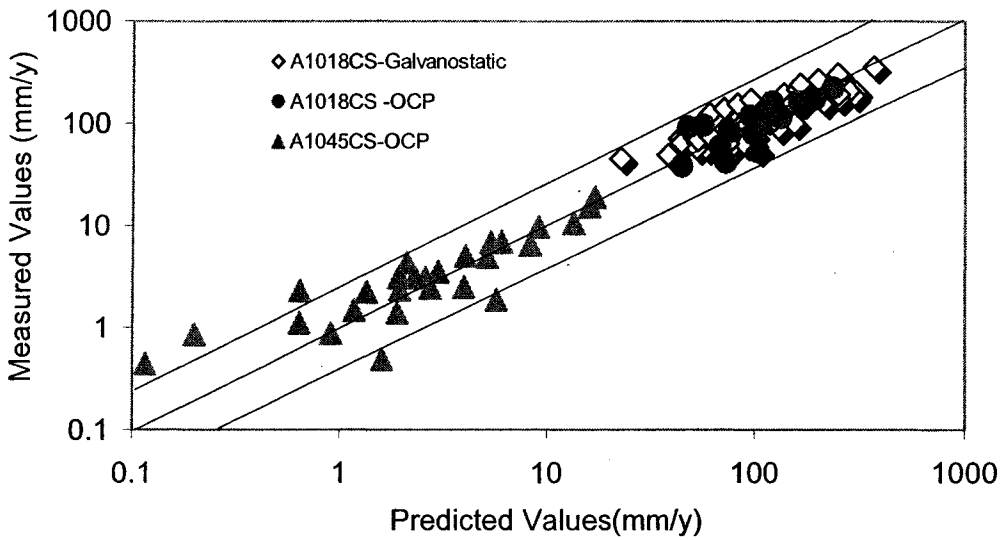

Figure 5-26. Comparison of the values measured and experimental for total weight loss.

References:

Blatt, W. K., Lotz, U. and Heitz, E. 1989. Influence of Hydrodynamics on Erosion-Corrosion in Two-phase Liquid-particle Flow. Corrosion **45(10):** 793-804.

Coeuret, F. and Legrand, J. 1981. Mass Transfer at the Electrodes of Concentric Cylindrical Reactors Combining Axial Flow and Rotation of the Inner Cylinder. Electrochemical Acta, **26:** 865-872.

Gosman, A. D., Tahry, S. El. and Launder. B. E. 1981. The Two-and Three-Dimensional Dispersal of a Passive Scalar in a Turbulent Boundary Layer. International Journal of Heat and Mass Transfer, **24 (1):** 35-46

Jiang, X., Li, S., Tao, D. and Yang, J. 1993. Accelerative Effect of Wear on Corrosion of High Alloy Stainless Steel. Corrosion, **49(10):** 836-841.

Kolman, D. G., Gaudett, M. A. and Scully, J. R. 1998. Modeling of Anodic Current Transients Resulting From Oxide Rupture of Plastically Strained Beta plus Alpha Titanium. Journal of the Electrochemical Society, **145(6):**1829-1840.

Lutz, U. and Postlethwaite, J. 1990. Erosion-Corrosion in Disturbed Two Phase Liquid/Particle Flow. Corrosion Science, **30(1):** 95-105.

Lindsley, B. A. and Marder, A. R. 1998. Solid Particle Erosion of a Fe-Fe Sub 3C Metal Matrix Composite. Metallurgical and Materials Transactions A: Physical Metallurgy and Materials Science. **29A (3):** 1071-1079.

Lu, B. T. and Luo, J. L. 2004. Chemo-Mechanical Effect in Erosion-Corrosion Process of Carbon Steel. CORROSION 2004, New Orleans, March 28-April 1, 2004.

Madsen, B. W. 1985. Study of Parameters Using a New Constant Wear-Rate Slurry Test. Wear of Materials, ASME, New York, 345-354.

Neville, A and Hu, X. 2001. Mechanical and Electrochemical Interactions during Liquid-Solid Impingement on High-Alloy Stainless Steels. Wear, **250-251:** 1284-1294

Poalson, B. 1983. Electrochemical Measurements in Flowing Solution. Corrosion Science, **23(4):** 391-430

Postlethwaite, J., Dobbin, M. H. and Bergevin, K. 1986. The Mechanism of Erosion-Corrosion in Slurry Pipelines. Materials Science Forum, **8:** 13-22.

Sankaran, S. R. 2004. Erosion-corrosion in Simulated Oil Sand Slurry Transportation. Master Thesis of University of Alberta.

Shadley, J. S., Sherazi, S. A., Dayalan, E., Ismail, M. and Rybicki, E. F. 1996. Erosion-Corrosion of Carbon Steel Elbow in a Carbon Dioxide Environment. Corrosion, **52:** 714-723.

Sapate, S. G., Rao, A. V. R. and Garg, N. K. 2000. Solid Particle Erosion Studies of Weld Hardfacing Deposits. Materials and Manufacturing Processes, **15(5):** 747-759

Wentzel, E. J. and Allen, C. 1997. Erosion-Corrosion Resistance of Tungsten Carbide Hard Metals. International Journal of Refractory Metals and Hard Materials, **15 (1-3):** 81-87.

Yong, X., Lin, Y., Liu, J. and Liu, S. 2000. Erosion-corrosion of Duplex Stainless Steel in Flowing Neutral Chloride Containing Sand. Acta Metallurgical Sinica, **37(7):** 745-748

Zheng, Y. G., Yang, F. F., Yao, Z. M. and Ke, W. 2000. On the Critical Flow Velocity for Erosion-Corrosion of Cu-Ni Alloy BFe30-1-1 in Artificial Sea Water, Zeitschrift für Metallkunde Materials Research and Advanced Techniques, **91(4):** 323-328

CHAPTER 6. CONCLUSIONS AND FUTURE WORK

6.1. Conclusions

The erosion-corrosion behavior of two carbon steels, A1018 and A1045, was investigated experimentally. Based on the theoretical model developed by Lu and Luo(2004) and the experimental observations, following conclusions were achieved.

(1). The relative contribution of total corrosion to the total material loss of carbon steels in the flowing slurries of near-neutral pH at the open circuit potential is less than 3%. The contribution of synergistic effect results mainly from the corrosion-enhanced erosion and it decreases with the flow velocity and sand concentration. In the flowing slurry with the sand concentration of 6 %wt and apparent flow velocity of 11.5m/s, the relative contribution of corrosion-enhanced erosion is about 61.59 %, but, when the sand concentration is 40%wt and the apparent flow velocity is raised to 11.5m/s, the wastage of corrosion-enhanced erosion is negligible.

(2). The experimental data of the present study confirm again that the pure mechanical erosion rate increases with decreasing hardness, the normalized wastage induced by the corrosion-enhanced erosion w_e^c / w_e^0 can be formulated as a linear function of the logarithm of corrosion current density and normalized wastage induced by the

corrosion-enhanced erosion w_c^e / w_c^0 can be formulated as a power function of wastage of pure erosion, as theoretically predicted.

(3). According to the regression analysis of experimental data, predictive models are established for the wastage of carbon steel caused by slurry erosion-corrosion. It can be used to formulate the effect of apparent flow velocity, sand concentration in slurry and anodic current density on each wastage component in the slurry erosion-corrosion.

(4). The interface electrochemical reaction dominates the corrosion process of carbon steels in flowing near-neutral pH slurries. Depending on the hydrodynamic conditions and corrosivity of media, the corrosion of carbon steels in flowing solutions free of solid particles may be controlled by the diffusion in surface scale or a mixed mode of diffusion in surface scale and interface reaction.

6.2. Future Work

The theoretical model of interaction of mechanical-chemical effects is well confirmed by the results of experiments under the range of flow rate 4-16 m/s and sand concentration 10-60% wt. In order to use the model in industry, the experiments in the flow loop should be performed.

Under our setup of erosion-corrosion and our experimental conditions, the weight loss of erosion-corrosion can be formulated as equation (5-33); it provides an experimental relationship between the weight loss with flow rate, sand concentration and

corrosion current. More tests, especially in the flow loop, are needed to confirm if it is suitable to other conditions.

APPENDIX A. EXPERIMENTAL DATA OF A1018CS IN TAINLING WATER SLURRY

A1. Test Conditions of Total Weight Loss for A1018CS

Order No.	Sample No.	Speed A	Sand B	Current C	Speed m/s	Sand wt%	Current mA/cm 2
1	902	-2	0.33	0	4.2	25	1
2	903	-2	0.33	0.75	4.2	25	2
3	113	-1.65	0	0	4.6	20	1
4	14	-1	-1	-0.75	5.9	10	0.5
5	F54	-1	-1	1	5.9	10	2.5
6	54"	-1	-1	1	5.9	10	2.5
7	54	-1	-1	1.65	5.9	10	4.6
8	42	-1	0.33	-1.65	5.9	25	0.25
9	43	-1	0.33	-0.75	5.9	25	0.5
10	44	-1	0.33	0	5.9	25	1
11	45	-1	0.33	0.75	5.9	25	2
12	46	-1	0.33	1.65	5.9	25	4.6
13	34	-1	1	-1.65	5.9	40	0.5
14	74	-1	1	1	5.9	40	2.5
15	F74	-1	1	1	5.9	40	2.5
16	f121	0	-1.65	0	8.5	6.5	1
17	69	0	-1.65	0.75	8.5	6.5	2
18	526	0	-1	0	8.5	10	1
19	521	0	-1	0.75	8.5	10	2
20	f131	0	0	-1.65	8.5	20	0.25
21	f91	0	0	0	8.5	20	1
22	f101	0	0	0	8.5	20	1
23	70	0	0	0.75	8.5	20	2

24	f161	0	0	1.65	8.5	20	4.6
25	562	0	0	1.65	8.5	20	4.6
26	5680	0	1	0	8.5	40	1
27	71	0	1	0.75	8.5	40	2
28	556	0	1.33	0	8.5	50	1
29	552	0	1.33	0.75	8.5	50	2
30	f151	0	1.65	0	8.5	60	1
31	72	0	1.65	0.75	8.5	60	2
32	62	0.2	-1	-1.65	9.5	10	0.25
33	63	0.2	-1	-0.75	9.5	10	0.5
34	64	0.2	-1	0	9.5	10	1
35	65	0.2	-1	0.75	9.5	10	2
36	66	0.2	-1	1.65	9.5	10	4.6
37	A132	0.2	0.33	-1.8	9.5	25	0.01
38	103	0.2	0.33	-1.65	9.5	25	0.25
39	162	0.2	0.33	-0.75	9.5	25	0.5
40	162'	0.2	0.33	-0.75	9.5	25	0.5
41	A32	0.2	0.33	0	9.5	25	1
42	b12	0.2	0.33	0.5	9.5	25	1.6
43	A162	0.2	0.33	0.75	9.5	25	2
44	A162*	0.2	0.33	1.65	9.5	25	4.6
45	62*	0.2	0.33	-1.65	9.5	25	0.25
46	63*	0.2	0.33	-0.75	9.5	25	0.5
47	64*	0.2	0.33	0	9.5	25	1
48	65*	0.2	0.33	0.75	9.5	25	2
49	B32	0.2	1.33	-1.8	9.5	50	0.01
50	152	0.2	1.33	-1.65	9.5	50	0.25
51	A102	0.2	1.33	-0.75	9.5	50	0.5
52	A152	0.2	1.33	0	9.5	50	1
53	b42	0.2	1.33	0.6	9.5	50	1.6
54	b52	0.2	1.33	0.75	9.5	50	2

55	652	0.2	1.33	1.65	9.5	50	4.6
56	821	1	-1	-1.65	12.3	10	0.25
57	22	1	-1	-0.75	12.3	10	0.5
58	62	1	-1	0.75	12.3	10	2
59	62"	1	-1	1	12.3	10	2.5
60	F62	1	-1	1	12.3	10	2.5
61	822	1	-1	1.65	12.3	10	4.6
62	82	1	0.33	-1.65	12.3	25	0.25
63	83	1	0.33	-0.75	12.3	25	0.5
64	84	1	0.33	0	12.3	25	1
65	85	1	0.33	0.75	12.3	25	2
66	852	1	0.33	1.65	12.3	25	4.6
67	42	1	1	-0.75	12.3	40	0.5
68	F162	1	1	0	12.3	40	1
69	82	1	1	1	12.3	40	2.5
70	82	1	1.33	-1.65	12.3	50	0.25
71	83	1	1.33	-0.75	12.3	50	0.5
72	84	1	1.33	0	12.3	50	1
73	85	1	1.33	0.75	12.3	50	2
74	86	1	1.33	1.65	12.3	50	4.6
75	144	1.45	0.33	0	14.5	25	1
76	68	1.45	0.33	0.75	14.5	25	2
77	184	1.45	1.33	1.65	14.5	50	6.4
78	144	1.65	0	0	15.7	20	1
79	102	1.65	-0.75		16	12	OCP
80	424	-1	-0.75		6.5	12	OCP
81	468	-1	0.75		6.5	34	OCP
82	480	-1	1		6.5	40	OCP
83	4120	-1	1.65		6.5	60	OCP
84	12o	0.75	-1.65		11.5	6	OCP
85	24o'	0.75	-0.75		11.5	12	OCP

86	40o	0.75	0		11.5	20	OCP
87	68o	0.75	0.75		11.5	34	OCP
88	80o	0.75	1		11.5	40	OCP
89	120o	0.75	1.65		11.5	60	OCP
90	304	-1.65	0		4.5	20	OCP
91	404	-1	0		6.5	20	OCP
92	554	0	0		8.5	20	OCP
93	40o	0.75	0		11.5	20	OCP
94	814	1	0		13	20	OCP
95	124	1.65	0		16	20	OCP

A2. Test Conditions of Pure Erosion Loss for A1018CS

Order	Sample	Speed	Sand	Current	Speed	Sand	Current
No.	No.	A	B	C	m/s	wt%	mA/cm2
101	114c	-2	0.33		4.2	25	cp
102	113c	-1.65	0		4.6	20	cp
103	380	-1.65	1		4.6	40	cp
104	14c	-1	-1		5.9	10	cp
105	41	-1	0.33		5.9	25	cp
106	34c	-1	1		5.9	40	cp
107	f121c	0	-1.65		8.5	6.5	cp
108	510	0	-1		8.5	10	cp
109	f91c	0	0		8.5	20	cp
110	5680c	0	1		8.5	40	cp
111	550	0	1.33		8.5	50	cp
112	f151c	0	1.65		8.5	60	cp
113	61	0.2	-1		9.5	10	cp
114	93c	0.2	0.33		9.5	25	cp

115	93c	0.2	0.33		9.5	25	cp
116	61*	0.2	0.33		9.5	25	cp
117	152c'	0.2	1.33		9.5	50	cp
118	152c'	0.2	1.33		9.5	50	cp
119	22c	1	-1		12.3	10	cp
120	81	1	0.33		12.3	25	cp
121	81	1	0.33		12.3	25	cp
122	42c	1	1		12.3	40	cp
123	81	1	1.33		12.3	50	cp
124	144c	1.45	0.33		14.5	25	cp
125	184c	1.45	1.33		14.5	50	cp
126	144c	1.65	0		15.7	20	cp
127	1010	1.65	-1		15.7	10	cp
128	1040	1.65	1		15.7	40	cp
129	102	1.65	-0.75		16	12	cp
130	424	-1	-0.75		6.5	12	cp
131	468	-1	0.75		6.5	34	cp
132	480	-1	1		6.5	40	cp
133	4120	-1	1.65		6.5	60	cp
134	12o	0.75	-1.65		11.5	6	cp
135	24o'	0.75	-0.75		11.5	12	cp
136	40o	0.75	0		11.5	20	cp
137	68o	0.75	0.75		11.5	34	cp
138	80o	0.75	1		11.5	40	cp
139	120o	0.75	1.65		11.5	60	cp
140	304	-1.65	0		4.5	20	cp
141	404	-1	0		6.5	20	cp
142	554	0	0		8.5	20	cp
143	40o	0.75	0		11.5	20	cp
144	814	1	0		13	20	cp
145	124	1.65	0		16	20	cp

A3. Raw Data of Total Weight Loss on A1018CS in tailing water slurry

Order	Weight loss (g/cm2-hr.)				
No.	1	2	3	4	w
1	3.57E-03	4.41E-03	3.63E-03		3.87E-03
2	5.94E-03	5.09E-03	4.24E-03		5.09E-03
3	4.14E-03	3.89E-03	3.79E-03		3.94E-03
4	1.97E-03	2.50E-03	1.58E-03		2.02E-03
5	8.25E-03	7.29E-03	5.00E-03		6.85E-03
6	2.80E-03	3.61E-03	4.16E-03		5.19E-03
7	8.17E-03	7.04E-03	8.79E-03		8.00E-03
8	7.80E-03	2.26E-03	3.50E-03		4.52E-03
9	6.62E-03	6.27E-03	5.57E-03	2.63E-03	5.28E-03
10	5.57E-03	9.14E-03	5.32E-03	4.33E-03	6.09E-03
11	8.60E-03	5.32E-03	8.50E-03		7.47E-03
12	9.97E-03	9.81E-03	1.07E-02	1.41E-02	1.12E-02
13	5.30E-03	6.04E-03	5.53E-03		5.62E-03
14	6.75E-03	6.94E-03	6.37E-03		9.64E-03
15	1.36E-02	1.44E-02	9.84E-03		1.26E-02
16	3.34E-03	3.26E-03	3.58E-03		3.40E-03
17	1.02E-02	8.33E-03	9.28E-03		9.28E-03
18	5.67E-03	3.82E-03	4.75E-03		4.75E-03
19	7.68E-03	5.51E-03	5.13E-03		6.10E-03
20	6.21E-03	6.21E-03	6.88E-03	5.48E-03	6.19E-03
21	8.66E-03	9.62E-03	7.23E-03		8.50E-03
22	1.01E-02	6.66E-03	7.20E-03		7.98E-03
23	1.33E-02	7.20E-03	9.52E-03		1.00E-02
24	1.20E-02	1.12E-02	1.30E-02		1.21E-02
25	1.20E-02	1.30E-02	1.28E-02		1.26E-02
26	1.90E-02	2.00E-02	1.87E-02		1.92E-02
27	2.62E-02	2.00E-02	2.18E-02		2.27E-02

28	3.27E-02	1.42E-02	2.35E-02		2.35E-02
29	1.92E-02	2.90E-02	3.43E-02		2.75E-02
30	2.80E-02	2.23E-02	2.93E-02		2.65E-02
31	3.37E-02	2.60E-02	2.99E-02		2.99E-02
32	3.95E-03	5.10E-03	5.10E-03		4.71E-03
33	4.68E-03	4.62E-03	4.04E-03	1.03E-02	5.90E-03
34	4.08E-03	5.61E-03	1.05E-02		6.72E-03
35	6.82E-03	8.22E-03	1.14E-02		8.82E-03
36	9.68E-03	1.36E-02	1.16E-02		1.16E-02
37	7.50E-03	7.37E-03	5.14E-03		6.67E-03
38	8.15E-03	7.79E-03	6.04E-03		7.32E-03
39	5.76E-03	6.66E-03	7.60E-03		7.60E-03
40	7.68E-03	8.92E-03	9.00E-03		8.53E-03
41	9.00E-03	1.01E-02	1.05E-02		9.86E-03
42	1.15E-02	9.90E-03	1.18E-02		1.11E-02
43	1.13E-02	1.19E-02	1.16E-02		1.16E-02
44	1.36E-02	1.49E-02	1.62E-02		1.49E-02
45	9.04E-03	9.11E-03	8.41E-03		8.85E-03
46	1.05E-02	9.97E-03	1.10E-02		1.05E-02
47	1.24E-02	1.27E-02	1.06E-02		1.19E-02
48	1.14E-02	1.31E-02	1.40E-02		1.28E-02
49	1.03E-02	1.70E-02	1.43E-02		1.39E-02
50	1.68E-02	1.67E-02	8.84E-03	1.63E-02	1.47E-02
51	1.15E-02	2.04E-02	1.55E-02		1.58E-02
52	2.25E-02	1.37E-02	1.51E-02		1.71E-02
53	1.67E-02	1.72E-02	1.69E-02		1.69E-02
54	1.98E-02	1.87E-02	2.09E-02		1.98E-02
55	2.58E-02	1.82E-02	2.20E-02		2.20E-02
56	5.16E-03	4.36E-03	4.76E-03		4.76E-03
57	4.95E-03	5.24E-03	5.92E-03		5.37E-03
58	5.84E-03	9.52E-03	7.48E-03		7.62E-03

59	8.25E-03	9.39E-03	8.82E-03		8.82E-03
60	7.48E-03	7.36E-03	8.12E-03		8.24E-03
61	1.19E-02	9.46E-03	1.19E-02		1.11E-02
62	5.84E-03	5.00E-03	5.42E-03		5.42E-03
63	6.37E-03	5.51E-03	7.23E-03		6.37E-03
64	7.74E-03	8.95E-03	5.73E-03		7.47E-03
65	1.01E-02	8.65E-03	7.20E-03		8.65E-03
66	1.87E-02	1.62E-02	1.97E-02		1.82E-02
67	2.63E-02	2.77E-02	2.70E-02		2.70E-02
68	2.56E-02	2.55E-02	2.55E-02		2.55E-02
69	2.99E-02	3.15E-02	2.94E-02	3.19E-02	3.07E-02
70	1.09E-02	1.45E-02	1.19E-02		1.24E-02
71	1.78E-02	1.45E-02	1.12E-02		1.45E-02
72	1.49E-02	1.42E-02	1.55E-02		1.49E-02
73	1.79E-02	1.84E-02	1.82E-02		1.82E-02
74	2.46E-02	2.05E-02	2.25E-02		2.25E-02
75	1.87E-02	2.62E-02	2.35E-02		2.28E-02
76	2.27E-02	2.18E-02	2.35E-02		2.27E-02
77	3.63E-02	3.17E-02	3.24E-02		3.35E-02
78	1.28E-02	1.27E-02	1.53E-02		1.36E-02
79	6.84E-03	8.54E-03			8.54E-03
80	5.57E-03	6.82E-03	6.11E-03		6.46E-03
81	3.82E-03	3.89E-03	4.65E-03		4.27E-03
82	5.29E-03	4.78E-03			5.03E-03
83	9.59E-03	1.08E-02	1.22E-02		1.15E-02
84	9.49E-03	9.30E-03	9.39E-03		9.39E-03
85	8.76E-03	8.85E-03	8.81E-03		8.81E-03
86	1.35E-02	1.39E-02	1.29E-02	7.64E-03	1.20E-02
87	9.97E-03	1.50E-02	1.93E-02		1.48E-02
88	1.22E-02	2.07E-02	1.90E-02		1.73E-02
89	2.20E-02	2.05E-02	2.13E-02		2.13E-02

90	3.86E-03	3.96E-03	3.96E-03		3.96E-03
91	6.21E-03	5.99E-03	6.10E-03		6.10E-03
92	5.03E-03	4.59E-03	1.06E-02		6.74E-03
93	1.29E-02	7.64E-03	1.03E-02		1.03E-02
94	1.63E-02	6.85E-03	8.79E-03		1.06E-02
95	1.33E-02	1.08E-02	8.79E-03		1.10E-02

A4. Raw Data of Pure Erosion Loss on A1018CS on Tailing Water Slurry

Order	Weight loss (g/cm2-hr.)				
No.	1	2	3	4	we0
101	1.85E-03	1.34E-03	1.84E-03		1.67E-03
102	1.74E-03	2.56E-03	1.83E-03		2.05E-03
103	4.97E-03	3.50E-03	4.24E-03		4.24E-03
104	1.27E-03	1.34E-03	1.42E-03		1.34E-03
105	2.58E-03	3.41E-03	3.28E-03		3.09E-03
106	3.81E-03	3.96E-03	4.46E-03		4.08E-03
107	1.49E-03	1.32E-03	1.43E-03		1.41E-03
108	2.85E-03	3.18E-03	2.52E-03		2.85E-03
109	5.67E-03	5.91E-03	4.71E-03		5.31E-03
110	1.13E-02	1.73E-02	1.43E-02		1.43E-02
111	2.18E-02	1.70E-02	1.94E-02		1.94E-02
112	1.72E-02	2.40E-02	2.13E-02		2.08E-02
113	3.69E-03	3.25E-03	3.47E-03		3.47E-03
114	5.26E-03	5.43E-03	7.17E-03		5.95E-03
115	5.26E-03	5.43E-03	7.17E-03		5.95E-03
116	9.14E-03	1.07E-02	7.99E-03		7.61E-03

117	1.33E-02	1.94E-02	1.19E-02	8.32E-03	1.33E-02
118	1.33E-02	1.19E-02	8.32E-03		1.12E-02
119	3.68E-03	3.47E-03	3.89E-03		3.68E-03
120	3.38E-03	5.67E-03	4.52E-03		4.52E-03
121	1.19E-02	1.24E-02	1.04E-02		1.16E-02
122	2.03E-02	2.16E-02	1.91E-02		2.03E-02
123	1.19E-02	1.24E-02	1.22E-02		1.22E-02
124	1.49E-02	1.66E-02	1.80E-02		1.65E-02
125	2.26E-02	3.71E-02	2.86E-02		2.94E-02
126	9.75E-03	9.11E-03	9.43E-03		9.43E-03
127	4.11E-03	4.84E-03	4.47E-03		4.47E-03
128	2.24E-02	2.24E-02			2.24E-02
129	4.65E-02	7.61E-03	7.20E-03		7.40E-03
130	2.83E-02	5.22E-03	5.35E-03	2.93E-03	4.50E-03
131	2.32E-02	4.01E-03	3.38E-03		3.69E-03
132	2.92E-02	4.65E-03	4.97E-03		4.65E-03
133	6.96E-02	1.11E-02	1.07E-02	7.17E-03	1.11E-02
134	3.63E-03	3.38E-03	3.44E-03		3.48E-03
135	6.88E-03	7.39E-03	7.13E-03		7.13E-03
136	1.22E-02	1.20E-02	8.37E-03		1.09E-02
137	1.52E-02	1.08E-02	1.58E-02		1.39E-02
138	2.54E-02	1.71E-02	1.29E-02	1.31E-02	1.71E-02
139	2.71E-02	1.70E-02	2.20E-02		2.20E-02
140	1.56E-03	1.94E-03	1.55E-03		1.68E-03
141	4.93E-03	4.93E-03			4.93E-03
142	5.61E-03	5.56E-03	5.58E-03		5.58E-03
143	1.22E-02	8.37E-03	6.88E-03		9.10E-03
144	9.46E-03	9.72E-03	9.59E-03		9.59E-03
145	1.20E-02	9.87E-03	1.09E-02		1.09E-02

A5. Total Weight Loss and its Components

Order No.	W g/cm2-hr	We 0 g/cm2-hr	Wc0 g/cm2-hr	Wc g/cm2-hr	We g/cm2-hr	Ws g/cm2-hr	Wce g/cm2-hr	Wec g/cm2-hr
1	3.9E-03	1.7E-03	7.1E-06	1.0E-03	2.8E-03	2.2E-03	1.0E-03	1.2E-03
2	5.1E-03	1.7E-03	7.1E-06	2.1E-03	3.0E-03	3.4E-03	2.1E-03	1.3E-03
3	3.9E-03	2.0E-03	9.0E-06	1.0E-03	2.9E-03	1.9E-03	1.0E-03	8.5E-04
4	2.0E-03	1.3E-03	9.8E-06	5.2E-04	1.5E-03	6.7E-04	5.1E-04	1.5E-04
5	6.8E-03	1.3E-03	9.8E-06	2.6E-03	4.2E-03	5.5E-03	2.6E-03	2.9E-03
6	5.2E-03	1.3E-03	9.8E-06	2.6E-03	2.6E-03	3.8E-03	2.6E-03	1.2E-03
7	8.0E-03	1.3E-03	9.8E-06	4.8E-03	3.2E-03	6.6E-03	4.8E-03	1.9E-03
8	4.5E-03	3.1E-03	9.8E-06	2.6E-04	4.3E-03	1.4E-03	2.5E-04	1.2E-03
9	5.3E-03	3.1E-03	9.8E-06	5.2E-04	4.8E-03	2.2E-03	5.1E-04	1.7E-03
10	6.1E-03	3.1E-03	9.8E-06	1.0E-03	5.0E-03	3.0E-03	1.0E-03	2.0E-03
11	7.5E-03	3.1E-03	9.8E-06	2.1E-03	5.4E-03	4.4E-03	2.1E-03	2.3E-03
12	1.1E-02	3.1E-03	9.8E-06	4.8E-03	6.4E-03	8.1E-03	4.8E-03	3.3E-03
13	5.6E-03	4.1E-03	9.8E-06	5.2E-04	5.1E-03	1.5E-03	5.1E-04	1.0E-03
14	9.6E-03	4.1E-03	9.8E-06	2.6E-03	7.0E-03	5.6E-03	2.6E-03	3.0E-03
15	1.3E-02	4.1E-03	9.8E-06	2.6E-03	1.0E-02	8.5E-03	2.6E-03	5.9E-03
16	3.4E-03	1.4E-03	1.1E-05	1.0E-03	2.4E-03	2.0E-03	1.0E-03	9.4E-04
17	9.3E-03	1.4E-03	1.1E-05	2.1E-03	7.2E-03	7.9E-03	2.1E-03	5.8E-03
18	4.7E-03	2.9E-03	1.1E-05	1.0E-03	3.7E-03	1.9E-03	1.0E-03	8.5E-04
19	6.1E-03	2.9E-03	1.1E-05	2.1E-03	4.0E-03	3.2E-03	2.1E-03	1.2E-03
20	6.2E-03	5.3E-03	1.1E-05	2.6E-04	5.9E-03	8.7E-04	2.5E-04	6.2E-04
21	8.5E-03	5.3E-03	1.1E-05	1.0E-03	7.5E-03	3.2E-03	1.0E-03	2.2E-03
22	8.0E-03	5.3E-03	1.1E-05	1.0E-03	6.9E-03	2.7E-03	1.0E-03	1.6E-03
23	1.0E-02	5.3E-03	1.1E-05	2.1E-03	7.9E-03	4.7E-03	2.1E-03	2.6E-03
24	1.2E-02	5.3E-03	1.1E-05	4.8E-03	7.3E-03	6.8E-03	4.8E-03	2.0E-03
25	1.3E-02	5.3E-03	1.1E-05	4.8E-03	7.8E-03	7.3E-03	4.8E-03	2.5E-03
26	1.9E-02	1.4E-02	1.1E-05	1.0E-03	1.8E-02	4.9E-03	1.0E-03	3.9E-03

27	2.3E-02	1.4E-02	1.1E-05	2.1E-03	2.1E-02	8.3E-03	2.1E-03	6.3E-03
28	2.3E-02	1.9E-02	1.1E-05	1.0E-03	2.2E-02	4.0E-03	1.0E-03	3.0E-03
29	2.7E-02	1.9E-02	1.1E-05	2.1E-03	2.5E-02	8.1E-03	2.1E-03	6.0E-03
30	2.7E-02	2.1E-02	1.1E-05	1.0E-03	2.5E-02	5.6E-03	1.0E-03	4.6E-03
31	3.0E-02	2.1E-02	1.1E-05	2.1E-03	2.8E-02	9.0E-03	2.1E-03	7.0E-03
32	4.7E-03	3.5E-03	1.5E-05	2.6E-04	4.5E-03	1.2E-03	2.5E-04	9.8E-04
33	5.9E-03	3.5E-03	1.5E-05	5.2E-04	5.4E-03	2.4E-03	5.1E-04	1.9E-03
34	6.7E-03	3.5E-03	1.5E-05	1.0E-03	5.7E-03	3.2E-03	1.0E-03	2.2E-03
35	8.8E-03	3.5E-03	1.5E-05	2.1E-03	6.7E-03	5.3E-03	2.1E-03	3.3E-03
36	1.2E-02	3.5E-03	1.5E-05	4.8E-03	6.8E-03	8.1E-03	4.8E-03	3.4E-03
37	6.7E-03	6.0E-03	1.5E-05	1.0E-05	6.7E-03	7.0E-04	4.2E-06	7.1E-04
38	7.3E-03	6.0E-03	1.5E-05	2.6E-04	7.1E-03	1.4E-03	2.5E-04	1.1E-03
39	7.6E-03	6.0E-03	1.5E-05	5.2E-04	7.1E-03	1.6E-03	5.1E-04	1.1E-03
40	8.5E-03	6.0E-03	1.5E-05	5.2E-04	8.0E-03	2.6E-03	5.1E-04	2.1E-03
41	9.9E-03	6.0E-03	1.5E-05	1.0E-03	8.8E-03	3.9E-03	1.0E-03	2.9E-03
42	1.1E-02	6.0E-03	1.5E-05	1.7E-03	9.4E-03	5.1E-03	1.7E-03	3.4E-03
43	1.2E-02	6.0E-03	1.5E-05	2.1E-03	9.5E-03	5.6E-03	2.1E-03	3.6E-03
44	1.5E-02	6.0E-03	1.5E-05	4.8E-03	1.0E-02	9.0E-03	4.8E-03	4.2E-03
45	8.9E-03	7.6E-03	1.5E-05	2.6E-04	8.6E-03	1.2E-03	2.5E-04	9.8E-04
46	1.0E-02	7.6E-03	1.5E-05	5.2E-04	1.0E-02	2.8E-03	5.1E-04	2.3E-03
47	1.2E-02	7.6E-03	1.5E-05	1.0E-03	1.1E-02	4.3E-03	1.0E-03	3.2E-03
48	1.3E-02	7.6E-03	1.5E-05	2.1E-03	1.1E-02	5.2E-03	2.1E-03	3.1E-03
49	1.4E-02	1.3E-02	1.5E-05	2.1E-04	1.4E-02	6.2E-04	1.9E-04	4.2E-04
50	1.5E-02	1.3E-02	1.5E-05	2.6E-04	1.4E-02	1.4E-03	2.5E-04	1.1E-03
51	1.6E-02	1.3E-02	1.5E-05	5.2E-04	1.5E-02	2.5E-03	5.1E-04	2.0E-03
52	1.7E-02	1.3E-02	1.5E-05	1.0E-03	1.6E-02	3.8E-03	1.0E-03	2.8E-03
53	1.7E-02	1.3E-02	1.5E-05	1.7E-03	1.5E-02	3.7E-03	1.7E-03	2.0E-03
54	2.0E-02	1.3E-02	1.5E-05	2.1E-03	1.8E-02	6.5E-03	2.1E-03	4.4E-03
55	2.2E-02	1.1E-02	1.5E-05	4.8E-03	1.7E-02	1.1E-02	4.8E-03	6.0E-03
56	4.8E-03	3.7E-03	2.4E-05	2.6E-04	4.5E-03	1.1E-03	2.4E-04	8.2E-04
57	5.4E-03	3.7E-03	2.4E-05	5.2E-04	4.9E-03	1.7E-03	5.0E-04	1.2E-03

58	7.6E-03	3.7E-03	2.4E-05	2.1E-03	5.5E-03	3.9E-03	2.1E-03	1.9E-03
59	8.8E-03	3.7E-03	2.4E-05	2.6E-03	6.2E-03	5.1E-03	2.6E-03	2.5E-03
60	8.2E-03	3.7E-03	2.4E-05	2.6E-03	5.6E-03	4.5E-03	2.6E-03	2.0E-03
61	1.1E-02	3.7E-03	2.4E-05	4.8E-03	6.3E-03	7.4E-03	4.8E-03	2.6E-03
62	5.4E-03	4.5E-03	2.4E-05	2.6E-04	5.2E-03	8.8E-04	2.4E-04	6.4E-04
63	6.4E-03	4.5E-03	2.4E-05	5.2E-04	5.8E-03	1.8E-03	5.0E-04	1.3E-03
64	7.5E-03	4.5E-03	2.4E-05	1.0E-03	6.4E-03	2.9E-03	1.0E-03	1.9E-03
65	8.6E-03	4.5E-03	2.4E-05	2.1E-03	6.6E-03	4.1E-03	2.1E-03	2.0E-03
66	1.8E-02	1.2E-02	2.4E-05	4.8E-03	1.3E-02	6.6E-03	4.8E-03	1.8E-03
67	2.7E-02	2.0E-02	2.4E-05	5.2E-04	2.6E-02	6.7E-03	5.0E-04	6.2E-03
68	2.6E-02	2.0E-02	2.4E-05	1.0E-03	2.4E-02	5.2E-03	1.0E-03	4.2E-03
69	3.1E-02	2.0E-02	2.4E-05	2.6E-03	2.8E-02	1.0E-02	2.6E-03	7.7E-03
70	1.2E-02	1.2E-02	2.4E-05	2.6E-04	1.2E-02	2.4E-04	2.4E-04	5.0E-06
71	1.4E-02	1.2E-02	2.4E-05	5.2E-04	1.4E-02	2.3E-03	5.0E-04	1.8E-03
72	1.5E-02	1.2E-02	2.4E-05	1.0E-03	1.4E-02	2.7E-03	1.0E-03	1.7E-03
73	1.8E-02	1.2E-02	2.4E-05	2.1E-03	1.6E-02	6.0E-03	2.1E-03	3.9E-03
74	2.3E-02	1.2E-02	2.4E-05	4.8E-03	1.8E-02	1.0E-02	4.8E-03	5.6E-03
75	2.3E-02	1.6E-02	2.1E-05	1.0E-03	2.2E-02	6.3E-03	1.0E-03	5.3E-03
76	2.3E-02	1.6E-02	2.1E-05	2.1E-03	2.1E-02	6.2E-03	2.1E-03	4.1E-03
77	3.3E-02	2.9E-02	2.1E-05	1.0E-03	3.2E-02	4.0E-03	1.0E-03	3.0E-03
78	1.4E-02	9.4E-03	2.3E-05	1.0E-03	1.3E-02	4.1E-03	1.0E-03	3.1E-03
79	8.5E-03	7.4E-03	2.4E-05	2.1E-04	8.3E-03	1.1E-03	1.8E-04	9.3E-04
80	6.5E-03	4.5E-03	1.1E-05	7.3E-05	6.4E-03	2.0E-03	6.2E-05	1.9E-03
81	4.3E-03	3.7E-03	1.1E-05	2.2E-04	4.0E-03	5.6E-04	2.1E-04	3.5E-04
82	5.0E-03	4.6E-03	1.1E-05	1.7E-04	4.9E-03	3.7E-04	1.6E-04	2.1E-04
83	1.2E-02	1.1E-02	1.1E-05	1.8E-04	1.1E-02	4.2E-04	1.7E-04	2.5E-04
84	9.4E-03	3.5E-03	2.2E-05	1.3E-04	9.3E-03	5.9E-03	1.0E-04	5.8E-03
85	8.8E-03	7.1E-03	2.2E-05	1.4E-04	8.7E-03	1.6E-03	1.2E-04	1.5E-03
86	1.2E-02	1.1E-02	2.2E-05	2.0E-04	1.2E-02	1.1E-03	1.8E-04	9.1E-04
87	1.5E-02	1.4E-02	2.2E-05	2.4E-04	1.5E-02	8.0E-04	2.2E-04	5.8E-04
88	1.7E-02	1.7E-02	2.2E-05	2.1E-04	1.7E-02	1.5E-04	1.9E-04	3.8E-05

89	2.1E-02	2.2E-02	2.2E-05	2.3E-04	2.1E-02	-8.0E-04	2.1E-04	1.0E-03
90	4.0E-03	1.6E-03	9.0E-06	6.0E-05	3.9E-03	2.3E-03	5.1E-05	2.3E-03
91	6.1E-03	4.9E-03	1.1E-05	1.1E-04	6.0E-03	1.2E-03	9.8E-05	1.1E-03
92	6.7E-03	5.6E-03	1.1E-05	1.7E-04	6.6E-03	1.1E-03	1.6E-04	9.8E-04
93	1.0E-02	9.1E-03	2.2E-05	2.3E-04	1.0E-02	1.2E-03	2.1E-04	9.6E-04
94	1.1E-02	9.6E-03	2.4E-05	2.3E-04	1.0E-02	1.0E-03	2.1E-04	8.2E-04
95	1.1E-02	1.1E-02	2.4E-05	2.3E-04	1.1E-02	7.7E-06	2.1E-04	2.2E-04

A6. Normalized Synergies and Percentages of Components

No.	We^c/We^0	Wc^e/Wc^0	Ws/W	We^c/W	Wc^e/W	We^0/W	Wc^0/W	We/W	Wc/W
1	0.69	145	0.57	0.30	0.27	0.43	0.002	0.73	0.27
2	0.79	292	0.67	0.26	0.41	0.33	0.001	0.59	0.41
3	0.42	115	0.48	0.22	0.26	0.52	0.002	0.74	0.26
4	0.12	52	0.33	0.08	0.25	0.67	0.005	0.74	0.26
5	2.16	266	0.80	0.42	0.38	0.20	0.001	0.62	0.38
6	0.92	266	0.74	0.24	0.50	0.26	0.002	0.50	0.50
7	1.39	490	0.83	0.23	0.60	0.17	0.001	0.40	0.60
8	0.38	26	0.31	0.26	0.06	0.68	0.002	0.94	0.06
9	0.54	52	0.41	0.32	0.10	0.59	0.002	0.90	0.10
10	0.63	106	0.49	0.32	0.17	0.51	0.002	0.83	0.17
11	0.74	212	0.59	0.31	0.28	0.41	0.001	0.72	0.28
12	1.06	490	0.72	0.29	0.43	0.28	0.001	0.57	0.43
13	0.25	52	0.27	0.18	0.09	0.73	0.002	0.91	0.09
14	0.73	266	0.58	0.31	0.27	0.42	0.001	0.73	0.27
15	1.45	266	0.68	0.47	0.21	0.32	0.001	0.79	0.21
16	0.67	94	0.58	0.28	0.30	0.42	0.003	0.69	0.31
17	4.09	189	0.85	0.62	0.22	0.15	0.001	0.78	0.22

18	0.30	94	0.40	0.18	0.22	0.60	0.002	0.78	0.22
19	0.41	189	0.53	0.19	0.34	0.47	0.002	0.66	0.34
20	0.12	23	0.14	0.10	0.04	0.86	0.002	0.96	0.04
21	0.41	94	0.37	0.25	0.12	0.62	0.001	0.88	0.12
22	0.31	94	0.33	0.20	0.13	0.67	0.001	0.87	0.13
23	0.49	189	0.47	0.26	0.21	0.53	0.001	0.79	0.21
24	0.37	436	0.56	0.16	0.40	0.44	0.001	0.60	0.40
25	0.47	436	0.58	0.20	0.38	0.42	0.001	0.62	0.38
26	0.27	94	0.25	0.20	0.05	0.75	0.001	0.95	0.05
27	0.44	189	0.37	0.28	0.09	0.63	0.000	0.91	0.09
28	0.16	94	0.17	0.13	0.04	0.83	0.000	0.96	0.04
29	0.31	189	0.29	0.22	0.08	0.71	0.000	0.92	0.08
30	0.22	94	0.21	0.17	0.04	0.79	0.000	0.96	0.04
31	0.33	189	0.30	0.23	0.07	0.70	0.000	0.93	0.07
32	0.28	17	0.26	0.21	0.05	0.74	0.003	0.94	0.06
33	0.55	35	0.41	0.32	0.09	0.59	0.002	0.91	0.09
34	0.64	70	0.48	0.33	0.15	0.52	0.002	0.85	0.15
35	0.94	141	0.60	0.37	0.23	0.39	0.002	0.76	0.24
36	0.97	326	0.70	0.29	0.41	0.30	0.001	0.59	0.41
37	0.12	0	0.11	0.11	0.00	0.89	0.002	1.00	0.00
38	0.19	17	0.19	0.15	0.03	0.81	0.002	0.96	0.04
39	0.19	35	0.22	0.15	0.07	0.78	0.002	0.93	0.07
40	0.35	35	0.30	0.24	0.06	0.70	0.002	0.94	0.06
41	0.48	70	0.40	0.29	0.10	0.60	0.001	0.89	0.11
42	0.58	113	0.46	0.31	0.15	0.54	0.001	0.85	0.15
43	0.60	141	0.49	0.31	0.18	0.51	0.001	0.82	0.18
44	0.70	326	0.60	0.28	0.32	0.40	0.001	0.68	0.32
45	0.13	17	0.14	0.11	0.03	0.86	0.002	0.97	0.03
46	0.31	35	0.27	0.22	0.05	0.73	0.001	0.95	0.05
47	0.43	70	0.36	0.27	0.09	0.64	0.001	0.91	0.09
48	0.41	141	0.41	0.24	0.16	0.59	0.001	0.84	0.16

49	0.03	13	0.04	0.03	0.01	0.95	0.001	0.98	0.02
50	0.09	17	0.09	0.08	0.02	0.90	0.001	0.98	0.02
51	0.15	35	0.16	0.13	0.03	0.84	0.001	0.97	0.03
52	0.21	70	0.22	0.16	0.06	0.78	0.001	0.94	0.06
53	0.15	113	0.22	0.12	0.10	0.78	0.001	0.90	0.10
54	0.33	141	0.33	0.22	0.10	0.67	0.001	0.89	0.11
55	0.54	326	0.49	0.27	0.22	0.51	0.001	0.78	0.22
56	0.22	10	0.22	0.17	0.05	0.77	0.005	0.95	0.05
57	0.32	21	0.31	0.22	0.09	0.68	0.004	0.90	0.10
58	0.50	87	0.51	0.24	0.27	0.48	0.003	0.73	0.27
59	0.69	109	0.58	0.29	0.29	0.42	0.003	0.70	0.30
60	0.53	109	0.55	0.24	0.31	0.45	0.003	0.68	0.32
61	0.71	201	0.67	0.23	0.43	0.33	0.002	0.57	0.43
62	0.14	10	0.16	0.12	0.04	0.83	0.004	0.95	0.05
63	0.29	21	0.29	0.21	0.08	0.71	0.004	0.92	0.08
64	0.42	43	0.39	0.26	0.14	0.61	0.003	0.86	0.14
65	0.45	87	0.47	0.24	0.24	0.52	0.003	0.76	0.24
66	0.16	201	0.36	0.10	0.26	0.64	0.001	0.74	0.26
67	0.30	21	0.25	0.23	0.02	0.75	0.001	0.98	0.02
68	0.21	43	0.20	0.16	0.04	0.80	0.001	0.96	0.04
69	0.38	109	0.34	0.25	0.08	0.66	0.001	0.92	0.08
70	0.00	10	0.02	0.00	0.02	0.98	0.002	0.98	0.02
71	0.15	21	0.16	0.12	0.03	0.84	0.002	0.96	0.04
72	0.14	43	0.18	0.11	0.07	0.82	0.002	0.93	0.07
73	0.32	87	0.33	0.22	0.11	0.67	0.001	0.89	0.11
74	0.46	201	0.46	0.25	0.21	0.54	0.001	0.79	0.21
75	0.32	48	0.28	0.23	0.04	0.72	0.001	0.95	0.05
76	0.25	97	0.27	0.18	0.09	0.73	0.001	0.91	0.09
77	0.10	48	0.12	0.09	0.03	0.88	0.001	0.97	0.03
78	0.33	45	0.31	0.23	0.07	0.69	0.002	0.92	0.08
79	0.13	8	0.13	0.11	0.02	0.87	0.003	0.98	0.02

80	0.42	6	0.30	0.29	0.01	0.70	0.002	0.99	0.01
81	0.09	19	0.13	0.08	0.05	0.87	0.003	0.95	0.05
82	0.05	15	0.07	0.04	0.03	0.92	0.002	0.97	0.03
83	0.02	16	0.04	0.02	0.01	0.96	0.001	0.98	0.02
84	1.66	5	0.63	0.62	0.01	0.37	0.002	0.99	0.01
85	0.21	5	0.19	0.17	0.01	0.81	0.003	0.98	0.02
86	0.08	8	0.09	0.08	0.01	0.91	0.002	0.98	0.02
87	0.04	10	0.05	0.04	0.02	0.94	0.001	0.98	0.02
88	0.00	9	0.01	0.00	0.01	0.99	0.001	0.99	0.01
89	0.05	10	0.04	0.05	0.01	1.04	0.001	0.99	0.01
90	1.39	6	0.59	0.57	0.01	0.41	0.002	0.98	0.02
91	0.21	9	0.19	0.17	0.02	0.81	0.002	0.98	0.02
92	0.18	15	0.17	0.15	0.02	0.83	0.002	0.97	0.03
93	0.11	9	0.11	0.09	0.02	0.88	0.002	0.98	0.02
94	0.09	9	0.10	0.08	0.02	0.90	0.002	0.98	0.02
95	0.02	9	0.00	0.02	0.02	1.00	0.002	0.98	0.02

APPENDIX B. EXPERIMENTAL DATA OF A1018CS IN THE SLURRY WITH DIFFERENT pH SOLUTION

B1. Test Conditions of Total Weight Loss for A1018CS in the Slurry with Different pH Solution

Order No.	Sample No.	pH	Speed m/s	Sand wt.%	Current mA/cm^2	Time Hour
201	551	5.5	9.5	25	cp	0.25
202	552	5.5	9.5	25	0.25	0.25
203	553	5.5	9.5	25	0.5	0.25
204	554	5.5	9.5	25	1	0.25
205	555	5.5	9.5	25	2	0.25
206	556	5.5	9.5	25	4.6	0.25
207	F94	5.5	12.3	25	cp	0.25
208	F114	5.5	12.3	25	0.25	0.25
209	F124	5.5	12.3	25	0.5	0.25
210	F134	5.5	12.3	25	1	0.25
211	F144	5.5	12.3	25	2	0.25
212	F154	5.5	12.3	25	4.6	0.25
213	152c	5.5	9.5	50	cp	0.5
214	562	5.5	9.5	50	0.25	0.25
215	563	5.5	9.5	50	0.5	0.25
216	564	5.5	9.5	50	1	0.25
217	565	5.5	9.5	50	2	0.25
218	566	5.5	9.5	50	4.6	0.25
219	701	7	9.5	25	cp	0.25

220	702	7	9.5	25	0.25	0.25
221	703	7	9.5	25	0.5	0.25
222	704	7	9.5	25	1	0.25
223	705	7	9.5	25	2	0.25
224	706	7	9.5	25	4.6	0.25
225	801	7	1.23	25	cp	0.25
226	802	7	1.23	25	0.25	0.25
227	803	7	1.23	25	0.5	0.25
228	804	7	1.23	25	1	0.25
229	805	7	1.23	25	2	0.25
230	806	7	1.23	25	4.6	0.25
231	901	8.5	9.5	25	cp	0.25
232	902	8.5	9.5	25	0.25	0.25
233	903	8.5	9.5	25	0.5	0.25
234	904	8.5	9.5	25	1	0.25
235	905	8.5	9.5	25	2	0.25
236	906	8.5	9.5	25	4.6	0.25

B2. Raw Data of the Weight Losses

Order			Weight Loss (g/cm2-hr.)		
No.	R1	R2	R3	R4	w
201	9.26E-03	7.17E-03			8.21E-03
202	9.43E-03	9.04E-03	9.81E-03		9.43E-03
203	1.03E-02	8.79E-03			9.54E-03
204	1.05E-02	9.68E-03	1.13E-02		1.05E-02
205	9.71E-03	1.64E-02	1.12E-02		1.24E-02
206	1.57E-02	1.35E-02			1.57E-02
207	8.64E-03	8.66E-03	1.06E-02		9.40E-03

208	1.01E-02	1.15E-02			1.08E-02
209	1.11E-02				1.11E-02
210	1.27E-02	1.18E-02			1.23E-02
211	1.33E-02	1.41E-02			1.37E-02
212	1.38E-02	1.69E-02			1.62E-02
213	1.62E-02	2.30E-02			1.96E-02
214	2.30E-02	2.39E-02	2.53E-02	9.71E-03	2.05E-02
215	1.85E-02	1.64E-02	2.00E-02	3.20E-02	2.17E-02
216	2.21E-02	1.70E-02	2.73E-02		2.21E-02
217	2.13E-02	2.92E-02			2.53E-02
218	3.46E-02	2.31E-02			2.88E-02
219	9.49E-03	8.92E-03			9.20E-03
220	1.25E-02	8.69E-03			1.06E-02
221	9.84E-03	1.32E-02			1.15E-02
222	1.13E-02	1.42E-02			1.27E-02
223	1.24E-02	1.68E-02			1.46E-02
224	1.98E-02	1.66E-02			1.82E-02
225	1.24E-02	1.23E-02	1.06E-02		1.13E-02
226	1.11E-02	1.85E-02	1.02E-02		1.32E-02
227	1.55E-02	1.16E-02			1.36E-02
228	1.63E-02	1.31E-02			1.47E-02
229	1.28E-02	1.68E-02	2.04E-02		1.67E-02
230	1.94E-02	2.23E-02			2.08E-02
231	1.03E-02	5.43E-03	7.17E-03	5.26E-03	7.04E-03
232	8.41E-03	7.99E-03			7.99E-03
233	9.08E-03	1.13E-02			1.02E-02
234	1.07E-02	0.00E+00			1.07E-02
235	1.28E-02	1.28E-02			1.28E-02
236	1.94E-02	1.42E-02			1.68E-02

B3. Total Weight Losses and its Components of A1018CS in the Slurry with Different pH Solution

Order No.	W g/cm^2-hr.	We^0 g/cm^2-hr.	Wc g/cm^2-hr.	We^c g/cm^2-hr.	We g/cm^2-hr.	We^c/We^0	We/W	Wc/W
201	8.21E-03	8.21E-03	0.0E+00	0.0E+00	8.21E-03	0.000	1.000	0.000
202	9.43E-03	8.21E-03	2.60E-04	9.56E-04	9.17E-03	0.116	0.972	0.028
203	9.54E-03	8.21E-03	5.21E-04	8.07E-04	9.02E-03	0.098	0.945	0.055
204	1.05E-02	8.21E-03	1.04E-03	1.26E-03	9.47E-03	0.153	0.901	0.099
205	1.24E-02	8.21E-03	2.08E-03	2.14E-03	1.03E-02	0.260	0.832	0.168
206	1.57E-02	8.21E-03	4.79E-03	2.73E-03	1.09E-02	0.332	0.695	0.305
207	9.40E-03	9.40E-03	0.0E+00	0.0E+00	9.40E-03	0.000	1.000	0.000
208	1.08E-02	9.40E-03	2.60E-04	1.14E-03	1.05E-02	0.121	0.976	0.024
209	1.11E-02	9.40E-03	5.21E-04	1.13E-03	1.05E-02	0.121	0.953	0.047
210	1.23E-02	9.40E-03	1.04E-03	1.85E-03	1.13E-02	0.197	0.915	0.085
211	1.37E-02	9.40E-03	2.08E-03	2.24E-03	1.16E-02	0.238	0.848	0.152
212	1.62E-02	9.40E-03	4.79E-03	1.97E-03	1.14E-02	0.209	0.703	0.297
213	1.96E-02	1.96E-02	0.0E+00	0.0E+00	1.96E-02	0.000	1.000	0.000
214	2.05E-02	1.96E-02	2.60E-04	6.07E-04	2.02E-02	0.031	0.987	0.013
215	2.17E-02	1.96E-02	5.21E-04	1.61E-03	2.12E-02	0.082	0.976	0.024
216	2.21E-02	1.96E-02	1.04E-03	1.49E-03	2.11E-02	0.076	0.953	0.047
217	2.53E-02	1.96E-02	2.08E-03	3.59E-03	2.32E-02	0.183	0.918	0.082
218	2.88E-02	1.96E-02	4.79E-03	4.43E-03	2.40E-02	0.226	0.834	0.166
219	9.20E-03	9.20E-03	0.0E+00	0.0E+00	9.20E-03	0.000	1.000	0.000
220	1.06E-02	9.20E-03	2.60E-04	1.14E-03	1.03E-02	0.124	0.975	0.025
221	1.15E-02	9.20E-03	5.21E-04	1.77E-03	1.10E-02	0.193	0.955	0.045
222	1.27E-02	9.20E-03	1.04E-03	2.49E-03	1.17E-02	0.271	0.918	0.082
223	1.46E-02	9.20E-03	2.08E-03	3.35E-03	1.26E-02	0.364	0.858	0.142
224	1.82E-02	9.20E-03	4.79E-03	4.19E-03	1.34E-02	0.455	0.736	0.264

225	1.13E-02	1.13E-02	0.0E+00	0.0E+00	1.13E-02	0.000	1.000	0.000
226	1.32E-02	1.13E-02	2.60E-04	1.71E-03	1.30E-02	0.152	0.980	0.020
227	1.36E-02	1.13E-02	5.21E-04	1.80E-03	1.31E-02	0.160	0.962	0.038
228	1.47E-02	1.13E-02	1.04E-03	2.41E-03	1.37E-02	0.214	0.929	0.071
229	1.67E-02	1.13E-02	2.08E-03	3.35E-03	1.46E-02	0.298	0.875	0.125
230	2.08E-02	1.13E-02	4.79E-03	4.76E-03	1.60E-02	0.422	0.770	0.230
231	7.04E-03	7.04E-03	0.0E+00	0.0E+00	7.04E-03	0.000	1.000	0.000
232	7.99E-03	7.04E-03	2.60E-04	6.91E-04	7.73E-03	0.098	0.967	0.033
233	1.02E-02	7.04E-03	5.21E-04	2.63E-03	9.67E-03	0.373	0.949	0.051
234	1.07E-02	7.04E-03	1.04E-03	2.62E-03	9.66E-03	0.372	0.903	0.097
235	1.28E-02	7.04E-03	2.08E-03	3.68E-03	1.07E-02	0.522	0.837	0.163
236	1.68E-02	7.04E-03	4.79E-03	4.95E-03	1.20E-02	0.703	0.714	0.286

APPENDIX C. EXPERIEMTNAL DATA OF A1045CS IN THE TAP WATER SLURRY

C1. Test Conditions of A1045CS in the Tap Water Slurry

Order No.	Sample No.	Speed A	Sand B	AB	Flow Rate m/s	Sand (%)
301	80	-2.2	-1	2.2	2.6	10
302	81	-2.2	0	0	2.6	20
303	33	-2.2	0.33	-0.726	2.6	25
304	82	-2.2	1	-2.2	2.6	40
305	26	-1	-1	1	4	10
306	111	-1	0	0	4	20
307	112	-1	0.6	-0.6	4	30
308	0	-1	1	-1	4	40
309	113	-0.4	0	0	5	20
310	114	-0.4	0.6	-0.24	5	30
311	75	0	-1	0	6	10
312	72	0	0	0	6	20
313	115	0	0	0	6	20
314	116	0	0.6	0	6	30
315	30	0	0.33	0	6	25
316	30	0	0.33	0	6	25
317	29	0	0.33	0	6	25
318	78	0	1	0	6	40
319	13	0	1.33	0	6	50
320	117	0.6	0	0	7	20
321	118	0.6	0.6	0.36	7	30
322	22	1	-1	-1	8	10

323	119	1	0	0	8	20
324	120	1	0.6	0.6	8	30
325	24	1	1	1	8	40
326	24	1	1	1	8	40
327	73	1.33	-1	-1.33	9.2	10
328	74	1.33	0	0	9.2	20
329	10	1.33	0.33	0.4389	9.2	25
330	71	1.33	1	1.33	9.2	40
331	76	1.33	1.33	1.7689	9.2	50

C2. Total Weight Losses and Their Components of A1045CS in the Tap Water Slurry

Order	W	We^0	Wc^0	Wc	We	Ws	Wc^e	We^c
No.	g/cm^2-hr	g/cm^2-hr	g/cm^2-hr	g/cm^2-hr	g/cm^2-hr	g/cm^2-hr	g/cm^2-hr	g/cm^2-hr
301	7.7E-06	8.7E-07	5.0E-07	5.8E-06	1.9E-06	6.3E-06	5.3E-06	9.9E-07
302	8.7E-06	3.1E-06	5.0E-07	5.2E-06	3.6E-06	5.1E-06	4.7E-06	4.6E-07
303	1.0E-05	4.4E-06	5.0E-07	5.5E-06	4.7E-06	5.3E-06	5.0E-06	3.2E-07
304	1.8E-05	5.8E-06	5.0E-07	7.3E-06	1.0E-05	1.1E-05	6.8E-06	4.6E-06
305	1.4E-04	3.1E-05	2.2E-06	6.4E-06	1.4E-04	1.1E-04	4.2E-06	1.1E-04
306	8.1E-05	3.4E-05	2.2E-06	6.6E-06	7.4E-05	4.5E-05	4.4E-06	4.0E-05
307	1.7E-04	9.0E-05	2.2E-06	7.4E-06	1.6E-04	7.8E-05	5.2E-06	7.2E-05
308	3.9E-04	3.4E-04	2.2E-06	7.7E-06	3.8E-04	4.5E-05	5.6E-06	4.0E-05
309	1.1E-04	6.8E-05	2.2E-06	7.4E-06	9.8E-05	3.5E-05	5.2E-06	2.9E-05
310	1.8E-04	1.1E-04	2.2E-06	8.3E-06	1.7E-04	6.6E-05	6.1E-06	5.9E-05
311	5.7E-05	2.8E-05	2.2E-06	7.1E-06	5.0E-05	2.8E-05	4.9E-06	2.3E-05
312	5.7E-05	3.5E-05	2.2E-06	8.4E-06	4.9E-05	2.0E-05	6.2E-06	1.4E-05

313	1.2E-04	8.4E-05	2.2E-06	8.1E-06	1.1E-04	3.4E-05	5.9E-06	2.8E-05
314	2.7E-04	1.9E-04	2.2E-06	9.1E-06	2.6E-04	7.6E-05	6.9E-06	7.0E-05
315	2.3E-04	1.5E-04	2.2E-06	9.2E-06	2.2E-04	8.2E-05	7.0E-06	7.5E-05
316	2.1E-04	9.2E-05	2.2E-06	9.2E-06	2.0E-04	1.1E-04	7.0E-06	1.1E-04
317	1.7E-04	9.2E-05	2.2E-06	9.2E-06	1.6E-04	7.9E-05	7.0E-06	7.2E-05
318	4.0E-04	3.1E-04	2.2E-06	9.9E-06	3.9E-04	8.9E-05	7.7E-06	8.2E-05
319	4.5E-04	3.0E-04	2.2E-06	1.2E-05	4.4E-04	1.5E-04	9.5E-06	1.4E-04
320	1.7E-04	1.1E-04	2.4E-06	8.8E-06	1.6E-04	6.2E-05	6.4E-06	5.5E-05
321	3.6E-04	2.6E-04	2.6E-06	9.9E-06	3.5E-04	9.7E-05	7.3E-06	9.0E-05
322	2.4E-04	2.0E-04	3.0E-06	9.4E-06	2.3E-04	3.9E-05	6.4E-06	3.2E-05
323	1.9E-04	1.4E-04	3.0E-06	9.4E-06	1.8E-04	4.2E-05	6.4E-06	3.6E-05
324	4.8E-04	4.0E-04	3.0E-06	1.1E-05	4.7E-04	7.4E-05	7.6E-06	6.6E-05
325	1.1E-03	9.4E-04	3.0E-06	1.3E-05	1.1E-03	1.7E-04	9.7E-06	1.6E-04
326	1.2E-03	9.8E-04	3.0E-06	1.3E-05	1.2E-03	2.2E-04	9.7E-06	2.1E-04
327	3.5E-04	2.1E-04	4.2E-06	7.4E-06	3.5E-04	1.4E-04	3.2E-06	1.3E-04
328	6.8E-04	4.6E-04	4.2E-06	1.1E-05	6.7E-04	2.2E-04	6.5E-06	2.2E-04
329	6.5E-04	4.8E-04	4.2E-06	1.3E-05	6.3E-04	1.6E-04	9.0E-06	1.5E-04
330	1.3E-03	7.8E-04	4.2E-06	1.4E-05	1.3E-03	5.6E-04	1.0E-05	5.5E-04
331	1.6E-03	7.2E-04	4.2E-06	1.5E-05	1.6E-03	8.8E-04	1.0E-05	8.7E-04

C3. Normalized Synergies and Percentage of the Components in the Tap Water Slurry

No.	We^c/We^0	Wc^e/Wc^0	Ws/W	We^c/W	Wc^e/W	We^0/W	Wc^0/W	We/W	Wc/W
301	1.14	10.74	0.82	0.13	0.69	0.11	0.06	0.24	0.76
302	0.15	9.42	0.59	0.05	0.54	0.35	0.06	0.41	0.59

303	0.07	10.08	0.52	0.03	0.49	0.43	0.05	0.46	0.54
304	0.79	13.64	0.64	0.26	0.38	0.33	0.03	0.59	0.41
305	3.38	1.96	0.77	0.74	0.03	0.22	0.02	0.96	0.04
306	1.20	2.04	0.56	0.50	0.05	0.42	0.03	0.92	0.08
307	0.80	2.43	0.46	0.43	0.03	0.53	0.01	0.96	0.04
308	0.12	2.59	0.12	0.10	0.01	0.88	0.01	0.98	0.02
309	0.43	2.39	0.33	0.28	0.05	0.65	0.02	0.93	0.07
310	0.55	2.82	0.37	0.34	0.04	0.61	0.01	0.95	0.05
311	0.82	2.25	0.48	0.39	0.09	0.48	0.04	0.88	0.12
312	0.41	2.81	0.35	0.25	0.11	0.61	0.04	0.85	0.15
313	0.33	2.68	0.28	0.23	0.05	0.70	0.02	0.93	0.07
314	0.37	3.16	0.29	0.26	0.03	0.70	0.01	0.97	0.03
315	0.52	3.20	0.36	0.33	0.03	0.63	0.01	0.96	0.04
316	1.15	3.20	0.55	0.51	0.03	0.44	0.01	0.96	0.04
317	0.78	3.20	0.46	0.42	0.04	0.53	0.01	0.95	0.05
318	0.26	3.52	0.22	0.20	0.02	0.77	0.01	0.98	0.02
319	0.47	4.31	0.33	0.31	0.02	0.66	0.00	0.97	0.03
320	0.51	2.64	0.36	0.32	0.04	0.63	0.01	0.95	0.05
321	0.35	2.78	0.27	0.25	0.02	0.72	0.01	0.97	0.03
322	0.16	2.11	0.16	0.13	0.03	0.83	0.01	0.96	0.04
323	0.25	2.09	0.22	0.19	0.03	0.76	0.02	0.95	0.05
324	0.16	2.49	0.15	0.14	0.02	0.84	0.01	0.98	0.02
325	0.17	3.20	0.15	0.14	0.01	0.84	0.00	0.99	0.01
326	0.21	3.20	0.18	0.17	0.01	0.82	0.00	0.99	0.01
327	0.62	0.77	0.39	0.38	0.01	0.60	0.01	0.98	0.02
328	0.48	1.54	0.33	0.32	0.01	0.67	0.01	0.98	0.02
329	0.32	2.14	0.25	0.24	0.01	0.74	0.01	0.98	0.02
330	0.71	2.40	0.42	0.41	0.01	0.58	0.00	0.99	0.01
331	1.20	2.49	0.55	0.54	0.01	0.45	0.00	0.99	0.01

APPENDIX D. REGRESSION ANALYSIS OF THE SYNERGY FROM CORROSION ENHANCED ERORION

Regression Formula: Y=0.477-0.146A-0.1B+0.148C

K	A	B	C	AB	AC	BC	ABC
0.4772	-0.1457	-0.0998	0.1484	-0.0535	-0.0436	-0.0205	0.0183

D1. Regression Analysis Data

Order	Sample	Speed	Sand	Current					We^c/We_0
No.	No.	A	B	C	AB	AC	BC	ABC	Y
1	902	-2	0.33	0	-0.66	0.00	0.00	0.00	0.69
2	903	-2	0.33	0.75	-0.66	-1.50	0.25	-0.50	0.79
3	113	-1.65	0	0	0.00	0.00	0.00	0.00	0.42
4	14	-1	-1	-0.75	1.00	0.75	0.75	-0.75	0.12
5	54"	-1	-1	1	1.00	-1.00	-1.00	1.00	0.92
6	54	-1	-1	1.65	1.00	-1.65	-1.65	1.65	1.39
7	42	-1	0.33	-1.65	-0.33	1.65	-0.54	0.54	0.38
8	43	-1	0.33	-0.75	-0.33	0.75	-0.25	0.25	0.54
9	44	-1	0.33	0	-0.33	0.00	0.00	0.00	0.63
10	45	-1	0.33	0.75	-0.33	-0.75	0.25	-0.25	0.74
11	46	-1	0.33	1.65	-0.33	-1.65	0.54	-0.54	1.06
12	34	-1	1	-1.65	-1.00	1.65	-1.65	1.65	0.25
13	74	-1	1	1	-1.00	-1.00	1.00	-1.00	0.73
14	F74	-1	1	1	-1.00	-1.00	1.00	-1.00	1.45

15	f121	0	-1.65	0	0.00	0.00	0.00	0.00	0.67
16	526	0	-1	0	0.00	0.00	0.00	0.00	0.30
17	521	0	-1	0.75	0.00	0.00	-0.75	0.00	0.41
18	f131	0	0	-1.65	0.00	0.00	0.00	0.00	0.12
19	f91	0	0	0	0.00	0.00	0.00	0.00	0.41
20	f101	0	0	0	0.00	0.00	0.00	0.00	0.31
21	70	0	0	0.75	0.00	0.00	0.00	0.00	0.49
22	f161	0	0	1.65	0.00	0.00	0.00	0.00	0.37
23	562	0	0	1.65	0.00	0.00	0.00	0.00	0.47
24	5680	0	1	0	0.00	0.00	0.00	0.00	0.27
25	71	0	1	0.75	0.00	0.00	0.75	0.00	0.44
26	556	0	1.33	0	0.00	0.00	0.00	0.00	0.16
27	552	0	1.33	0.75	0.00	0.00	1.00	0.00	0.31
28	f151	0	1.65	0	0.00	0.00	0.00	0.00	0.22
29	72	0	1.65	0.75	0.00	0.00	1.24	0.00	0.33
30	62	0.2	-1	-1.65	-0.20	-0.33	1.65	0.33	0.28
31	63	0.2	-1	-0.75	-0.20	-0.15	0.75	0.15	0.55
32	64	0.2	-1	0	-0.20	0.00	0.00	0.00	0.64
33	65	0.2	-1	0.75	-0.20	0.15	-0.75	-0.15	0.94
34	66	0.2	-1	1.65	-0.20	0.33	-1.65	-0.33	0.97
35	A132	0.2	0.33	-1.8	0.07	-0.36	-0.59	-0.12	0.12
36	103	0.2	0.33	-1.65	0.07	-0.33	-0.54	-0.11	0.19
37	162	0.2	0.33	-0.75	0.07	-0.15	-0.25	-0.05	0.19
38	162'	0.2	0.33	-0.75	0.07	-0.15	-0.25	-0.05	0.35
39	A32	0.2	0.33	0	0.07	0.00	0.00	0.00	0.48
40	b12	0.2	0.33	0.5	0.07	0.10	0.17	0.03	0.58
41	A162	0.2	0.33	0.75	0.07	0.15	0.25	0.05	0.60
42	A162*	0.2	0.33	1.65	0.07	0.33	0.54	0.11	0.70
43	62*	0.2	0.33	-1.65	0.07	-0.33	-0.54	-0.11	0.13
44	63*	0.2	0.33	-0.75	0.07	-0.15	-0.25	-0.05	0.31
45	64*	0.2	0.33	0	0.07	0.00	0.00	0.00	0.43

46	65*	0.2	0.33	0.75	0.07	0.15	0.25	0.05	0.41
47	B32	0.2	1.33	-1.8	0.27	-0.36	-2.39	-0.48	0.03
48	152	0.2	1.33	-1.65	0.27	-0.33	-2.19	-0.44	0.05
49	A102	0.2	1.33	-0.75	0.27	-0.15	-1.00	-0.20	0.15
50	A152	0.2	1.33	0	0.27	0.00	0.00	0.00	0.21
51	b42	0.2	1.33	0.6	0.27	0.12	0.80	0.16	0.15
52	b52	0.2	1.33	0.75	0.27	0.15	1.00	0.20	0.33
53	652	0.2	1.33	1.65	0.27	0.33	2.19	0.44	0.54
54	821	1	-1	-1.65	-1.00	-1.65	1.65	1.65	0.22
55	22	1	-1	-0.75	-1.00	-0.75	0.75	0.75	0.32
56	62	1	-1	0.75	-1.00	0.75	-0.75	-0.75	0.50
57	62"	1	-1	1	-1.00	1.00	-1.00	-1.00	0.69
58	F62	1	-1	1	-1.00	1.00	-1.00	-1.00	0.53
59	822	1	-1	1.65	-1.00	1.65	-1.65	-1.65	0.71
60	82	1	0.33	-1.65	0.33	-1.65	-0.54	-0.54	0.14
61	83	1	0.33	-0.75	0.33	-0.75	-0.25	-0.25	0.29
62	84	1	0.33	0	0.33	0.00	0.00	0.00	0.42
63	85	1	0.33	0.75	0.33	0.75	0.25	0.25	0.45
64	852	1	0.33	1.65	0.33	1.65	0.54	0.54	0.16
65	42	1	1	-0.75	1.00	-0.75	-0.75	-0.75	0.30
66	F162	1	1	0	1.00	0.00	0.00	0.00	0.21
67	82	1	1	1	1.00	1.00	1.00	1.00	0.54
68	82	1	1.33	-1.65	1.33	-1.65	-2.19	-2.19	0.00
69	83	1	1.33	-0.75	1.33	-0.75	-1.00	-1.00	0.15
70	84	1	1.33	0	1.33	0.00	0.00	0.00	0.08
71	85	1	1.33	0.75	1.33	0.75	1.00	1.00	0.32
72	86	1	1.33	1.65	1.33	1.65	2.19	2.19	0.46
73	144	1.45	0.33	0	0.48	0.00	0.00	0.00	0.32
74	68	1.45	0.33	0.75	0.48	1.09	0.25	0.36	0.25
75	184	1.45	1.33	1.65	1.93	2.39	2.19	3.18	0.10
76	144	1.65	0	0	0.00	0.00	0.00	0.00	0.33

77	12o	0.75	-1.65	-1.65	-1.24	-1.24	2.72	2.04	1.68
78	24o'	0.75	-0.75	-1.65	-0.56	-1.24	1.24	0.93	0.22
79	40o	0.75	0	-1.65	0.00	-1.24	0.00	0.00	0.09
80	68o	0.75	0.75	-1.65	0.56	-1.24	-1.24	-0.93	0.05
81	80o	0.75	1	-1.65	0.75	-1.24	-1.65	-1.24	0.00
82	120o	0.75	1.65	-1.65	1.24	-1.24	-2.72	-2.04	0.00
83	304	-1.65	0	-1.65	0.00	2.72	0.00	0.00	1.39
84	404	-1	0	-1.65	0.00	1.65	0.00	0.00	0.21
85	554	0	0	-1.65	0.00	0.00	0.00	0.00	0.18
86	40o	0.75	0	-1.65	0.00	-1.24	0.00	0.00	0.11
87	814	1	0	-1.65	0.00	-1.65	0.00	0.00	0.09
88	124	1.65	0	-1.65	0.00	-2.72	0.00	0.00	0.00

D2. Results of Regression Analysis

SUMMARY OUTPUT

Regression Statistics	
Multiple R	0.8248
R Square	0.6804
Adjusted R Square	0.6524
Standard Error	0.1689
Observations	88

ANOVA

	df	SS	MS	F	Sign. F
Regression	7	4.8601	0.6943	24.326	2E-17
Residual	80	2.2833	0.0285		
Total	87	7.1434			

Coefficients		Error	t Stat	P-value	Low 95%	Up 95%	Low95.0%	Up 95.0%
K	0.4772	0.0196	24.307	1E-38	0.4381	0.5163	0.4381	0.5163
A	-0.1457	0.0235	-6.1929	2E-08	-0.1925	-0.0989	-0.1925	-0.0989
B	-0.0998	0.025	-3.9968	0.0001	-0.1495	-0.0501	-0.1495	-0.0501
C	0.1484	0.0172	8.6154	5E-13	0.1141	0.1827	0.1141	0.1827
AB	-0.0535	0.036	-1.4858	0.1413	-0.1251	0.0181	-0.1251	0.0181
AC	-0.0436	0.0208	-2.0985	0.039	-0.085	-0.0023	-0.085	-0.0023
BC	-0.0205	0.0238	-0.8593	0.3927	-0.0678	0.0269	-0.0678	0.0269
ABC	0.0183	0.0302	0.6065	0.5459	-0.0418	0.0784	-0.0418	0.0784

D3 Parameters of Regression Analysis

RESIDUAL OUTPUT			PROBABILITY OUTPUT		
Observation	Predicted Y	Residuals	Residuals	Percentile	Y
1	0.77	-0.08	-0.51	0.57	-0.04
2	0.93	-0.14	-0.86	1.70	0.00
3	0.72	-0.30	-1.86	2.84	0.00
4	0.50	-0.38	-2.35	3.98	0.03
5	0.90	0.02	0.15	5.11	0.05
6	1.05	0.34	2.11	6.25	0.08
7	0.31	0.07	0.42	7.39	0.09
8	0.47	0.07	0.41	8.52	0.10
9	0.61	0.03	0.17	9.66	0.11
10	0.74	0.00	0.02	10.80	0.12
11	0.90	0.16	0.97	11.93	0.12

12	0.32	-0.07	-0.45	13.07	0.12
13	0.73	0.00	-0.03	14.20	0.13
14	0.73	0.72	4.44	15.34	0.13
15	0.64	0.03	0.16	16.48	0.13
16	0.58	-0.28	-1.71	17.61	0.13
17	0.70	-0.29	-1.81	18.75	0.14
18	0.23	-0.11	-0.71	19.89	0.15
19	0.48	-0.07	-0.45	21.02	0.15
20	0.48	-0.17	-1.05	22.16	0.15
21	0.59	-0.10	-0.59	23.30	0.16
22	0.72	-0.35	-2.16	24.43	0.16
23	0.72	-0.25	-1.54	25.57	0.19
24	0.38	-0.11	-0.67	26.70	0.19
25	0.47	-0.04	-0.22	27.84	0.21
26	0.34	-0.19	-1.17	28.98	0.21
27	0.44	-0.13	-0.78	30.11	0.22
28	0.31	-0.09	-0.56	31.25	0.22
29	0.40	-0.06	-0.40	32.39	0.25
30	0.30	-0.02	-0.11	33.52	0.25
31	0.44	0.11	0.68	34.66	0.27
32	0.56	0.08	0.48	35.80	0.28
33	0.68	0.27	1.64	36.93	0.29
34	0.82	0.15	0.93	38.07	0.30
35	0.17	-0.05	-0.31	39.20	0.30
36	0.19	0.00	-0.02	40.34	0.31
37	0.31	-0.12	-0.75	41.48	0.31
38	0.31	0.04	0.22	42.61	0.31
39	0.41	0.07	0.44	43.75	0.32
40	0.48	0.10	0.61	44.89	0.32
41	0.51	0.09	0.54	46.02	0.32
42	0.63	0.07	0.44	47.16	0.32

43	0.19	-0.06	-0.38	48.30	0.33
44	0.31	0.00	-0.02	49.43	0.33
45	0.41	0.01	0.09	50.57	0.33
46	0.51	-0.10	-0.62	51.70	0.35
47	0.09	-0.06	-0.36	52.84	0.36
48	0.11	-0.06	-0.38	53.98	0.37
49	0.21	-0.06	-0.40	55.11	0.38
50	0.30	-0.09	-0.56	56.25	0.41
51	0.37	-0.22	-1.35	57.39	0.41
52	0.39	-0.06	-0.34	58.52	0.41
53	0.49	0.04	0.26	59.66	0.42
54	0.31	-0.08	-0.52	60.80	0.42
55	0.40	-0.09	-0.53	61.93	0.43
56	0.56	-0.06	-0.37	63.07	0.44
57	0.59	0.10	0.61	64.20	0.45
58	0.59	-0.06	-0.37	65.34	0.46
59	0.66	0.05	0.28	66.48	0.47
60	0.11	0.03	0.20	67.61	0.48
61	0.20	0.09	0.56	68.75	0.49
62	0.28	0.14	0.87	69.89	0.50
63	0.36	0.09	0.57	71.02	0.53
64	0.45	-0.29	-1.82	72.16	0.53
65	0.10	0.20	1.25	73.30	0.54
66	0.18	0.03	0.17	74.43	0.54
67	0.28	0.25	1.57	75.57	0.54
68	-0.04	0.04	0.25	76.70	0.55
69	0.05	0.10	0.59	77.84	0.58
70	0.13	-0.05	-0.29	78.98	0.60
71	0.20	0.12	0.72	80.11	0.61
72	0.30	0.16	1.01	81.25	0.63
73	0.21	0.11	0.70	82.39	0.64

74	0.27	-0.02	-0.15	83.52	0.67
75	0.18	-0.08	-0.51	84.66	0.69
76	0.24	0.10	0.59	85.80	0.69
77	0.39	0.14	0.87	86.93	0.70
78	0.27	0.08	0.50	88.07	0.71
79	0.18	-0.05	-0.30	89.20	0.71
80	0.08	0.05	0.32	90.34	0.73
81	0.05	0.04	0.25	91.48	0.74
82	-0.04	0.00	0.00	92.61	0.79
83	0.35	0.36	2.20	93.75	0.92
84	0.31	0.30	1.85	94.89	0.94
85	0.23	0.08	0.51	96.02	0.97
86	0.18	-0.05	-0.30	97.16	1.06
87	0.16	-0.05	-0.30	98.30	1.39
88	0.11	-0.11	-0.67	99.43	1.45

D5. Figures of Residuals and fits for the Parameters

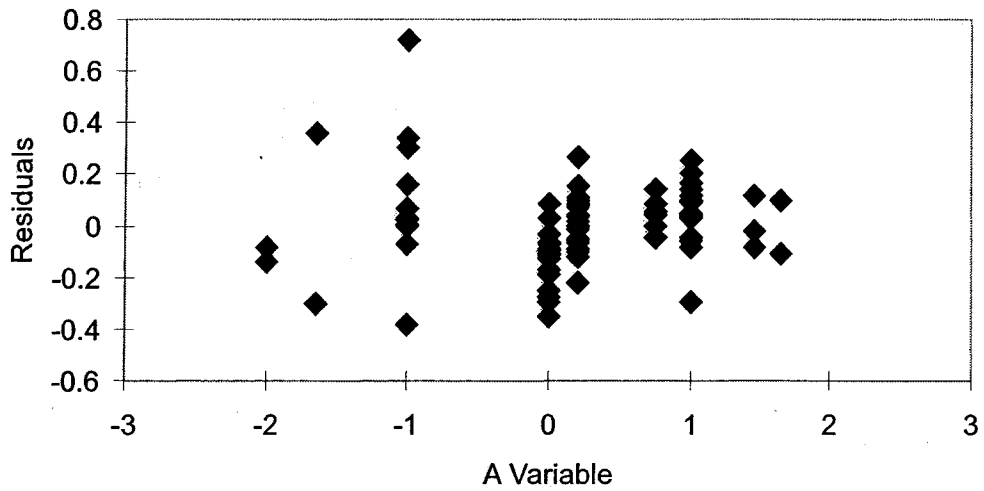

Figure D5-1. Residuals vs. the parameter of flow rate

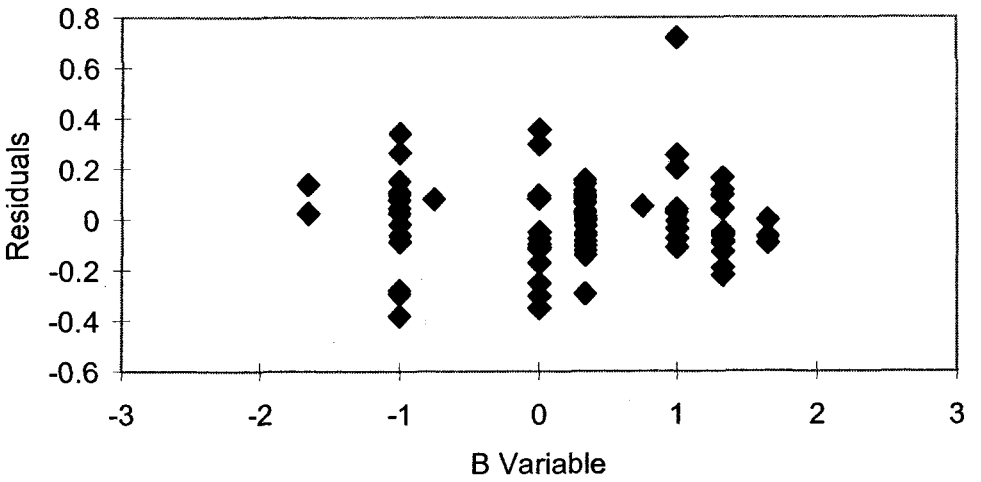

Figure D5-2. Residuals vs. the parameter of sand concentration

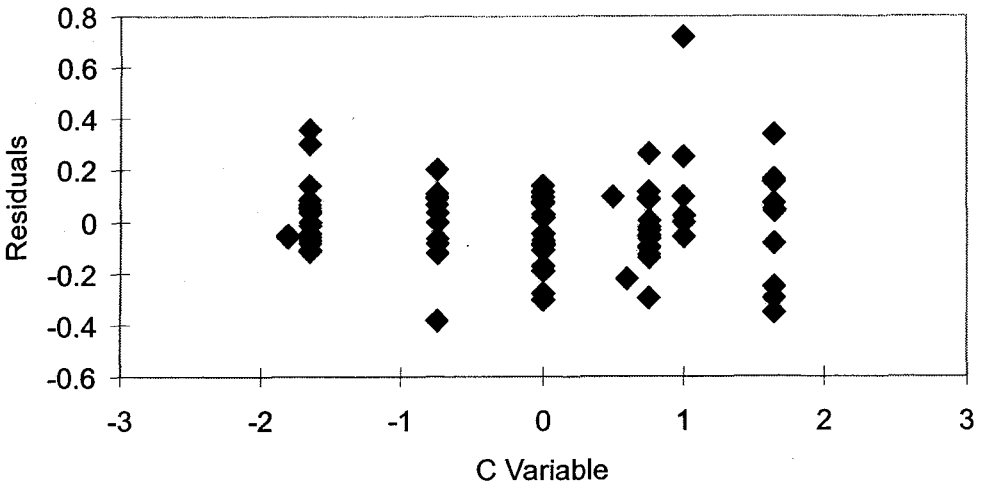

Figure D5-3. Residuals vs. the parameter of anodic current

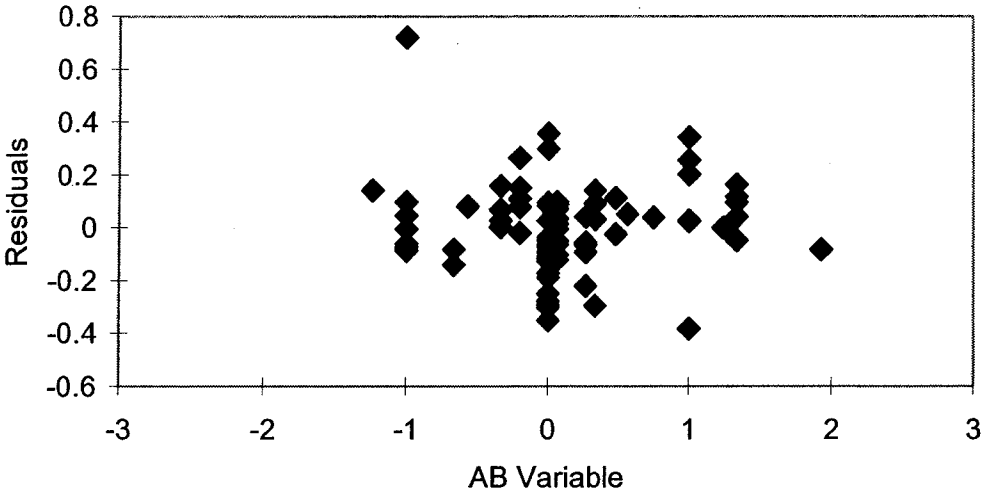

Figure D5-4. Residuals vs. the inter-parameter of flow rate and sand concentration

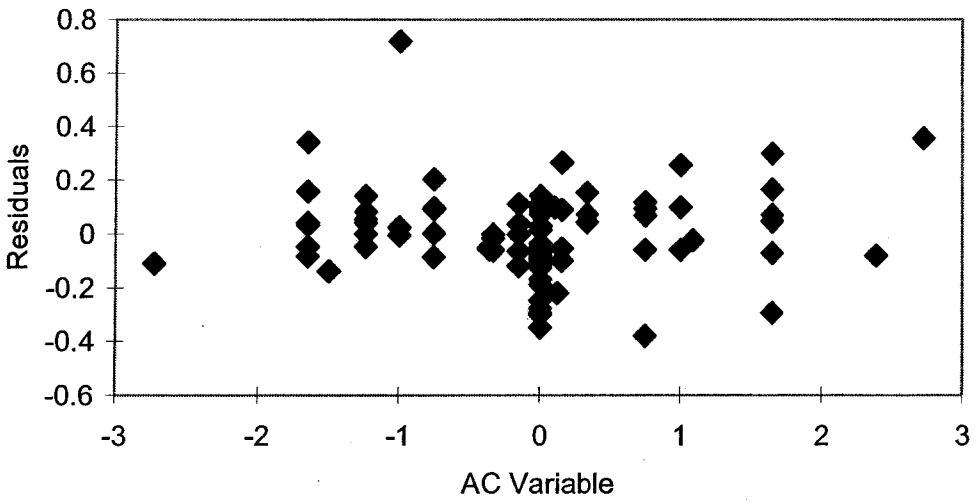

Figure D5-6. Residuals vs. the inter-parameter of flow rate and anodic current

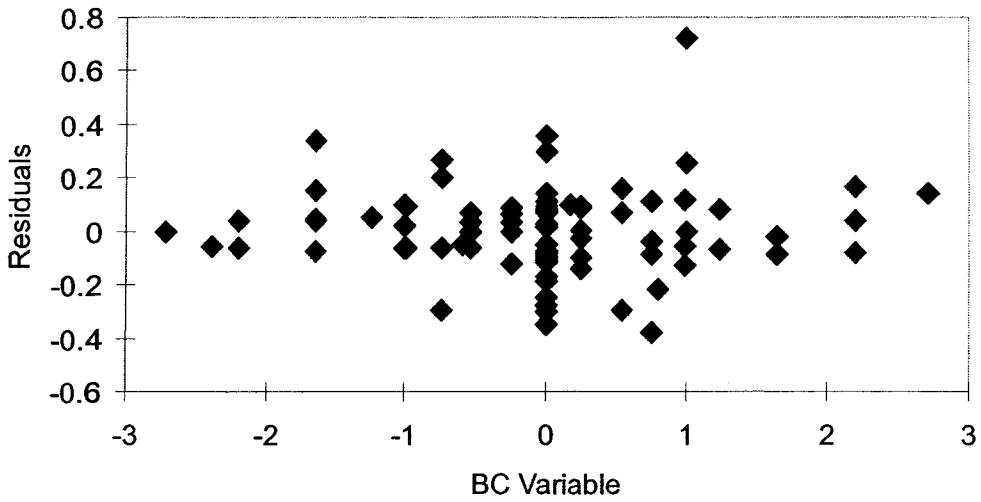

Figure D5-6. Residuals vs. the inter-parameter of sand concentration and anodic current

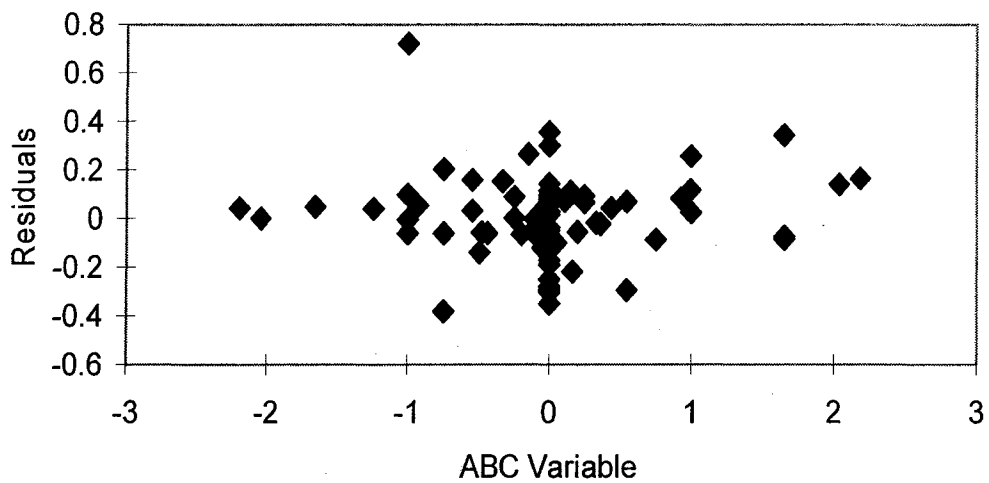

Figure D5-7. Residuals vs. the inter-parameter of flow rate, sand concentration and anodic current

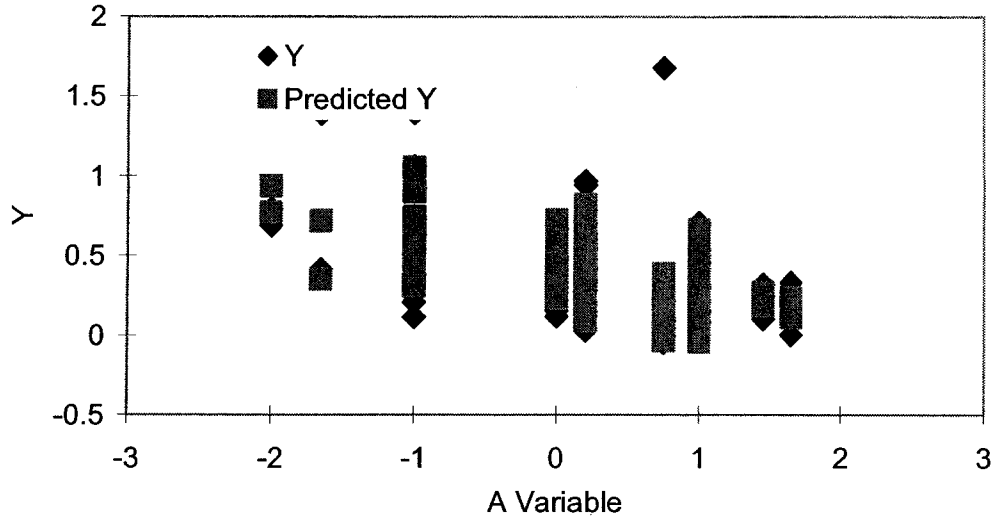

Figure D5-8. Fits of the values measured and predicted vs. factor of flow rate

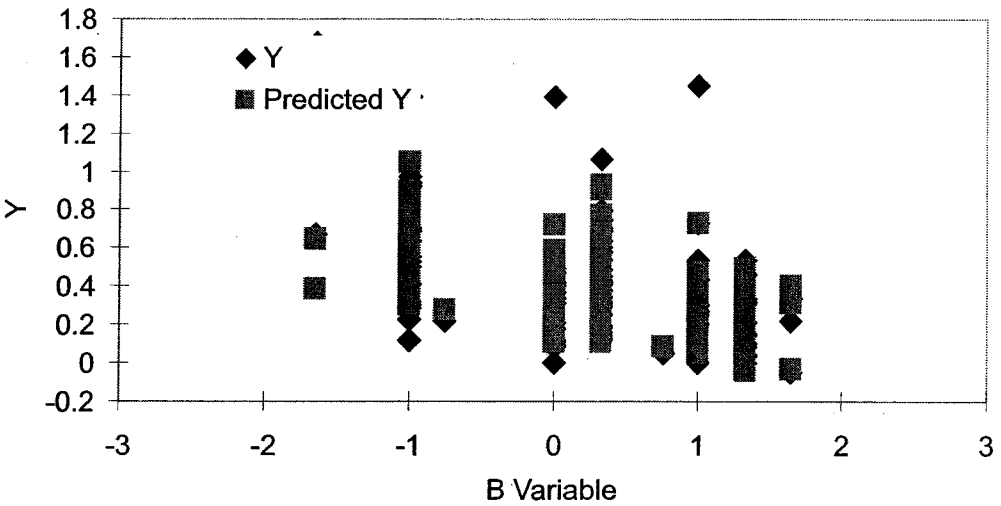

Figure D5-9. Fits of the values measured and predicted vs. factor of sand concentration

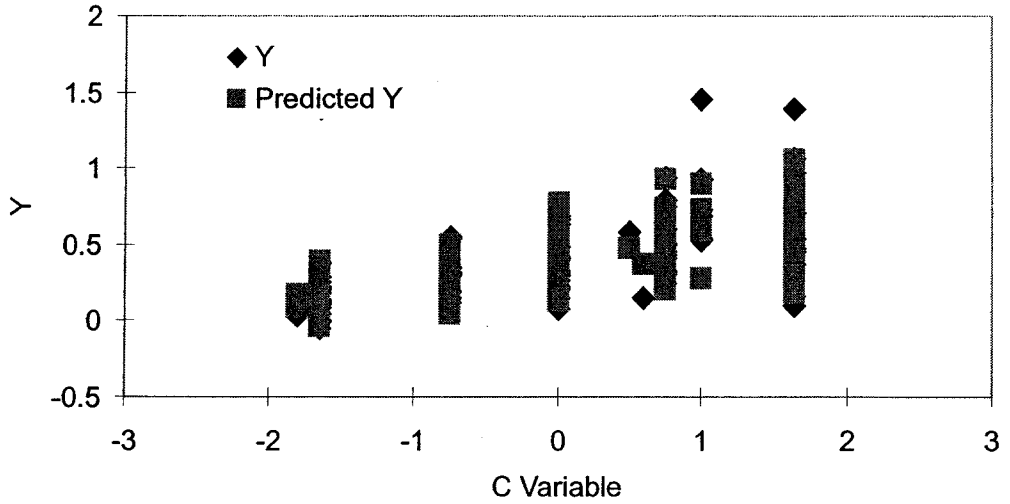

Figure D5-10. Fits of the values measured and predicted vs. factor of anodic current

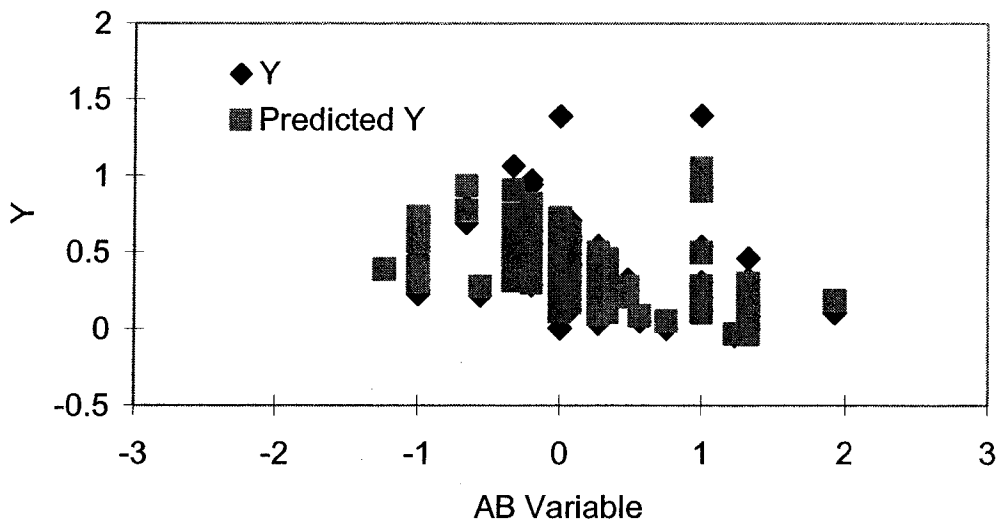

Figure D5-11. Fits of the values measured and predicted vs. inter-factors of flow rate and sand concentration

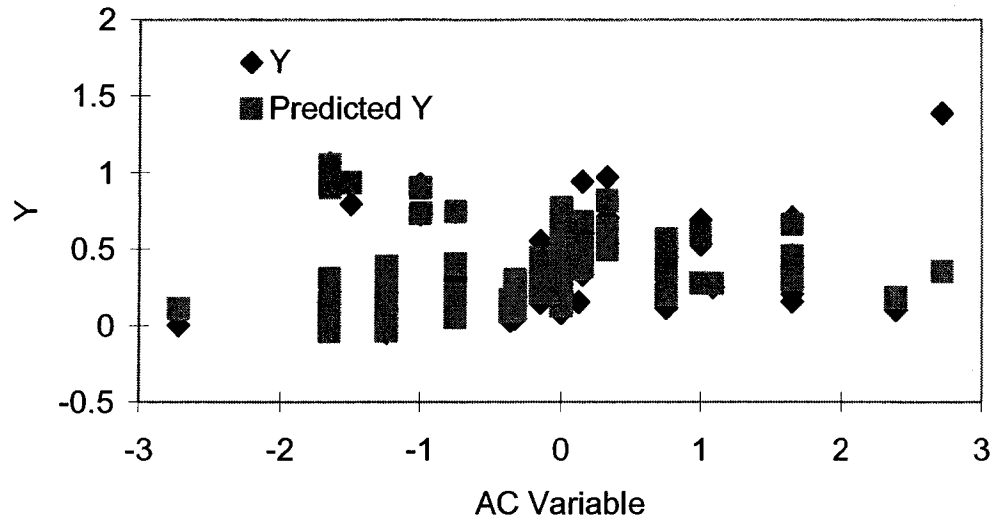

Figure D5-11. Fits of the values measured and predicted vs. inter-factors of flow rate and sand concentration

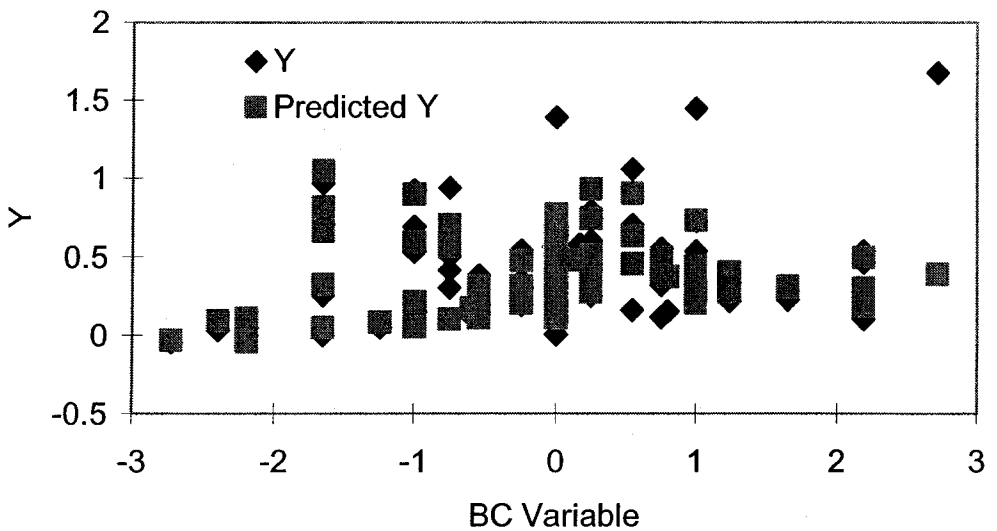

Figure D5-11. Fits of the values measured and predicted vs. inter-factors of flow rate and sand concentration

Appendix D. Publications

C. W. Chen, T. Yu, B.T. Lu and J. L. Luo, "Interaction of mechanical and chemical factors in erosion-corrosion process occurring in oil sand wastewater transportation", Proceedings of the Second International Symposium on Aerospace materials and Manufacturing: Development, Testing and Life Cycle Issues-Honoring William Wallace, P.C. Patnaik, M. Elboujdaïni, M. Jahazi and J. Luo Eds., 43rd Annual Conference of Metallurgists of CIM, MET SOC, Montreal, Quebec, pp. 493-503, 2004.

C.W. Chen, B.T. Lu, J. L. Luo and T. Yu, "Effect of Corrosivity of Wastewater Slurry on Synergism of Erosion-Corrosion", Poster in the 43rd Annual Conference of Metallurgists of CIM, Hamilton, Ontario, Canada, August 22-25, 2004.

B.T. Lu, C.W. Chen, J.L. Luo and B.D. Campbell, "Micorbiatically Influenced Corrosion In a Depressurization Well Piping", Proceedings of the Second International Symposium on Environmental Degradation of Materials and Corrosion Control In Metals, J. Luo, M. Elboujdaïni, D. Shoesmith and P.C. Patnaik Eds., 42nd Conference of Metallurgists of CIM, MET SOC, Montreal, Quebec, pp. 341-353, 2003.

C.W. Chen, B.T. Lu, J.L. Luo and S. Chiovelli, "Electrochemical Noise and Corrosion Mechanism of Pipeline Steel under Slurry-Erosion Conditions", Proceedings of the Second International Symposium on Environmental Degradation of Materials and Corrosion Control In Metals, J. Luo, M. Elboujdaïni , D. Shoesmith and P.C. Patnaik Eds., 42nd Conference of Metallurgists of CIM, MET SOC, Montreal, Quebec, pp. 21-29, 2003.